Tracing the Footprints of Alzheimer's in the Locus Coeruleus:

A Longitudinal Investigation of LC-NE System Integrity and Cognitive Performance Across the AD Spectrum Using a Custom LC NM-MRI Processing Method

Ahmad Sibahi

Thesis submitted to the University of Ottawa
in partial fulfillment of the requirements for the
Doctorate in Philosophy degree in Neuroscience

Cellular and Molecular Medicine
Faculty of Medicine
University of Ottawa

Qur’anic Reflection

بِسْمِ اللَّهِ الرَّحْمَـٰنِ الرَّحِيمِ

اللَّهُ خَلَقَكُمْ ثُمَّ يَتَوَفَّاكُمْ ۚ وَمِنكُم مَّن يُرَدُّ إِلَىٰ أَرْذَلِ الْعُمُرِ لِكَيْلَا يَعْلَمَ بَعْدَ عِلْمٍ شَيْئًا ۚ إِنَّ اللَّهَ عَلِيمٌ قَدِيرٌ

(سورة النحل، الآية ٧٠)

"Allah created you, then He will take your souls. And some of you will be reduced to the most abject stage of life so that they may know nothing after having known much. Surely Allah is All-Knowing, Most-Powerful."
— **Surah An-Nahl (16:70)**

This verse eloquently captures the essence of age-related cognitive decline, such as observed in Alzheimer’s disease. It serves as a profound reminder of the human journey—from knowledge to frailty—and underscores the spiritual and biological realities of aging. The study of neurodegeneration not only advances science but also resonates with timeless truths conveyed in the Qur’an.

Abstract

Alzheimer's disease (AD) is increasingly recognized as involving early degeneration of the locus coeruleus (LC), the brain's primary source of norepinephrine and a key regulator of cognitive functions such as attention and memory. Despite its importance, the progression and consequences of LC deterioration have remained elusive due to challenges in reliably imaging this small brainstem nucleus in vivo. This thesis addresses that gap by employing neuromelanin-sensitive MRI (NM-MRI) and introducing a novel automated LC segmentation technique, the funnel-tip (FT) method, to quantify LC integrity across aging and AD stages.

In the first set of experiments, we validated the FT approach using a cross-sectional cohort (n = 190) across the Alzheimer's spectrum. The FT method demonstrated high agreement with manual tracing (ICC = 0.91), strong association with AD diagnosis, Braak stage, and cognition, and robust test–retest reliability (ICC = 0.82).

Building on this, we conducted a longitudinal analysis in 266 older adults, including cognitively normal individuals, patients with mild cognitive impairment (MCI), and those with AD, followed over four years with annual NM-MRI, PET imaging for amyloid and tau, and neuropsychological testing.

This study's main findings were that the LC signal declined significantly in early AD (Aβ+, Braak stages 1-3), but remained stable in late stages of AD and healthy aging. Notably, Aβ-negative individuals at baseline exhibited an unexpected LC signal increase linked to early tau accumulation, suggesting a transient biological response before

neuronal loss. LC signal was also positively correlated with cognitive performance, particularly in memory and object recognition tasks among AD patients.

In conclusion, this work identifies LC degeneration as a dynamic, early feature of AD and introduces a scalable method for its in vivo assessment. The FT segmentation technique, combined with multimodal biomarkers, enhances our ability to track disease progression and opens new avenues for early diagnosis and intervention in AD.

Acknowledgements

First and foremost, I thank God, the Most Merciful and Compassionate, for guiding me through every step of this journey. It is by His will and grace that I was granted the strength, resilience, and patience to pursue and complete this work. In moments of doubt and exhaustion, His presence gave me clarity and comfort, and I am forever grateful.

I would like to express my deepest gratitude to my supervisor, Dr. Clifford Cassidy, for his exceptional mentorship, unwavering support, and insightful guidance throughout my PhD. Your belief in me, both personally and professionally, has been instrumental in shaping my academic growth and research path. It has been an honour to work under your supervision.

To my Thesis Advisory Committee—Dr. Simon Chen, Dr. Jason Steffener, and Dr. Tharick Pascoal—thank you for your thoughtful feedback and consistent encouragement throughout the years. Your input helped refine my research and challenged me to think more critically.

I am also deeply thankful to my PhD defense committee members—Dr. Simon Chen, Dr. Paul Albert, Dr. Melanie Sekeres, and Dr. David Clewett—for generously offering your time, expertise, and valuable perspectives, all of which contributed greatly to the quality and impact of this dissertation.

To my family, your love and support have been the foundation upon which this entire journey was built. To my beloved mother Aliya and father Mohammad, your prayers, sacrifices, and unconditional love gave me the courage to chase my dreams

across continents. To my dear sisters Sirine and Sally, and my brothers Ibrahim and Youssef, thank you for your constant encouragement, for always believing in me, and for being my anchor through it all.

I also extend my heartfelt gratitude to my aunt Souad Aboukar, whose generosity and warmth have been a blessing in my life. Even before I arrived in Canada, she opened her heart and home to me, offering me a place to stay and the emotional support that helped me settle and thrive in a new country. Her care and kindness made Ottawa feel like home when everything was unfamiliar.

To my dearest friend Youssef Al Falah, thank you for being by my side since the beginning of this journey. From deciding to move to Canada together to supporting one another through each challenge and triumph, your friendship has been a constant source of strength and motivation. To my Ottawa new best friends Baker Zyad and Abdelrahman Alshouali, thank you for the laughter, encouragement, and companionship that brought light to the long days and made this journey so much more enjoyable.

To my incredible wifey Jana Jarjour, thank you for your unwavering love, patience, and inspiration. You have been my greatest supporter, my calm during chaos, and my reason to keep going when the path felt heavy. Your presence has filled my life with joy, balance, and meaning. I am endlessly grateful for the beautiful memories we've created together during this chapter and for your strength and grace throughout it all. I cannot wait to begin our next chapter with the arrival of our son Amir, who we look forward to welcoming this summer. You both are my heart and my future.

Dedication

I dedicate this thesis to the soul of my beloved grandmother, ***Dalal Ghrawi****, who passed away from Alzheimer's disease during the first year of my PhD. Her struggle with this illness inspired me to pursue this research, with the hope of contributing to a better understanding of the disease and helping others who face its devastating effects. This work is a tribute to her memory and to all those touched by Alzheimer's.*

TABLE OF CONTENTS

Title i

Qur'anic Reflection ii

Abstract iii

Acknowledgements v

Dedication vii

Table of Contents viii

List of Abbreviations xiii

List of Figures xv

List of Tables xvi

Chapter 1. Literature Review 1

1.1. Background on Alzheimer's Disease 2

1.1.1. Epidemiology & Impact 2

1.1.2. Prevalence of AD 2

1.1.3. Risk Factors of AD 3

1.1.3.1 Genetic Factors 3

1.1.3.2 Behavioral Factors 4

1.1.3.3 Metabolic and Cardiovascular Factors 4

1.1.3.4 Social and Environmental Factors 5

1.1.4. The Role of Iron in AD 5

1.1.5 Societal and Economic Impacts of Alzheimer's Disease-Related Neurodegeneration 6

1.1.6 AD Course of Illness 7

1.1.7. Comparison Between AD and Other Dementias 9

1.1.8. Pathological Hallmarks 10
1.1.8.1 Amyloid-Beta 11
1.1.8.2 Tau Neurofibrillary Tangles 12
1.1.8.3 Synaptic Loss 13
1.1.8.4. Various Forms of Alzheimer's Disease 14
1.1.8.5. Oxidative Stress & Neuroinflammation as Etiological Factors 14
1.1.8.5.1. Neuroinflammation 14
1.1.8.5.2. Oxidative Stress 16
1.1.8.6 Cholinergic System Involvement 17
1.1.8.7. Cascade of Change 17
1.1.9. Neuropsychiatric Symptoms 18
1.2. Locus Coeruleus Norepinephrine System Function and its Relevance to AD 19
1.2.1. The Human Locus Coeruleus 20
1.2.1.1. Anatomical Review 20
1.2.1.2. Noradrenergic Projection Pathways 20
1.2.1.3. Norepinephrine Receptors 21
1.2.1.4. Neurotrophic Factors 22
1.2.1.5. Formation of Neuromelanin Pigment 22
1.2.2. The functional relevance of the Locus Coeruleus in cognitive processes 25
1.2.2.1. Arousal, Attention, and the LC-NE system 25
1.2.2.2. Novelty detection and memory processing 26
1.2.3. LC-NE system in Animal Models 27
1.2.3.1. LC Activation and Cognitive Improvement 27
1.2.3.2. Stress-induced cognitive decline and LC hyperactivity 28
1.2.3.3. Models of Neurodegenerative Disease and LC Dysfunction 28

1.2.3.4. Therapeutic Strategies in Animal Models 29

1.2.4. The LC in Neurodegenerative Diseases and Healthy Aging 30

1.2.4.1. LC Aging and Integrity 30

1.2.4.2. Evidence Connecting Pathology of Alzheimer's Disease and Cognitive Decline to Early Locus Coeruleus Degeneration 31

1.2.5. Noradrenergic Hypothesis of Alzheimer's Disease 32

1.3. Importance of NM-MRI LC Imaging and Automated Segmentation 33

1.3.1. Introduction to MRI's and Neuromelanin Imaging Physics 34

1.3.2. Neuromelanin-sensitive MRI 35

1.3.3. From Manual to Automated Segmentation 36

1.3.4. NM-MRI Studies and Neurodegenerative Diseases 37

1.3.5. Use of LC Imaging in Human Aging and AD Research 38

1.4. Aims and Hypotheses 40

1.4.1. Aim 1 40

1.4.2. Hypothesis 1 40

1.4.3. Aim 2 40

1.4.4. Hypothesis 2 40

1.4.5. Aim 3 41

1.4.6. Hypothesis 3 41

Chapter 2. Methods Used For All Aims in This Doctoral Thesis 42

2.1. Methods for Aim 1 43

2.1.1. Participants and clinical measures 43

2.1.2. Image acquisition 45

2.1.3. Manual LC segmentation 46

2.1.4. Automated LC segmentation 47

2.1.5. 3D reconstruction of LC structure by FT method 53

2.1.6. PET Acquisition and Analysis 53

2.1.7. Statistical Analysis 54

2.2. Methods for Aim 2 and 3 55

2.2.1. Participants and clinical measures 55

2.2.2. Image acquisition 57

2.2.3. PET Acquisition and Analysis 57

2.2.4. NM-MRI processing 57

2.2.5. Cognitive Tests 60

2.2.6. Statistical Analysis 62

Chapter 3. Results of the characterization of an automated method to segment the human locus coeruleus 64

3.1. Evaluation of Different LC Segmentation Methods 65

3.1.1. LC Signal Values 65

3.1.2. Agreement between LC metrics 66

3.1.3. Sensitivity to Signal Loss Associated with AD 72

3.2. Reproducibility Across and within NM-MRI sequences 74

3.2.1. Reliability of Scan-Rescan and LC location 74

3.2.2. LC Signal Cross-Sequences Consistency 76

3.3. FT-based 3D LC Reconstructions' Structural Validity 76

Chapter 4. Results for the longitudinal investigation of locus coeruleus norepinephrine system integrity and cognitive performance across the Alzheimer’s spectrum 85

4.1. Longitudinal change in LC signal 86

4.2. LC change proximal to AD onset 90

4.3. Association of LC integrity to cognition 92

Chapter 5. Discussions For the Aims in This Doctoral Thesis 102

5.1. Discussion for Aim 1 103

5.2. Discussion for Aims 2 and 3 108

Chapter 6. Limitations, Strengths, Future Directions, and Conclusions 117

6.1 Strengths and Limitations for Chapter 2 118

6.2 Strengths and Limitations for Chapter 3 120

6.3 Future Directions 122

6.4 Conclusions 124

References 127

LIST OF ABBREVIATIONS

AD	Alzheimer's Disease
Aβ	Amyloid-beta
PET	Positron Emission Tomography
NM-MRI	Neuromelanin-Sensitive Magnetic Resonance Imaging
LC	Locus Coeruleus
NE	Norepinephrine
MCI	Mild Cognitive Impairment
CN	Cognitively Normal
FT	Funnel-Tip (segmentation method)
ICC	Intraclass Correlation Coefficient
CNR	Contrast-to-Noise Ratio
BORB	Birmingham Object Recognition Battery
MMSE	Mini Mental State Examination
CDR	Clinical Dementia Rating
TMT-A/B	Trail Making Test Part A / B
WAIS	Wechsler Adult Intelligence Scale
RAVLT	Rey Auditory Verbal Learning Test
ROI	Region of Interest
TE	Echo Time
TR	Repetition Time
MPRAGE	Magnetization Prepared Rapid Acquisition Gradient Echo
SUVR	Standardized Uptake Value Ratio

APOE ε4	Apolipoprotein E epsilon 4 allele
DTI	Diffusion Tensor Imaging
VMAT	Vesicular Monoamine Transporter
VaD	Vascular Dementia

LIST OF FIGURES

Figure 1. Step-by-step Process of Neuromelanin Organelle Creation from Dopamine 24

Figure 2. LC segmentation via FT method 51

Figure 3. Three different LC segmentation approaches 52

Figure 4. Schematic map of the LC with colors reflecting coefficients for each LC section derived from a logistic regression with CN status as dependent variable 59

Figure 5. Bland-Altman plot examining proportional bias between LC signal measured using the manual and FT methods 70

Figure 6. Heatmap showing proportion of subjects where the manual and FT LC masks overlapped 71

Figure 7. Linear structure of the FT LC mask 78

Figure 8. Effect of time on LC integrity 86

Figure 9. Relationship between change in LC integrity and tau accumulation over time in older adults with little to no evidence of AD at study baseline 88

Figure 10. LC schematic maps association of NM-MRI signal across all LC sections to cognitive measures 95

Figure 11. Longitudinal loss in LC integrity is associated with reduction in object recognition over time in AD participants 96

Supplementary Figure 1. Raw data of LC patternCN metric change over time in every single participant across all Braak stages. 89

Supplementary Figure 2. BORB combined scores versus LC patternCN across Braak staging 98

Supplementary Figure 3. Working Memory scores versus LC patternCN across Braak staging 99

Supplementary Figure 4. Logical Memory scores versus LC patternCN across Braak staging 100

Supplementary Figure 5. Verbal Fluency scores versus LC patternCN across Braak staging 101

LIST OF TABLES

Table 1a. Demographic characteristics of the sample of older adults (Aim 1) 44

Table 1b. Clinical, cognitive and demographic measures (Aims 2-3) 56

Table 2a. LC signal (CNR) as measured by different LC segmentation approaches and level of agreement (ICC (2,k)) between these metrics 68

Table 2b. LC signal (CNR) as measured by different LC segmentation approaches and level of agreement (ICC (3,k)) between these metrics 69

Table 3. Effect size estimates of the relationship between LC signal metrics and AD severity measures 73

Table 4. Reproducibility of LC signal 75

Table 5. Angle of LC fit lines relative to y-axis 79

Table 6. Fraction of FT peak-intensity voxels deviating from linear structure 80

Table 7. Error in linear fit of LC coordinates per LC section 81

Table 8. Error in linear fit of LC coordinates from FT method and control conditions 82

Table 9. Relation of LC $pattern_{CN}$ to cognitive measures in study subgroups 94

Chapter 1. Literature Review

1.1. Background on Alzheimer's Disease

1.1.1. Epidemiology & Impact

Cognitive decline, memory loss, and functional disability define the progressive neurodegenerative condition known as Alzheimer's disease (AD). Affecting millions of people globally, it is the common cause of dementia in the elderly[1,2]. The progressive decline eventually affects the patient’s daily activities and quality of life after the sequential decrease in behavioral, cognitive, and motor functions[3]. The prevalence of Alzheimer's continues to rise, as the population ages, at an alarming rate, posing significant challenges and socio-economic burdens to the patients, communities, and the healthcare systems worldwide[4,5].

1.1.2. Prevalence of AD

In 2020, the prevalent cases of AD cases and other dementias around the world were more than 55 million cases according to the World Health Organization (WHO) where AD accounted for 60-70 percent of these cases[6]. This number is expected to triple by 2050 to reach 139 million cases globally. In 2019, the prevalence rate (age-standardized) due to AD and other dementias increased by 5.7% to be 682.5 per 100,000 individuals globally[7]. Regionally, the highest scores were for the regions of Middle East and North Africa (777.6) and East Asia (781.4), while Western Sub-Saharan Africa (469.8) and South Asia (428.4) recorded the lowest rates[7]. Moreover, East Asia and high-income Asia Pacific regions had the highest increase (28.3% and 19% respectively) in regional prevalence rates since 1990, whereas Western Sub-Saharan Africa recorded a decrease of -2.4%. Country-wise, the prevalence rates are the highest in Turkey (805.1) and Bahrain (801.1), while it is the lowest in Nigeria (441.4) and India (416.4)[7].

A recent report (2023) showed that only in the United States of America there is an estimated 6.7 million people above the age of 64 are currently living with Alzheimer's dementia[8]. While this number is expected to double by 2060 to reach around 13.8 million cases. In 2020, a report recorded that the prevalence rate of AD was doubled among persons who identify themselves as Black/African American than those of a white race[8].

In 2019, AD was recorded as a cause of death for 121,499 cases in America, and it was listed as the sixth leading cause of death before COVID-19 entered the top ten pushing it to the seventh place[8]. However, it remains fifth on the list of Americans' death certificates who are age 65 or older. Since the beginning of 2000, the death rates decreased for HIV, stroke, and heart disease, while recorded deaths from AD increased by more than 145%[8].

1.1.3. Risk Factors of AD

Although a lot of studies have been done, the precise etiology of Alzheimer's disease is still unknown; yet certain risk factors have been found to help explain its onset. Early diagnosis, prevention plans, and proper illness management all depend on an awareness of these risk factors. The most important risk factors linked with Alzheimer's disease—including genetic predisposition, lifestyle choices, cardiovascular diseases, and environmental exposures—as explored in this literature review will be discussed.

1.1.3.1 Genetic factors

Among the most firmly recognized risk factors for Alzheimer's disease is genetic inclination. An elevated risk of late-onset or sporadic Alzheimer's disease is linked to the Apolipoprotein E (APOE) gene, especially the APOE ε4 allele. Studies have found that persons with one copy of the APOE e4 allele had a two- to threefold greater risk; those with two copies have up to a

twelve-fold risk[9,10]. Furthermore, early-onset or familial Alzheimer's disease is connected to mutations in genes including APP, PSEN1, and PSEN2[11]. Characteristic of Alzheimer's disease, these genetic factors contribute to amyloid-beta accumulation and tau protein pathology, which are known as the hallmark features of AD[12,13]. Also, these genes are highly penetrant compared to APOE ε4 allele carriers, and mutations to these genes can lead to symptomatic onset as early as the third or fourth decade of life[14].

1.1.3.2. Behavioral Factors

New research points to a major influence of lifestyle decisions on Alzheimer's risk. An increased risk of the disease has been linked to physical inactivity, bad eating patterns, smoking, and excessive alcohol consumption[15,16]. Consistent physical activity and a balanced diet—especially the Mediterranean diet[17] has been shown to reduce risk. Additionally, protective factors include social interaction and cognitive stimulation. Studies show that those who pursue lifetime learning and keep close relationships show less cognitive deterioration[15,18].

1.1.3.3. Metabolic and Cardiovascular Factors

Alzheimer's disease and cardiovascular health are clearly connected. Among the risk factors are hypertension, diabetes mellitus, hypercholesterolemia, and obesity[15,19]. Reduced brain perfusion and vascular injury help explain neurodegenerative alterations; insulin resistance may aggravate amyloid plaque development and neurofibrillary tangles[20]. Also, efficient control of cardiovascular risk factors has shown a reduction in the incidence of Alzheimer's and associated dementias[21].

1.1.3.4. Social and Environmental Factors

Also linked with the etiology of Alzheimer's disease are environmental exposures including heavy metal toxicity and air pollution. Long-term particulate matter and pollution exposure to nitrogen dioxide, nitrous oxide, ozone, and carbon monoxide can set off inflammatory reactions and oxidative stress, therefore causing brain damage[15,22]. Furthermore, very important in risk modulation are socioeconomic elements including the degree of education and availability of healthcare facilities. Reduced educational level and socioeconomic hardship are connected to higher sensitivity to cognitive deterioration[5,15]. This is known by a concept called “cognitive reserve” defined by an individual's ability to sustain cognitive function despite age related degeneration or brain damage, where the brain's resilience and adaptability make it easier to compensate for cognitive decline[23]. Multiple factors affect this reserve as years of education, category of occupation, and consistent engagement in brain-stimulating activities[23].

1.1.4. The Role of Iron in AD

Proper iron balance within the brain is crucial for neurological function and cognitive health. Dysregulated iron homeostasis has increasingly been directly implicated in the pathogenesis and progression of Alzheimer's disease[24,25]. Accumulation of iron in the brain can induce oxidative stress and generate reactive oxygen species, resulting in neuronal injury and the induction of neuroinflammation[24,26]. Moreover, elevated iron levels might promote amyloid-beta peptide and tau protein aggregation—two defining features of Alzheimer's disease pathology[25].

A prominent idea posits that iron deposition in the brain interferes with normal cellular processes, allowing toxic protein aggregates to form and inducing cognitive deterioration.

Certain experimental treatments have tried reducing brain iron stores by chelation or diet modification, however, clinical information is limited and sometimes conflicting[26]. Additionally, systemic abnormalities of iron metabolism, as characterized by elevated serum ferritin levels, have similarly been linked to heightened risks of cognitive impairment, suggesting that deregulation of iron may spread its negative effects well beyond the brain[25].

In order to establish new and effective treatment strategies, it is important to expand our knowledge of the role of iron in neurodegeneration. Prevention of iron-induced neurotoxicity may provide new strategies for the treatment of Alzheimer's disease progression and patient quality of life.

1.1.5. Societal and Economic Impacts of Alzheimer's Disease-Related Neurodegeneration

With the increasing burden of Alzheimer's disease (AD), it has emerged as a significant public health concern that demands immediate attention. The primary cause of this increase is the aging population, which imposes a tremendous burden on families, communities, and healthcare systems globally[27]. The economic cost of Alzheimer's disease is significant and far-reaching, including direct healthcare costs, long-term care costs, and informal home care by family.

Healthcare spending on Alzheimer's Disease has increased in affluent nations such as Canada due to the increasing demand for specialist services and long-term care. The additional demand usually results in the placement of patients in care facilities, further exacerbating financial expenses. With the aging population, economic pressures will increase, mandating the introduction of legislative bills to efficiently ration resources[27]. The financial burden of AD extends beyond the direct medical costs. The socioeconomic impact involves diminishing

productivity, in that both patient and caregiver both experience increasing obstacles to maintaining their job. Family members also tend to become primary caregivers, forgoing professional aspirations to spend time and energy on tending to their loved ones. Such a persistent workload generates a significant emotional and mental burden, resulting in many caregivers becoming overwhelmed, drained, and even depressed[28,29]. Communities are challenged to accommodate to support individuals with dementia while meeting the needs of impacted families. Policies encouraging caregiver well-being, as well as public and community education activities and educational campaigns, are central in relief from family and system burden. Early detection and treatment are critical in slowing down the development of illness, while public education can greatly increase health awareness, thereby increasing the likelihood of early detection[27].

1.1.6. AD Course of Illness

Alzheimer's disease progresses through various stages, each with its own challenges concerning cognitive decline and activities of daily living. Knowledge of the disease course is important for clinicians and caregivers as it informs clinical decisions and care planning. The initial phase, mild cognitive impairment (MCI), is gradual and may go undetected and it is not specific as some MCI cases may not go on to develop AD. MCI individuals may, forget things at times, be slow to collect their thoughts or have difficulty completing complicated tasks. Sadly, the symptoms are misdiagnosed as normal symptoms of aging, resulting in delayed treatment and diagnosis[30,31].

As the disease progresses to its early stage, memory loss becomes more significant, particularly with respect to recent things or recently learned information. Changes in mood,

including anxiety and depression, may emerge, disrupting daily life and social relationships[32]. During the second stage, cognitive impairment severely disrupts daily activities and makes every day a challenging task. The patients will have to depend more and more on caregivers to accomplish simple tasks such as bathing, dressing, and administering medicines. Changes in behavior such as irritability, restlessness, and disturbed sleep patterns are commonly established, making caregiving more demanding[31].

The final stage of AD is preceded by a severe loss of cognitive and physical functions. Communication may be restricted or cut off, resulting in patients not knowing their nearest relatives. A normal activity such as swallowing and eating may become a problem, requiring constant observation as well as psychotic-like symptoms would be shown in many cases[31]. Immobility is a major issue, with the risk of infection, especially pneumonia, being a top cause of death[30].

One intriguing feature of the progression of Alzheimer's disease is that the characteristic neuropathological manifestations, i.e., amyloid plaques and neurofibrillary tangles, do not always correspond to symptoms complained by the patients, while the Braak staging developed by Braak and Braak explains the illness progression based on the spread of tau and amyloid in the brain, which can now be tracked in vivo with the utilization of PET imaging[33–35].

Braak & Braak's theory holds that the initial changes—stage I—start in the transentorhinal cortex, where amyloid deposits are either small or absent and tau building is only beginning[35]. The disease starts to migrate into the entorhinal cortex in stage II, but at this phase, cognitive decline is usually not present[36].

Tau tangles reach the limbic system and early neocortical areas as the disease moves into stages III and IV. This is regarded as the preclinical phase of AD; although they are usually not severe or easily observable, minor cognitive problems can start to show[36]. Amyloid plaques also become more noticeable in these phases, therefore adding to the pathogenic load on the brain[36].

Tau pathology has spread broadly over the neocortex by the time AD reaches stages V and VI. By this stage, the illness is completely developed, and people usually suffer from major cognitive impairment and extensive neuronal loss[37]. Though tau appears to be especially important in promoting neurodegeneration as AD develops, both amyloid and tau ultimately help to drive the disease process. Thus, it is imperative to assess both kinds of pathology jointly if one is to completely grasp and monitor Alzheimer's development[37,38].

Enhancing public awareness of the normal progression of Alzheimer's Disease and its warning signs can enable early intervention, with improved planning and more reflective care strategies. Ongoing research into Alzheimer's disease process mechanisms is central to the development of targeted therapy that can maximize patient outcomes and quality of life[39].

1.1.7. Comparison Between AD and Other Dementias

Alzheimer's disease (AD), the most common type of dementia, is known for memory impairment and cognitive function loss that are caused by the deposition of amyloid-beta (Aβ) plaques and tau tangles in the brain[40]. Comparatively, frontotemporal dementia (FTD) usually shows early personality changes and behavioral abnormalities rather than memory impairment and has different pathological markers including TDP-43 proteinopathies[41,42]. Although these diseases have common degenerative paths, their clinical patterns are quite different. While

FTD patients show executive dysfunction and changed social behavior early in the illness course, those with AD often show prominent memory impairment[43,44].

Moreover, vascular dementia (VaD) is known to have a distinct pathogenesis connected to cerebral ischemia and vascular factors[45]. While cognitive abilities can be impacted in both AD and VaD, the beginning of VaD usually coincides with strokes or cardiovascular diseases, therefore producing a varying cognitive history unlike the more slow cognitive decline seen in AD[46]. Different brain perfusion patterns across the several dementia types are indicated by a comparison of changes in cerebral blood flow (CBF) between VaD patients and those with AD and FTD, where VaD showed higher CBF than other types of dementia[47]. Similarly, Lewy body dementia (LBD), which includes Parkinson's disease dementia, has distinct symptoms such as visual hallucinations and parkinsonism that are not commonly seen in AD or FTD[48].

Dementia with Lewy bodies (DLB), the second type of LBD, further complicates the dementia spectrum because of its overlap with both AD and FTD, especially with relation to neuropsychiatric symptoms like hallucinations[49]. Lewy bodies, the pathogenic feature of DLB, differ from the amyloid plaques of AD and the TDP-43 inclusions observed in FTD, therefore contributing to different clinical presentations[50]. Neuroimaging studies have revealed significant biomarker differences between these dementias, with AD exhibiting increased amyloid and tau deposition, whereas DLB exhibits lower levels of dopaminergic function and distinct MRI characteristics when compared to both AD and FTD[48,51].

1.1.8. Pathological Hallmarks

Alzheimer's disease (AD) is a chronic neurodegenerative disease with characteristic pathological features, which are pivotal to its pathogenesis and progression. They are amyloid-

beta (Aβ) plaque deposition, tau neurofibrillary tangle formation, and synaptic loss. In addition, oxidative stress and neuroinflammation are increasingly considered pathogenic processes, in addition to global changes in the cholinergic system. Due to its multifactorial etiology, AD is a challenge to researchers and clinicians because they need to utilize effective therapeutic strategies and diagnostic markers. However, as you will see in the following sections, the biology of AD is becoming well characterized and significant progress has been made despite persistent challenges.

1.1.8.1. Amyloid-Beta

Amyloid-beta (Aβ) plaque accumulation in the brain is one of the most known pathogenic features of Alzheimer's disease. More precisely Aβ42, which is produced from the amyloid precursor protein (APP) by consecutive cleavages by beta- and gamma-secretase enzymes, these plaques mostly feature oligomerized Aβ peptides[52]. Aβ peptides synthesized often self-assemble and form insoluble fibrils, which build extracellularly in the brain in the compact form of plaques. These plaques are not only neurotoxic but also supposed to start inflammatory reactions in the brain.

According to the amyloid cascade theory, Aβ peptide deposition is the first event causing the later pathologic alterations in Alzheimer's disease[52]. With increasing cognitive function loss, deposited Aβ deranges synaptic activity and neural communication. It is well established that clinical presentation and amyloid load are tightly but nonlinearly linked. Some patients have extreme dementia but rather low amyloid loads; others have plenty of plaque but lack dementia[24]. Such variety has spurred discussion on the particular role Aβ plaques play in disease pathogenesis.

With the development of neuroimaging methods such as positron emission tomography (PET) radiotracers that enable in vivo identification of amyloid deposition, Aβ plaque research have advanced significantly. Longitudinal studies suggest that Aβ plaque development usually occurs several years before the onset of cognitive impairment and that early therapy of amyloid deposition may thus be beneficial[24].

1.1.8.2. Tau Neurofibrillary Tangles

Tau neurofibrillary tangles (NFTs) are the second inherent pathological feature of Alzheimer's disease (AD) and consist of hyperphosphorylated tau protein that exists in the form of filaments in the neurons. In healthy individuals, tau protein plays a role in the structural integrity of microtubules of the neuronal cytoskeleton; however, after hyperphosphorylation, it loses its functional activity and causes disassembly and tangle formation made of tau[24,53].

Compared with amyloid plaques, the topological distribution of tau pathology better correlates with the severity of cognitive deficits. Evolution of tau pathology follows a seemingly predictable course from the transentorhinal cortex to the hippocampus and neocortex with the progression of illness[24,54]. A spreading mechanism such as this aligns well with the clinical progression of Alzheimer's disease, and tau pathology serves as an accurate biomarker for monitoring the progression of illness as we discussed the Braak stage progression in the previous section on AD course of illness[35–37].

Tau pathology has been linked with axonal transport disruptions, which in turn compromise efficient communication between neurons. This ultimately results in synaptic dysfunction and neuronal cell death. It has been observed that tau pathology is more closely linked with clinical presentation than amyloid deposition because it directly disrupts neuronal

function[24]. Identifying the mechanisms underlying tau hyperphosphorylation and aggregation is significant for the development of therapeutic interventions aimed at this aspect of Alzheimer's disease pathology[24].

1.1.8.3. Synaptic Loss

Synaptic dysfunction and subsequent loss of synapses are directly related to the phenomenon of cognitive impairment in Alzheimer's disease (AD) patients, and these states usually occur many years before the development of obvious and overt pathology featuring amyloid or tau proteins. Extensive research has established a direct and significant correlation between the loss of synapses in the hippocampus, and also in other regions of the brain associated with memory, and the consequent impairment of cognitive function, [54]. The induction of synaptic loss can be due to a myriad of factors ranging from tau hyperphosphorylation, mitochondrial injury, to oxidative stress[55].

A salient feature of synaptic loss in Alzheimer's disease (AD) is the degeneration of the cholinergic system, which is involved in promoting learning and memory functions. In patients diagnosed with AD, extensive degeneration of the cholinergic neurons within the basal forebrain occurs, leading to decreased levels of acetylcholine. Such specific loss is associated with cognitive and memory impairment, and research is still ongoing to search for the effective medication for cognition since cholinergic medications didn’t show an improvement[54].

There is also accumulating evidence demonstrating disruption of synaptic plasticity in AD. Loss of dendritic spines, which play a role in synaptic transmission and plasticity, is a common finding in AD brains[54]. Synaptic loss is not only the consequence of tau and amyloid

pathologies but also plays a role in cognitive impairment by directly influencing neuronal communication and information processing[54].

1.1.8.4. Various Forms of Alzheimer's Disease

Alzheimer's disease, a complex and serious neurodegenerative disease, is routinely classified into two distinct forms: familial or early-onset Alzheimer's disease, and sporadic or late-onset Alzheimer's disease. Sporadic Alzheimer's disease is the most prevalent form of the disease and typically affects individuals after they have reached the age of 65 years, with no particular genetic link or familial factor that can be identified following family lines[24]. Familial Alzheimer's disease, however, is far less common and occurs as a direct result of mutations in the genes PSEN1, PSEN2, and APP, which have been documented as having fundamental roles in the causation of this form of the disease. These mutations cause changes in the processing of Aβ and result in a tremendous rise in plaque deposition at a very early age[24].

Elucidation of the molecular and genetic mechanisms of the different types of AD is important in the development of targeted intervention. Differential diagnosis between the familial and sporadic types also raises issues of screening and genetic counseling, especially in the early-onset dementia families[24]. Molecular investigations are also progressively giving insights into the molecular pathways involved and are offering opportunities for individualized therapeutic intervention[24].

1.1.8.5. Oxidative Stress and Neuroinflammation as Etiological Factors

1.1.8.5.1. Neuroinflammation

Neuroinflammation is one of the major causes of Alzheimer's disease pathogenesis, one of the key mechanisms that initiate and advance neurodegenerative changes. Increasingly, research shows that neuroinflammation is not simply an epiphenomenon of the pathological process of AD, but also an active promoter of the overall pathology of the disease. The brain immune cells, i.e., microglia and astrocytes, become activated with amyloid-beta (Aβ) deposition and release pro-inflammatory cytokines, chemokines, and reactive oxygen species (ROS)[56,57]. Inflammation, though helpful in its initial stage, turns to be harmful with chronic inflammation, causing neuronal injury and synaptic dysfunction[57].

The bidirectional interaction between amyloid-beta (Aβ) plaques and neuroinflammation reinforces a negative vicious cycle that drives the progression of Alzheimer's disease (AD). Aβ accumulation induces the activation of microglial receptors like Toll-like receptor 4 (TLR4) and NLRP3 inflammasomes, which result in the release of pro-inflammatory molecules like interleukin-1β (IL-1β) and tumor necrosis factor-alpha (TNF-α)[57]. The inflammatory mediators in question not only cause neuronal cell death but also impede the clearance of Aβ, thus allowing the continuous formation of plaques. This harmful cycle forms the basis of the neurodegenerative cascade seen in patients suffering from Alzheimer’s disease[57].

Current neuroimaging studies have shown strong correlations between amyloid accumulation and increased markers of neuroinflammation. Advances in imaging techniques, particularly with PET imaging for TSPO ligands, have shown that areas of high amyloid deposition have higher glial activation and inflammation relative to areas of low amyloid burden; these are indices of cognitive impairment and severity of symptoms[58]. Identification of the precise pathways by which neuroinflammation contributes to AD pathology is important to the

development of anti-inflammatory therapies directed at modulating microglial activation or blocking the release of pro-inflammatory cytokines[58].

1.1.8.5.2. Oxidative Stress

Oxidative stress is a key aspect of the pathophysiology of Alzheimer's disease since it is a final inducer for neuron injury and loss of synaptic integrity. It arises as a result of imbalance between the generation of reactive oxygen species (ROS) and the capacity of the brain to conduct antioxidant defense. In Alzheimer's disease, oxidative stress is further exacerbated by the accumulation of amyloid-beta (Aβ) and tau aggregates that cause mitochondrial dysfunction and enhanced production of reactive oxygen species (ROS)[56]. The heightened oxidative stress consequently results in the oxidation of vital biomolecules like lipids, proteins, and nucleic acids, with eventual cellular dysfunction and apoptosis[55].

Oxidative damage is pervasive in brain regions that are typified by heightened susceptibility to Alzheimer's disease (AD), namely the hippocampus and cortex. It has been revealed that the amyloid and tau pathologies are not just initiated by oxidative stress, but also modulated by it, which causes them to develop slowly. Oxidative alterations, however, can increase the risk of Aβ peptide aggregation along with promoting tau hyperphosphorylation, thus spreading the process of neurodegeneration[54].

Therapeutic approaches to reduce oxidative stress have included the use of antioxidants such as vitamin E, coenzyme Q10, and curcumin. These have been found to exert neuroprotection in preclinical models, but it has been extremely difficult to translate this to the clinical scenario[25]. Targeting oxidative stress remains an attractive strategy for decreasing the course of Alzheimer's disease and preserving cognitive function.

1.1.8.6. Cholinergic System Involvement

The cholinergic hypothesis of Alzheimer's disease postulates that cognitive decline is caused by extensive loss of cholinergic neurons, primarily from the basal forebrain. Acetylcholine (ACh) is a major neurotransmitter of learning and memory and its deficiency is commensurate with the degree of dementia[55]. Pathologic processes against the cholinergic neurons are synaptic degeneration, axonal injury, and defective neurotransmitter synthesis, all of which are harmful to cognitive functions[54].

The cholinergic dysfunction in AD has motivated the development of therapeutic strategies that enhance cholinergic transmission. Cholinesterase inhibitors such as donepezil, rivastigmine, and galantamine, which are in routine practice, act by increasing the amount of acetylcholine (ACh) available by inhibiting its breakdown. Pharmacological treatment is being employed for symptom relief by enhancing cholinergic transmission, with no impact on the disease pathology[54].

There is new evidence for a potential interaction of the cholinergic system with neuroinflammatory mechanisms. Cholinergic receptors-bearing activated microglia can modulate inflammatory processes in such a way that restoring cholinergic function can be employed to prevent neuroinflammatory damage[54]. Such interaction explains the effectiveness of combining cholinergic-targeted therapy with anti-inflammatory treatment to enhance therapeutic effectiveness in Alzheimer's disease[54].

1.1.8.7. Cascade of Change

The cascade model of Alzheimer's Disease (AD) states that pathological processes are not independent; they are, rather, linked with each other and give a sequential response during the

disease process. Early accumulation of amyloid generates tau pathology, followed by synaptic dysfunction and neurodegeneration[57]. The cascade model explains the cross-talk between amyloid, tau, neuroinflammation, oxidative stress, and cholinergic deficit that all facilitate cognitive impairment and disease progression.

An appreciation of the cascade effect is necessary to design multi-targeting therapeutic approaches that address multiple facets of AD pathology rather than targeting amyloid or tau individually. This type of approach can be expected to break the vicious cycle and halt disease progression[57].

1.1.9. Neuropsychiatric Symptoms

Neuropsychiatric symptoms (NPS) are prevalent in Alzheimer's disease and significantly impact patients' quality of life. Depression, anxiety, agitation, and apathy are frequent symptoms that complicate the management of the disease and enhance caregiver burden[59]. The knowledge of neurobiological substrates of NPS is imperative in formulating integrative treatment approaches targeting both cognitive and behavioral aspects of AD[59].

AD psychiatric symptoms often occur early in the course of illnesss and can precede cognitive impairment. Depression and anxiety are particularly difficult, associated with alterations in brain regions like the prefrontal cortex and limbic system[59]. Not only do these symptoms worsen the patient's quality of life but also accelerate cognitive loss, with eventual institutionalization a possibility[60].

The development of NPS in AD is believed to be the consequence of the neuropathology of neurotransmitter systems such as serotonergic and cholinergic systems. Besides this,

neuroinflammation initiates the disruption of mood and behavior by altering neurotransmission as well as neuroplasticity[57,59].

Neuroimaging research has established that the severity of depression symptoms is also associated with atrophy in the amygdala and cingulate gyrus areas of the brain. Such structural deficits in the respective areas hamper the regulation of emotion and control over cognition, and interventions may need to be designed specifically to target neuropsychiatric and cognitive activities of Alzheimer's disease[53].

1.2. Locus Coeruleus- Norepinephrine System Function and its Relevance to AD

Most famously known for its function in controlling a wide range of cognitive processes by the release of the neuromodulator norepinephrine (NE), the locus coeruleus (LC) is a small but fundamentally significant nucleus within the brainstem. The LC norepinephrine system is essential for sustaining alertness and thereby promotes attention, memory processing, and modulation of emotional response[61]. Although its total volume is small, the LC's broad projections allow the NE to affect almost every area of the central nervous system (CNS), hence regulating both cognitive and autonomic activity[62].

Knowing the anatomical organization and functional relevance of the locus coeruleus (LC) is especially crucial since it is fundamental for basic physiological and cognitive processes; moreover, its degeneration has been connected to a variety of neurodegenerative diseases including Alzheimer's and Parkinson's diseases[63,64]. This extensive review of the literature takes into account the anatomy of the LC, its function in memory and the processing of new stimuli, results of animal research, and the effect of aging on both the structural integrity and functional effectiveness of the LC.

1.2.1. The Human Locus Coeruleus

1.2.1.1. Anatomical Review

Located bilaterally in the dorsal pons of the brainstem, the LC lies near to the lateral boundary of the fourth ventricle[62]. The presence of neuromelanin in noradrenergic neurons—a crucial indicator of both localization and identification of locus coeruleus neurons—helps to explain its bluish-gray color[65]. The locus coeruleus is the main source of norepinephrine in the brain according to histological studies showing a high concentration of noradrenergic neurons, over 30,000 in human subjects[61].

A neural complex, the locus coeruleus stretches rostro-caudally through its projections in the pons and has a strongly concentrated distribution close to the fourth ventricle. Widespread efferent projections connect the LC to numerous cortical and subcortical areas, including the prefrontal cortex, thalamus, amygdala, hippocampus, cerebellum, and spinal cord[65]. High-resolution magnetic resonance imaging (MRI) has made it feasible to do in vivo LC studies, therefore enabling research into age-related alterations and degeneration[65,66].

1.2.1.2. Noradrenergic Projection Pathways

Forming some of the most common networks in the central nervous system, the noradrenergic projections from the LC, include both ascending and descending fibers[67]. Affecting higher cognitive functions including attention, arousal, memory, and emotional processing, the ascending paths mostly point to locations including the prefrontal cortex, hippocampus, amygdala, thalamus[63], and all other cortical areas, while it might have some weaker connections with some regions or a lack of direct projection in the case of the primary visual cortex (V1)[68]. Ascending projections would be maintaining arousal and adjusting

attentional focus depending on the wide innervation of the cerebral cortex, especially in the frontal and parietal lobes[69].

Descending projections from the LC reach the spinal cord and autonomic regions, thereby altering nociceptive processing, pain management, and motor behavior[70]. Descending neural pathways are crucial for the modulation of the sympathetic nervous system's functions which is essential for stress reactions and adaptive behaviors. These projections have dual character, which makes the LC an important hub combining cognitive processes with physiological reactions[70].

1.2.1.3. Norepinephrine Receptors

Norepinephrine (NE) interacts with two primary categories of adrenergic receptors: alpha (α) and beta (β) adrenergic receptors. The α-adrenergic receptors are categorized into subtypes α1, and α2, whereas the β-adrenergic receptors are distinguished into β1, β2, and β3 subtypes[71]. G-protein coupled receptors (GPCRs) play a crucial role in modulating neuronal excitability and neurotransmitter release by transducing signals via intracellular second messengers, notably cyclic adenosine monophosphate (cAMP) and inositol trisphosphate (IP3) pathways[71]. When NE is present, α1 receptors usually mediate excitatory effects that increase cellular activity and promote vasoconstriction, while α2 receptors primarily act as inhibitory autoreceptors that control NE signaling and reduce NE production. β-adrenergic receptors impact learning and memory by improving synaptic transmission and promoting long-term potentiation (LTP)[72,73].

The characteristics of the NE system elucidate the function of the LC in promoting arousal and wakefulness: in states of alertness, increased norepinephrine release amplifies

cortical neuron excitability, leading to EEG desynchronization, which is a hallmark of alertness[74,75]. Conversely, during sleep or times of reduced arousal, the activity of the locus coeruleus diminishes, promoting synchronized EEG patterns that indicate relaxation or sleep[74]. This delicate interplay between neurotrophic activities and NE receptor activation highlights the LC-NE system's crucial involvement in modulating cognitive functions required for adaptive behavior, maintaining awake, and enabling arousal.

1.2.1.4. Neurotrophic Factors

The neurotrophic effects of norepinephrine, particularly its involvement in signal transduction, are noteworthy. Norepinephrine (NE) plays a crucial role in promoting neuronal survival and augmenting neurogenesis, particularly within the hippocampus[76]. It affects the strength and plasticity of synapses by regulating signaling pathways associated with neurotrophic factors. The neurotrophic influence can enhance neuronal connectivity and promote survival in challenging environments, thereby improving cognitive functions such as memory and attention[76,77]. According to present research, norepinephrine from the LC can reduce microglial activation and the synthesis of pro-inflammatory cytokines, therefore reducing neurotoxicity[78].

1.2.1.5. Formation of Neuromelanin Pigment

Neuromelanin is a type of melanin that is dark brown pigmented and has a vital neuroprotective role against oxidative stress, it is found mainly in the Locus Coeruleus (LC) and Substantia Nigra (SN)[79]. The detailed step-by-step process for the creation of NM pigment is shown in Figure 1 (adapted from Zucca et al. 2017 to better explain the details). The process starts by oxidizing catecholamines such as norepinephrine or dopamine (DA), which are closely

related molecules, using Iron (FeIII) in order to get DA-o-quinoine, which in turn goes under three distinct routes. The first one undergoes cyclization, polymerization, and further oxidation to create Eumelanin. The second route is to have a conjugation with protein residues to create protein-DA adducts. And the last route is to react with L-cysteine or Glutathione to produce cysteinyl-DA compounds, which would turn into Pheomelanin after further oxidation. According to the mixed melanogenesis model, the last two routes are faster than the first one and thus produce more protein-pheomelanin which will be coated with eumelanin. This would produce an insoluble and undegradable pigment that is fused with lysosomes and autophagic vacuoles which contain mainly lipids and proteins, thus forming the neuromelanin organelle which continues to accumulate as people age[79] and cannot be removed unless neurons degenerate after which can be broken down and removed by microglia[79].

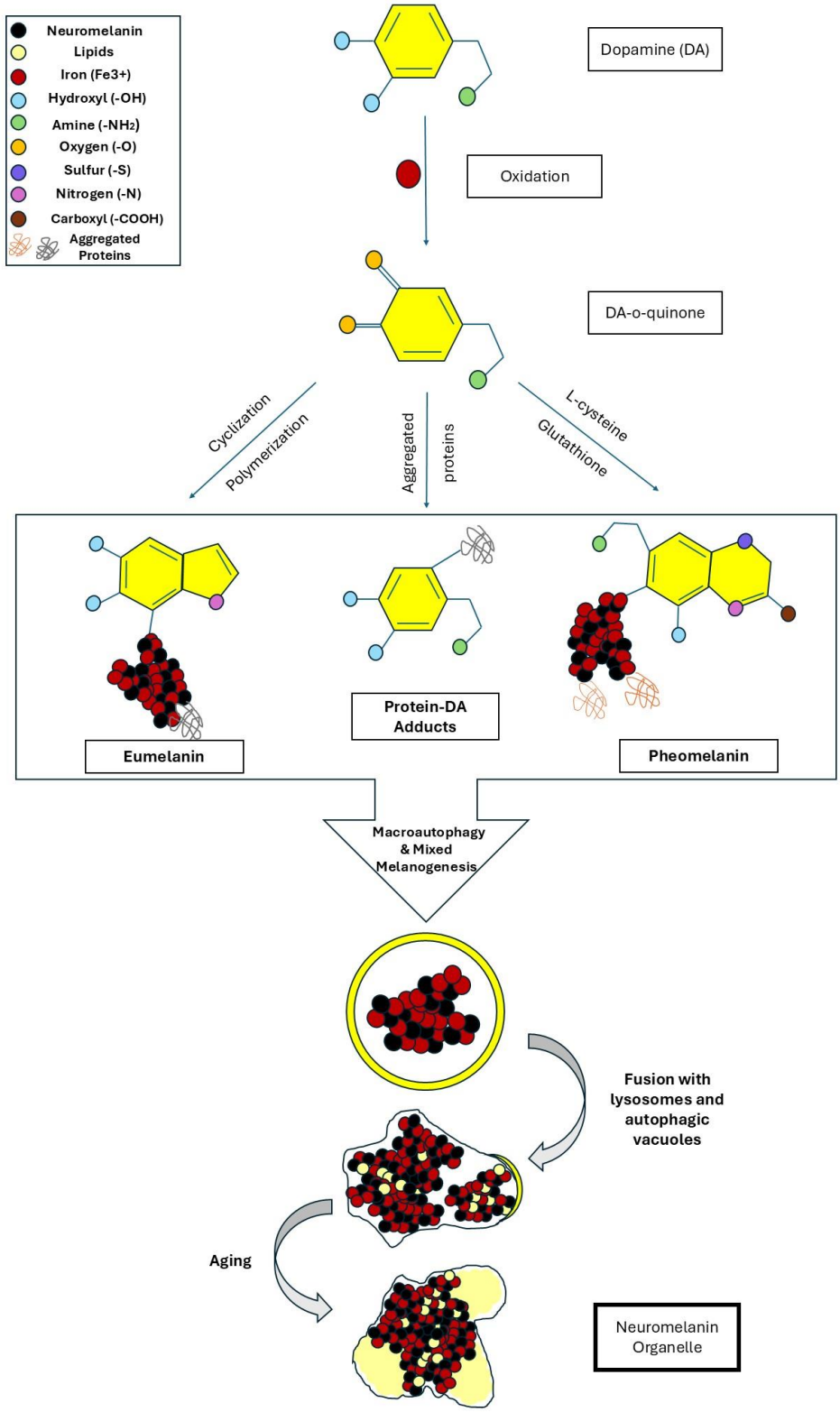

Figure 1. *Step-by-step Synthesis Process of Neuromelanin Organelle*

1.2.2. The functional relevance of the Locus Coeruleus in cognitive processes

1.2.2.1. Arousal, Attention, and the LC-NE system

The locus coeruleus is fundamental in the modulation of arousal and attention by regulating norepinephrine levels across the brain. The LC shows high-frequency phasic firing under periods of enhanced vigilance or stress, which releases bursts of norepinephrine, improving cognitive processing and enabling quick responses[80]. Conversely, low-frequency tonic firing preserves baseline arousal, which is essential for keeping attention over extended lengths of time[67].

The activation of the LC optimizes the brain's ability to respond to salient stimuli, thereby facilitating both involuntary and voluntary attentional mechanisms, by increasing general arousal levels[81]. Tonic LC activity increases the responsiveness of neuronal networks connected to attention and alertness, enhancing the ability to process incoming sensory information and engage in cognitive tasks[82]. Moreover, neurodegenerative diseases like Alzheimer's disease, where age-related LC degeneration can impair attention and higher cognitive abilities, have been linked to disruptions in the LC-NE system[83].

Furthermore, neuroimaging and physiological measurements are required to better understand the link between arousal and attention. Recent advances in event-related potential studies have revealed links between phasic arousal and neural correlates of attention allocation, emphasizing how the LC's modulation of attention is dependent on its ability to adjust arousal levels in response to both internal and external cues[81]. This dynamic interplay is important when considering how LC integrity predicts cognitive performance, where impaired norepinephrine signaling, particularly in the context of neurodegenerative diseases such as

Alzheimer's and Parkinson's disease, is associated with attention deficits and cognitive decline[83,84].

DSP-4, a neurotoxin that impairs LC-NE signaling, has been demonstrated to influence behaviors associated with neurodegenerative symptoms and cognitive impairments, underlining the system's significance in mood regulation and cognitive performance[85]. Furthermore, the LC-NE system's ability to adaptively manage blood flow and oxygen demand under heightened arousal highlights its crucial role in preserving cognitive efficiency and neuronal health, especially in age-related or pathological cognitive decline86. Understanding the LC-NE system has significant implications for creating tailored therapeutic approaches to improve attention deficiencies in Alzheimer's disease and other neurodegenerative illnesses.

1.2.2.2. Novelty detection and memory processing

The locus coeruleus has a vital role in memory processes, especially the encoding of information and consolidation of emotionally relevant information87. In response to new stimuli, phasic activation of the LC stimulates synaptic plasticity in memory-associated areas including the hippocampal region, therefore helping to consolidate long-term memory88.

The capacity of the locus coeruleus to adapt in response to environmental fluctuations contribute to its role in novelty detection. The LC's response to unexpected stimuli appears to be essential for encoding events of significance and enabling quick changes in behavior63. Apart from consolidating memory, this process has been shown to be facilitated through heightened noradrenergic transmission to hippocampus and amygdala, which enhances emotional tagging89.

1.2.3. LC-NE system in Animal Models

The functional relevance of the locus coeruleus and its involvement in a sequence of cognitive and physiological processes has been greatly clarified by animal models. Rodent studies have shed important light on the function of LC activation in memory consolidation, attention, arousal, and stress responses[90,91]. Using optogenetic stimulation, pharmacological modification, and lesion studies among other experimental approaches, scientists have demonstrated how variations in LC activity influence behavior and cognitive ability[92].

1.2.3.1 LC Activation and Cognitive Improvement

One very interesting result of studies on the locus coeruleus (LC) in animal models is the support of cognitive processes provided by focused stimulation. Particularly in demanding activities requiring constant attention, studies employing optogenetic techniques have demonstrated that selective activation of LC neurons is linked to enhanced attentional functioning and memory consolidation[90]. Increased norepinephrine levels underlie the facilitation of synaptic plasticity and long-term potentiation (LTP), both of which are crucially important in the storage of memories. These effects of LC stimulation are most obviously evident in the hippocampus [90].

pharmacological stimulation of LC function using adrenergic agonists has also shown positive effects on cognitive ability. Particularly in learning and memory paradigms, norepinephrine injection or pharmacological enhancement of noradrenergic transmission has been proven to specifically improve performance on tasks[91]. These investigations confirm the theory that LC-evoked norepinephrine release is a crucial control of cognitive enhancement, particularly in conditions requiring high alertness or quick decision-making.

1.2.3.2 Stress-induced cognitive decline and LC hyperactivity

However, elevated LC-NE function does not always provide a physiological benefit. Extended chronic stress has been demonstrated to induce hyperactivity in the locus coeruleus (LC), which increases norepinephrine release and thereby induces receptor desensitization. Particularly with regard to memory and attention, this hyperactivated condition has been related to deficits in cognitive function89. Longterm LC stimulation—which simulates stress—has been shown in studies utilizing animal models to result in cognitive impairment. These findings imply that, whereas prolonged hyperactivity may have deleterious effects, acute activation may enhance cognitive ability93.

Furthermore, animal models of stress have shown that LC hyperactivity is linked to decreased learning90 and more anxiety-like behaviors. This phenomenon probably reflects a maladaptive reaction whereby the constant norepinephrine release finally disturbs brain circuits in charge of balanced cognitive processing. Therefore, therapeutic strategies aimed at reducing stress-related cognitive impairment seek to control LC activity without causing hyperactivity90.

1.2.3.3 Models of Neurodegenerative Disease and LC Dysfunction

Particularly in models of Alzheimer's and Parkinson's disease, studies including animal models have been crucial in clarifying the degradation of locus coeruleus neurons in neurodegenerative disease and allow investigation of the mechanisms and consequences of LC degeneration on other pathophysiological processes and behavior. Reflecting the human patient patterns, some transgenic mice used to model AD show a significant loss of LC neurons94. Reduced levels of norepinephrine in such model systems correspond with significant deficits in spatial memory and attentional performance. Treatments targeting either LC integrity or

norepinephrine levels have successfully ameliorated cognitive impairment in animal models, implying possible treatment approaches for human neurodegenerative illness94.

The TgF344-AD rat model is a transgenic animal model that expresses mutant human APP and PS1 genes. This model recapitulates both amyloid and tau pathology and shows early tau accumulation in the LC prior to its spread to the hippocampus and entorhinal cortex[91]. Quantification of CP13+ phosphorylated tau in the LC, mEC, and hippocampus at 6 and 16 months confirms a progressive pathology, with significantly increased tau burden in TgF344-AD rats compared to wild-type controls. This study also showed the anatomical progression of p-tau and Aβ pathology with age, supporting the LC's role as a potential initiator of tau propagation. This model reflects early-stage tau-related changes prior to overt neurodegeneration, and is well-suited for mechanistic studies investigating LC-origin tau seeding and noradrenergic dysfunction in AD-like progression[91].

1.2.3.4 Therapeutic Strategies in Animal Models

Correcting cognitive impairment by pharmaceutically targeting the LC-NE system has shown encouraging results in animal models. Agents raising noradrenergic transmission—that is, those of adrenergic agonists and norepinephrine reuptake blockers—have shown improvements in attentional as well as mnemonic function92. Promising first results in preserving cognitive status in neurodegenerative models have also come from gene therapy targeted at re-establishing LC neuron activity94. The APP/PS1 mouse model is a well-known example of a model that mimics many of the alterations that are observed in the brain of people who have Alzheimer's disease (AD).

Absence of a preclinical model that faithfully replicates early tau accrual in LC, loss of LC innervation, and related behavioral deficits have hindered mechanistic insights and therapeutic development. Thus, researchers started using the TgF344-AD transgenic rat model, which expresses mutant human amyloid precursor protein (APP) and presenilin-1 (PS1), for histological and behavioral markers of LC dysfunction analogous to early AD. In these rats, hyperphosphorylated tau appears in the LC before its presence in the entorhinal cortex or hippocampus and correlates with reduced noradrenergic innervation in these regions. Progressive loss of norepinephrine and LC fibers was observed without significant LC neuron loss. In vitro, LC neurons expressing mutant tau showed reduced neurite length despite maintained viability, linking early tau pathology to structural degeneration. Behaviorally, TgF344-AD rats exhibited impaired cognitive flexibility, which was restored by chemogenetic LC activation via designer receptors exclusively activated by designer drugs (DREADDs)95. These findings support TgF344-AD rats as a robust model for early LC pathology in AD and highlight a promising therapeutic window targeting the LC-NE system95. Another study showed that α_{2A} adrenergic receptor activity is increased in the AD animal model compared to healthy ones96. Having an in vivo treatment to block this receptor decreases Aβ-induced glycogen synthase kinase 3β (GSK3β) activation and tau hyperphosphorylation, and as a result, it enhances cognitive function in AD mouse models and ameliorates AD-related pathological changes96.

Furthermore, animal models have proved crucial in evaluating lifestyle modifications that can help to slow down the deterioration of the locus coeruleus. Exercise and living in enriched conditions have proved to be helpful for LC neuron survival and norepinephrine retention, thereby enhancing cognitive resilience91. These results imply that in the face of aging and

disease, pharmacological as well as non-pharmacological treatments could perhaps offer protective advantages for LC functioning and support cognitive processes.

Thus, animal models offer priceless insights into the functional dynamics of the LC and its role in cognition and neuroprotection. Experimental manipulation of LC activity has advanced our knowledge of how noradrenergic modulation affects stress adaptation, memory, and attention. Translation of these discoveries into practical applications aiming at maintaining LC integrity and cognitive health depends on ongoing research in animal models.

1.2.4. The LC in neurodegenerative diseases and healthy aging

1.2.4.1. LC Aging and Integrity

The aging process entails a slow decrease in locus coeruleus neuron functionality as well as density. Reduced LC contrast in elderly people has been observed by neuroimaging studies; evidence of this points to neuronal death and lowered norepinephrine production97. These losses are linked to deficiencies in attention, memory, and executive function, so LC integrity presents a good biomarker for age-related cognitive decline98.

1.2.4.2. Evidence Connecting Pathology of Alzheimer's Disease and Cognitive Decline to Early Locus Coeruleus Degeneration

Strong evidence points to degeneration of the locus coeruleus (LC) in AD, implying that LC dysfunction may represent a potential clinical biomarker94. Early degeneration is associated with low norepinephrine levels in relevant brain regions such the hippocampal and cortical regions, which are critical for the consolidation of memory and executive function99.

Neuropathological studies show the presence of neurofibrillary tangles (NFTs) made of hyperphosphorylated tau proteins in the LC, clearly identifiable even in the preclinical stages of Alzheimer's disease. According to postmortem work, The LC accumulates tau before such pathology is spread into the entorhinal cortex, hippocampus, or any other brain region 99,100. Also, preceding to medial temporal lobe tau accumulation, there is confirmed LC integrity changes happening, suggesting that initial tau spreading originates from the LC and it starts seeding tau elsewhere through its neuronal projections100. This finding reveals the LC's selective vulnerability to AD tau pathology underscoring the relevance of a detailed understanding of LC pathology in AD.

Reduced levels of arousal and cognitive flexibility follow from compromised noradrenergic innervation of the cortex and hippocampal tissue resulting from neuronal loss in the LC. Thus, the disturbed norepinephrine signaling of the impaired LC has been connected to problems in attention control, memory loss, and increased sensitivity to stress101. Daily functioning depends on these cognitive abilities, hence, their loss seriously reduces the quality of life of those suffering from Alzheimer's disease.

A recent neuroimaging study implies that subjects displaying reduced integrity of the locus coeruleus, as measured by neuromelanin-sensitive magnetic resonance imaging (MRI), show a faster cognitive deterioration and exhibit increased accumulation of amyloid-beta and tau pathology98. Furthermore, postmortem studies show that LC degeneration is consistently linked to cognitive impairment and tau burden in the cortex99.

Apart from direct neuropathological data, investigations using animal models have revealed that lesions of the locus coeruleus cause lower cognitive capacities, which are

suggestive of the early memory loss usually connected to Alzheimer's disease91. The models also imply a higher buildup of amyloid-beta plaques following disturbance of LC function, implying that LC degradation can not only aggravate but also initiate amyloid-related pathologies94.

Human postmortem studies also corroborate the LC's early involvement in tau pathology. Based on histological scoring of tau severity in rostral, middle, and caudal LC segments, this study shows that tau pathology increases significantly with advancing Braak and Braak stage[94]. However, no significant differences were found along the rostrocaudal LC axis, suggesting uniform vulnerability across LC subregions. These findings were derived from aged human donors with varying degrees of AD pathology, reinforcing that LC tau accumulation occurs even in early or preclinical stages. This histological data adds important context to the interpretation of NM-MRI signal changes, helping to validate imaging biomarkers against cellular-level pathology[94].

1.2.5 Noradrenergic Hypothesis of Alzheimer's Disease

According to the noradrenergic theory of Alzheimer's disease, primary causes of the disease's development are degeneration of the locus coeruleus (LC) and consequent lack of norepinephrine. Not only does norepinephrine help to sustain arousal and attention, but it also modulates neuroinflammatory processes101. Degeneration of the LC might thus set off an unregulated inflammatory reaction that aggravates neuronal damage and accelerates cognitive decline78.

The fact that norepinephrine depletion aggravates the inflammatory response in animal models of Alzheimer's disease supports this notion even more; nonetheless, stimulation of

noradrenergic signaling has been shown to reverse cognitive deficits and lower amyloid deposition102. Thus, interventions meant to maintain the integrity of the locus coeruleus or to increase norepinephrine signaling could have potential in slowing down disease progress and improving cognitive results102.

Finally, mounting data emphasizes the important role that early LC degradation plays in the development of Alzheimer's disease. Both neuropathological and experimental findings point to the loss of LC neurons as a trigger for later amyloid and tau disease, hence aggravating cognitive decline95,100. More study is required to clarify the processes by which LC dysfunction fuels AD progression and to create focused treatments meant to maintain LC integrity and minimize cognitive loss.

1.3. Importance of NM-MRI LC Imaging and Automated Segmentation

Human neuroimaging has emerged as a critical technical advancement in understanding AD pathophysiology, considerably improving our ability to visualize and define the complex brain changes associated with this neurodegenerative disorder. Conventional neuroimaging modalities, such as structural magnetic resonance imaging, functional MRI, and positron emission tomography, have been instrumental in elucidating the anatomical and functional alterations linked to Alzheimer's disease, thereby aiding in early diagnosis and monitoring disease advancement103–105. These imaging modalities enable researchers to investigate critical biomarkers, including amyloid beta deposition and tau tangles, which are closely associated with cognitive impairment in Alzheimer's disease patients106,107.

Despite the invaluable insights derived from these traditional methodologies, substantial gaps persist in the investigation of neuroimaging correlates that could enhance knowledge and

prognostic capabilities for Alzheimer's disease, especially for the locus coeruleus-norepinephrine (LC-NE) system. This system, has not been thoroughly examined in relation to Alzheimer's disease, although recent research indicates that its degeneration may be associated with neurovascular dysfunction and cognitive decline108,109. The incorporation of machine learning and automation algorithms in neuroimaging applications is still nuanced and offers prospects for enhancing diagnostic criteria and tailoring treatment strategies, highlighting the necessity for more refined methodologies to interpret and analyze the extensive neuroimaging data currently accessible110,111. It is essential to identify and address existing gaps in the pursuit of enhancing outcomes for individuals at risk for AD112,113.

1.3.1. Introduction to MRI and Neuromelanin Imaging Physics

Using the magnetic characteristics of hydrogen nuclei, magnetic resonance imaging (MRI) is a non-invasive imaging method that produces comprehensive anatomical images. MRI's basic idea is found in the interaction of nuclear magnetic moments with a strong external magnetic field114. Because of their magnetic dipole moments, hydrogen nuclei (protons) align in a magnetic field and produce a net magnetization along the field axis115. A radiofrequency (RF) pulse then disturbs these aligned nuclei, leading to their entering an excited state and generating transverse magnetism116.

As the protons relax back to their equilibrium condition, the energy received during this excitation process is then discharged. Two processes underlie this relaxation: transverse relaxation (T2) and longitudinal relaxation (T1), which separately define the decrease of transverse magnetization and the recovery of net magnetism97. The MRI coils gather the

produced RF signals, then process their amplitude and phase to provide highly spatial resolution anatomical images114.

Using variations in T1 and T2 relaxation durations and also magnetization transfer dynamics, neuromelanin-sensitive MRI (NM-MRI) images brain areas high in neuromelanin, including the locus coeruleus (LC) and substantia nigra62. The high iron content of neuromelanin, gives it paramagnetic characteristics which contribute to its unique MRI contrast117. NM-MRI uses the contrast between neuromelanin-rich and neuromelanin-poor areas to improve imaging a tiny nucleus like the LC115.

High-field MRI (3T and 7T), which increases signal-to-noise ratios (SNR) and spatial resolution, has evolved from advances in MRI physics. These developments especially help to visualize small nuclei like the LC, which has a diameter of roughly 1-2 mm118. High-field MRI additionally enhances the contrast between neuromelanin-rich and neuromelanin-poor regions, therefore enabling exact anatomical localization and assessment of LC integrity115.

1.3.2. Neuromelanin-sensitive MRI

Recent advances in MRI technology have transformed our capacity to visualize noradrenergic nuclei, including the LC, and assess its integrity. By their unique contrast characteristics, high-resolution imaging methods including neuromelanin-sensitive MRI have become well-known for their capacity to distinguish between healthy and degenerative LC 114,115. Mostly accumulating in the LC and the substantia nigra, neuromelanin offers a special target for MRI research64,114. Postmortem studies were also used to validate that a reduction in neuromelanin signal is correlated with decreased dopaminergic neuronal populations in PD patients using NM-MRI, showing its ability to monitor AD or PD disease progression119,120.

Additional postmortem data highlights the extent of LC neuronal loss in AD and PD. A study demonstrates a significant (~55–82%) reduction in LC cell density in AD and PD patients relative to age-matched controls[135]. This reduction was quantified using immunohistochemical methods on human brainstem samples and visually confirmed via photomicrographs. Importantly, the population included clinically diagnosed AD and PD patients, enabling clear pathological group comparisons. Such cellular-level validation is critical for interpreting LC signal loss seen in NM-MRI and underlines the transdiagnostic relevance of LC degeneration across neurodegenerative diseases. In line with these findings, a study conducted a stereological analysis of human postmortem brains and demonstrated progressive reductions in both LC volume and neuronal counts across the clinical spectrum of AD, with significant losses evident even at early Braak stages. These observations highlight the vulnerability of the LC at preclinical and prodromal phases and further support its potential as an early-stage biomarker target for in vivo imaging approaches[136].

Research has shown that areas rich in neuromelanin, such as the LC, show particular MRI signal features reflecting their functional condition and neuronal integrity. The contrast shown in NM-MRI is especially related to the concentration of neuromelanin, a consequence of catecholamine metabolism. This approach has shown promise not only in discriminating between the LC and other cortical structures but also in revealing the dynamics of LC neuron health across the lifespan115,121. The LC has been evaluated using advanced imaging modalities, including magnetization transfer imaging at 3T and 7T, which are all considered NM-MRI studies, therefore enabling more exact examination of the integrity of noradrenergic pathways in humans114.

1.3.3. From Manual to Automated Segmentation

Conventional methods of LC segmentation in MRI images have mostly depended on manual segmentation. Time-consuming and prone to inter- and intra-observer variability69, these manual techniques usually entail visual inspection and expertly hand delineated boundaries. Furthermore, lacking standardization, manual segmentation affects data quality and reproducibility, and anatomical precision, which varies depending on different study sites or by several operators119. Large cohort analyses or meta-analyses are difficult to do since this unpredictability and labor greatly reduces the scalability of research.

Manual segmentation is further complicated by the complexity of LC architecture, which is marked by tiny size (about 1-2 mm in diameter) and proximity to adjacent brainstem structures62,114. Consequently, even minor errors in hand delineation can cause appreciable variations in volumetric and structural data122. The development of automated segmentation methods has become a main focus in neuroimaging research to overcome these difficulties.

Using cutting-edge algorithms, automated segmentation techniques localize and precisely define the LC. By means of anatomical landmarks and neuroanatomical atlases to standardize the segmentation process, these techniques aim to reduce human error and improve reproducability122. Moreover, automated methods provide high-throughput data processing, so enabling researchers to effectively examine vast databases and obtain more statistically significant findings69,123.

Often requiring fine-tuning for particular datasets, early automated techniques were limited in their capacity to generalize well across different populations and imaging technologies119. Recent developments, however, have included adaptive algorithms that may

change to fit different image qualities and subject demographics, therefore greatly improving the accuracy and resilience of LC segmentation114.

To guide accurate LC segmentation, histological reconstructions have been used to map the rostrocaudal axis of the LC in postmortem human brains[124]. This study visualized neuromelanin content using high-resolution microscopy, enabling 3D modeling of LC volume across individuals. Such histological atlases provide anatomical ground truth for validating NM-MRI signal localization and segmentation approaches, ensuring more precise extraction of LC metrics across studies. They are especially useful when standardizing across imaging centers or comparing different field strengths (e.g., 3T vs. 7T)[124].

Ultimately, moving from manual to automated segmentation marks a significant advance in the precise and quick evaluation of LC integrity. Particularly in studies involving aging and neurodegenerative diseases114,115, automated methods are probably going to become the gold standard as technology develops since they enable dependable, repeatable, and scalable analysis of LC structure.

1.3.4. NM-MRI and Neurodegenerative Diseases

NM-MRI's possible use as a biomarker in neurodegenerative illnesses is highlighted by newly published data indicating the detection of early LC degeneration. Reduced neuromelanin signal intensity has been linked to cognitive deficiencies and grey matter atrophy in AD, suggesting that this tool is a reliable non-invasive method that should be used more in research124,125. Also, research on patients with Parkinson's disease (PD) has shown that non-motor symptoms including apathy and cognitive decline121,126 are linked to reduction in LC integrity. These results highlight the need to evaluate LC integrity in clinical environments for

not only neurodegenerative illness diagnosis but also for understanding the intricate details of their progression.

1.3.5 Use of LC Imaging in Human Aging and AD Research

MRI LC visualization mostly depends on the neuromelanin NM-related hyperintensity seen in T1-weighted, turbo spin echo (TSE), and magnetizing transfer (MT) sequences. These sequences take advantage of NM's paramagnetic characteristics that accumulate gradually in LC neurons over adulthood79,127. The LC signal shows a distinct trend of increasing until midlife and then falling with age128,129.

Results from cognitively unimpaired older people imply that age-related LC signal decrease might not be benign. Reduced LC signal, particularly in the rostral LC, is linked in multiple studies to poorer memory function, lower cortical thickness, and greater cortical microstructural degeneration122,129,130. Reduced LC signal particularly corresponds with greater levels of plasma phosphorylated tau (pTau), a hallmark of AD pathology, therefore underlining the idea that LC degeneration in aging may communicate early pathogenic processes rather than physiological decline131.

LC-MRI studies consistently show reduced LC signal in people with mild cognitive impairment (MCI) and AD dementia compared to healthy controls132,133. Supporting LC-MRI as a possible prognostic marker, longitudinal data show that MCI patients with lower baseline LC signal are more likely to advance to AD dementia132.

In human in vivo imaging studies, NM-MRI signal from the LC has been linked to tau burden using PET tracers. Another study used longitudinal NM-MRI and tau PET imaging to show that lower LC integrity (measured as decreased NM-MRI signal) precedes medial temporal

lobe tau accumulation by approximately three years, as measured by standardized uptake value ratios (SUVRs) using the tau-specific tracer [^18F]flortaucipir (AV-1451). This tracer binds paired helical filament tau aggregates, thereby reflecting the regional burden of neurofibrillary tangle pathology. Crucially, this study demonstrated that LC-related tau spread followed a topographical pattern consistent with Braak staging and was associated with subsequent cognitive decline. These results come from cognitively unimpaired and MCI participants in the DIAN or ADNI cohorts, emphasizing the utility of LC signal as a surrogate marker for early tau pathology[100]. Notably, correlations with tau deposition were stronger than those seen for amyloid PET, aligning with neuropathological evidence suggesting the LC is more directly involved in tau propagation. The inclusion of large human cohorts enables stratified analysis and strengthens generalizability, though diverse racial and ethnic representation remains limited in such samples.

LC signal may be more tightly correlated to tau than amyloid measurements. For the entorhinal and temporal cortices, LC signal negatively correlates with tau PET levels, for instance; amyloid correlations seem more diffuse and indirect125,134. LC signal predicted future tau accumulation independent of amyloid load in autosomal dominant AD individuals, implying that LC-MRI could act as a surrogate for tau pathology131.

Beyond structural connections, LC integrity has been associated with several cognitive and behavioral traits of AD. Lower LC signal has been linked to poorer memory, attention, and executive function132,135–137. Furthermore, LC signal is related to neuropsychiatric symptoms and circadian rhythm disturbances because of its function in arousal and behavioral control125,130.

Finally, important new perspectives on the function of the noradrenergic system in aging and AD are offered by LC imaging using MRI. Evidence points to LC degeneration, observable in vivo, as not just a first sign of AD but also a possible cause of tau pathology and cognitive loss. Therefore, LC-MRI is not only a useful tool in AD research but may also have potential clinical application as a biomarker for early identification, risk assessment, and therapy monitoring in AD.

1.4 Aims and Hypotheses

This Ph.D. thesis is divided into 3 principal aims and hypotheses.

Aim 1:

To evaluate the accuracy and utility of the automated LC segmentation method developed by our group for assessing locus coeruleus (LC) integrity from neuromelanin-sensitive MRI (NM-MRI), in comparison to gold-standard manual segmentation and other methods.

Hypothesis 1:

We hypothesize that the FT method will demonstrate strong concordance with manual segmentation across multiple validation metrics—including signal contrast-to-noise ratio (CNR), test–retest reliability (ICC), and spatial agreement (DICE coefficient)—and will be as effective capture AD-related LC degeneration as alternative manual segmentation methods.

Aim 2:

To investigate the loss of LC integrity over time as measured with our segmentation method in older adults across the AD spectrum.

Hypothesis 2:

We hypothesize that LC integrity would decrease to a greater extent over time in AD participants compared to cognitively normal older adults.

Aim 3:

To examine the longitudinal relationship between LC integrity and cognitive performance across multiple domains in early and late stages of Alzheimer's disease, as well as in healthy aging.

Hypothesis 3:

We hypothesize that LC integrity will be positively associated with cognitive function in domains linked to noradrenergic function, including executive function, logical memory, and novel object recognition. While in healthy aging, LC signal is expected to show minimal association with cognition, consistent with preserved LC integrity in this group.

Chapter 2. Methods

2.1. Methods for Aim 1

2.1.1 Participants and clinical measures

The first study sample consisted of 190 participants from the community or outpatients at the McGill University Research Centre for Studies in Aging were enrolled in the Translational Biomarkers of Aging and Dementia (TRIAD) cohort138, McGill University, Canada. Clinical and demographic characteristics of the sample are shown in Table 1a. The cohort participants had a detailed clinical assessment, including the Clinical Dementia Rating Scale (CDR) and Mini-Mental State Examination (MMSE). Cognitively unimpaired participants had no objective cognitive impairment and a CDR score of 0. Mild cognitive impairment (MCI) individuals had subjective and objective cognitive impairment, preserved activities of daily living, and a CDR score of 0.5. Patients with mild-to-moderate sporadic Alzheimer's disease dementia had a CDR score between 0.5 and 2 and met the National Institute on Aging and the Alzheimer's Association criteria for probable Alzheimer's disease determined by a physician139. Participants were excluded if they had other inadequately treated conditions, active substance abuse, recent head trauma, or major surgery, or if they had MRI/PET safety contraindication.

The second and third study samples, used for aim 1, consisted of healthy individuals enrolled from the community (Sample 2: n=12, age=27.1±2.8 years, n=4 male, 8 female; Sample 3: n=30, age=42.1±16.2 years, n=16 male, 14 female). Study procedures were approved by the Douglas Institute Research Ethics Board (Sample 1) and the University of Ottawa Research Ethics Board (Samples 2 and 3). All participants provided written informed consent140.

Table 1a. Demographic characteristics of the sample of older adults (Aim 1)140

Age (n=190), mean (SD), y	71.42 (7.0)
Male (n=190), No. (%)	70 (36.85)
CN (n=190), No. (%)	118 (62.11)
AD (n=190), No. (%)	28 (14.74)
MCI (n=190), No. (%)	44 (23.16)
CDR score (n=188), mean (SD)	0.2 (0.37)
MMSE score (n=187), mean (SD)	27.74 (3.78)
Tau-positive (n=190), No. (%)	56 (29.47)
Braak stage 0-1 (n=160), No. (%)	92 (57.5)
Braak stage 2-3 (n=160), No. (%)	27 (16.88)
Braak stage 4-6 (n=160), No. (%)	41 (25.62)

2.1.2. Image acquisition

Neuroimaging data for Sample 1 were acquired at the Montreal Neurological Institute (MNI). Magnetic resonance (MR) images were acquired on a 3T Prisma scanner. NM-MRI images were collected via a turbo spin echo sequence with the following parameters: repetition time (TR) = 600 ms; echo time (TE) = 10 ms; flip angle = 120°; turbo factor = 4; in-plane resolution = 0.6875 × 0.6875 mm2; partial brain coverage overlaying the pons and midbrain with field of view = 165 × 220; number of slices = 20; slice thickness = 1.8 mm; number of averages = 7; acquisition time = 8.45 min. Whole-brain, T1-weighted MR images (resolution = 1 mm, isotropic) were acquired using an MPRAGE sequence for preprocessing of the NM-MRI and PET data. Quality of MRI images was visually inspected for artifacts immediately upon acquisition, and scans were repeated when necessary, time permitting140.

Neuroimaging data for Sample 2 and Sample 3, were acquired at the Brain Imaging Centre of the Royal Ottawa Institute for Mental Health Research on a 3T Siemens Biograph MR-PET scanner. For Sample 2, NM-MRI images were collected via a 2D gradient-recalled echo sequence with magnetization transfer pulse (2D-GRE with MT) sequence with the following parameters: repetition time (TR)=685 ms; echo time (TE)=3.97 ms; flip angle=50°; in-plane resolution=0.639 × 0.639 mm^2 ; partial brain coverage with field of view (FoV)=166×224; matrix=260×352; number of slices=18; slice thickness=2 mm; slice gap=0 mm; magnetization transfer frequency offset=1,200 Hz; number of excitations (NEX)=5. Whole-brain, T1-weighted MR images (resolution=1 mm, isotropic) were acquired using an MEMPRAGE sequence. The 2D-GRE MT sequence was acquired twice for all participants within the same hour and subjects were asked to get on and off the scanning table to reposition their head between the test and retest scans. Sample 3 protocol included a 2D-GRE sequence (very similar to that used in

Sample 2 but with 24 thinner (1.5 mm) slices), a TSE sequence (very similar to the sequence used in Sample 1), and the same MEMPRAGE sequence as Sample 2. Immediately after acquisition, quality of MRI images was visually inspected for smearing of banding artifacts affecting the midbrain or pons and scans were repeated when necessary, time permitting140.

2.1.3. Manual LC segmentation

We followed a commonly used protocol for manual LC segmentation101,118,127,141. This is a 2D segmentation method that localizes the LC on a single axial slice. Using MRIcron software for visualization, the LC was found by two trained raters (A.S., R.G.) on an axial slice 9 mm under the inferior colliculus (Sample 1; for sample 2 the distance was slightly different, 8 mm, due to a change in slice thickness). On this slice, the LC was defined on the left and right sides as a 5-voxel cross covering hyperintense voxels near the 4^{th} ventricle. In cases of discordance between raters, consensus was obtained between the raters and C.M.C. for a final mask. Contrast-to-noise ratio (CNR) was calculated using the same method as for the funnel tip segmentation (Section 2.4; for all LC segmentation methods the reference region was segmented in the same automated manner in order to isolate the impact of variability of LC segmentation on LC metrics by avoiding variability in measurement of the reference region signal). The LC signal values were calculated by averaging CNR values for all voxels under the mask. LC signal from the manual masks from the 2 raters prior to consensus showed excellent agreement, ICC=0.86 (within the range of interrater agreement reported previously for manual segmentation, ICC ranging from 0.84-0.98129,142). Three versions of the manual mask were generated, one retaining all 5 voxels per side, one with 4 voxels per side (dropping the voxel of lowest intensity in order to match the size of the LC mask generated by the automated method) and one with only a single, peak-intensity voxel per side (Figure 3). These smaller masks were generated in part

because the in-plane resolution of our images was lower than that of some prior NM-MRI studies[128,130], and therefore some voxels under a 4-voxel mask would be expected to show partial volume effects. We assumed partial volume effects would be minimal in the case of the peak-intensity voxel[143].

2.1.4. Automated LC segmentation

LC signal was measured using a semi-automated algorithm[146] incorporating steps similar to those described in previous studies[147,148]. This method performs an intensity-threshold-free cluster search within an overinclusive mask of the LC in native space. For simplicity we refer to it as a 'funnel tip' (FT) method, see Figure 2 for summary of the steps in the algorithm. Although LC signal is measured on native-space NM-MRI images, it is necessary to spatially normalize the NM-MRI images in order to register an overinclusive LC mask (referred to as the LC search mask) from MNI space to native space for each participant. Initial preprocessing steps were performed using ANTs software. To bring the NM-MRI image of each participant into standardized space, T1-weighted images were normalized to MNI152 space (MNI152NLin2009cAsym; 1 mm isotropic resolution), then NM-MRI images were coregistered to the T1-weighted images, and finally these two transforms were applied to the NM-MRI images. A visualization template (Figure 2) was created by averaging the spatially normalized NM-MRI images from all participants[143].

Subsequent steps used custom MATLAB scripts. An LC search mask was drawn over the MNI-space visualization template to cover the LC, defined as the hyperintense voxels at the anterior-lateral edge of the 4th ventricle spanning 15 mm in the rostrocaudal axis (from MNI space coordinates z= -16 to -30, see Figure 2). The rostrocaudal limits were set based on the

position of the LC from a brainstem atlas[149] and cell counting work[150], spanning from the inferior colliculus to the posterior recess of 4th ventricle, while excluding the extreme rostral and caudal ends to minimize edge effects. The mask was divided into 5 rostrocaudal sections of equal length (3 mm). The full LC search mask and the 5 mask sections were then warped to native space using the inverse transformation generated in the spatial normalization step and resampled to NM-MRI image space. This warped LC search mask defined a search space wherein to find the LC for each participant. A cluster-forming algorithm was used to segment the LC within this space, defined as the 4 adjacent voxels (total area=1.96 mm^2) on each side and axial slice with the highest mean signal. The automated segmentation was visually inspected and was found to perform some operations suboptimally, requiring manual correction (error rate Sample 1=1.2%, error rate Sample 2=4.6%, error rate Sample 3 MT=4.6%, TSE=4.6%). Manual corrections were performed if the automatically selected voxels appeared to be within a hyperintense artifact occasionally present within the bottom slices of the 4th ventricle or if they were far from the expected location of the LC based on anatomy (edge of 4th ventricle) and its position on adjacent slices (this issue most commonly occurs on the rostral and caudal ends where LC neurons are more scattered[150]). In most of these cases the LC was redrawn in a probable position near the edge of the 4th ventricle and in rare cases the LC mask was excluded from the slice if the hyperintense artifact appeared to obscuring the LC itself[143]. CNR for each voxel *v* in a given axial slice was then calculated as the relative difference in NM-MRI signal intensity *I* from a reference region *RR* in the same slice as:

$$CNR_{\mathrm{v}} = \frac{(I_v - mode(I_{RR}))}{mode(I_{RR})}$$

We selected a reference region used in our prior work[146,151], the central pons (Figure 2[20]), defined by a circle of radius 11.6 mm, centered on the midline, 32.6 mm anterior to the LC[143]. It was selected, by our group and other groups[128,152], as well since it has a close proximity to the LC and it is in the same axial slice throughout the full rostrocaudal extent of the LC. Also, it is considered large and contains relatively little signal variability, which facilitates estimation of signal from the structure and reduces the influence of noise. Thus, every LC-containing axial slice was linked to one of the 5 rostrocaudal LC sections based on which of the 5 sectioned LC masks was present on that slice (if 2 sectioned masks were present on the same slice, the LC section was defined for each side by the sectioned mask covering the most LC voxels). LC signal was calculated for each of the five sections by averaging CNR values from all LC voxels within the section (4-voxel version) or only the peak-intensity voxels from each side and slice within the section (peak-intensity voxel version). Each section covered between 1 and 2 slices in native space. For instance, for the middle LC section, 53% of cases had two slices assigned, 47% of cases had 1 slice assigned, and no cases were missing the section entirely[143].

In order to compare the FT (3D) method to the manual (2D) method, it was necessary to determine in which of the rostro-caudal LC sections from the FT method that the manual mask tended to be located. For 66.5% of participants, the manual mask fell in the middle LC section, for 27.7% in the mid-caudal section, for 5.0% in the mid-rostral section, for 0.8% in the extreme-caudal section, (see Figure 2D). Therefore, all analyses using the FT method (excepting those described in Section 2.5) retained only the LC signal from the middle section (MNI coordinates z=-22 to -24). Conveniently, the middle LC, has shown the greatest signal loss seen in AD in some studies[146] (though some studies have found the rostro-middle portion most affected[136,153]).

Finally, an alternative automated LC segmentation was applied using the conventional approach of applying a binary mask of the LC in standardized space NM-MRI images warped to standardized space (no smoothing applied). To better match to the other segmentation methods, only the portion of the standardized space mask covering MNI coordinates z=-22 to -24 (the middle LC segment defined with the FT method) was retained. One binary mask was taken from a prior publication[144] (standardized space mask 1, SS 1; Rigid and affine transformations in ANTs with nearest-neighbor interpolation brought the mask to MNI152NLin2009cAsym 1mm space.), and one was generated from our own dataset by thresholding the visualization template at CNR>11% (standardized space mask 2, SS 2; see Figure 3). The average of peak voxels from the left and right sides on all 3 slices was extracted for both masks and used in subsequent analyses[143].

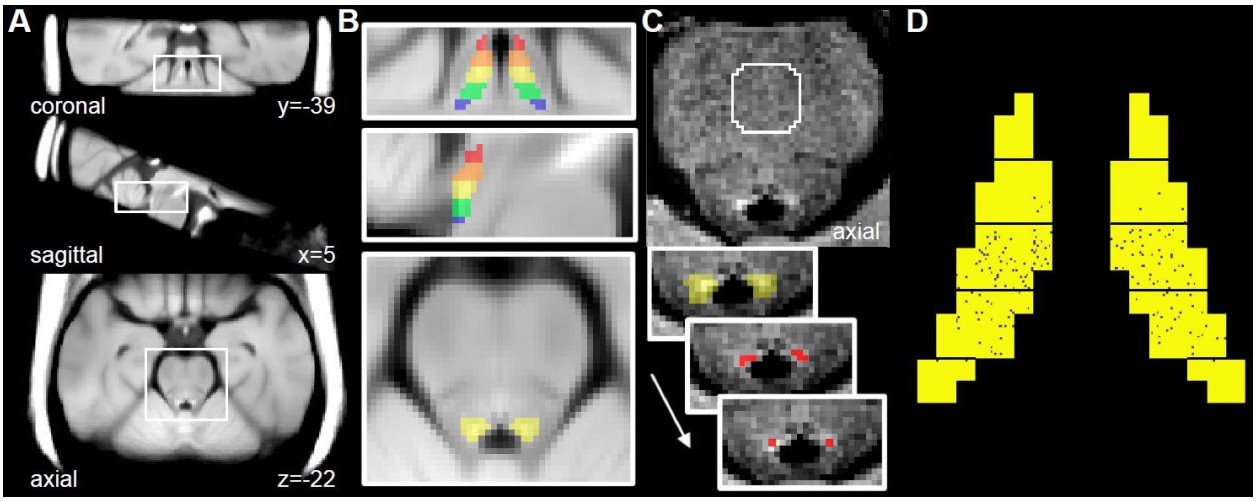

Figure 2. *LC segmentation via FT method. A: visualization template in MNI space created by averaging the spatially normalized NM-MRI images from participants in Sample 1. B: magnified views of the visualization template with the LC search mask overlaid. This mask was manually traced on the visualization template over the hyperintense region surrounding the LC and divided into five sections (displayed in different colors), each spanning 3mm in the z-axis. C: unprocessed NM-MRI image showing the pons of a representative individual; the central pons reference region is encircled in white. Contrast-to-noise ratio for all voxels was calculated relative to signal extracted from this region. The LC search mask (yellow, signifying the middle section) was deformed from MNI space to native space to provide a search space wherein the LC was identified on left and right sides as the four adjacent voxels with highest signal contrast. The peak-intensity voxel was then identified from these. D: Variability in manual LC mask position within the sections of the FT mask. Each black speck represents the position of the manual LC mask from a single participant from Sample 1. The greatest proportion of manual LC masks were located in the middle LC section so this section was selected when comparing to the manual mask*[143].

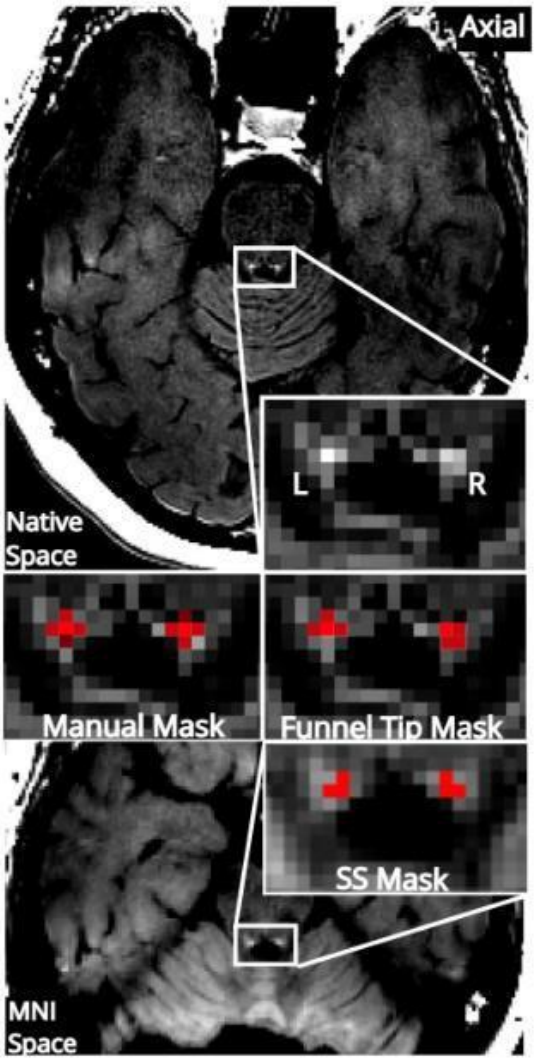

Figure 3. *Three different LC segmentation approaches. NM-MRI image from a representative participant is shown in native space (top) and standardized MNI space (bottom). Magnification around the fourth ventricle shows LC segmented using a manual approach, the funnel tip (FT) approach, and a mask in standardized space mask 2 (SS 2; the version created from this dataset is shown). For all subjects, full LC coverage was fixed as 4 voxels per slice (1.8 mm^2 on the left and right). The peak-intensity voxel is shown in bright red on the manual and FT masks. To concord with previous implementations, a 5-voxel version of the manual mask was created and the lowest-intensity voxel, excluded from the 4 voxel version, is shown in darker red*[143].

2.1.5. 3D reconstruction of LC structure by FT method

The previous tests only assessed the middle portion of the LC; therefore, an additional test was needed to assess the accuracy of the FT segmentation of the LC along its entire rostro-caudal extent. We leveraged the known structure of the LC as a roughly contiguous, rod-shaped structure and examined whether the position of FT-segmented peak-intensity voxels were consistent with a linear shape. Data was collected from 30 participants (Sample 3) scanned with both an 2D-GRE with MT sequence and a TSE sequence and linear fit was assessed for both sequence types[143].

To assess linear fit along the x-dimension, a linear regression was performed with the x-coordinates for peak voxel locations as the dependent variable and the z-coordinates as the independent variable. This was repeated for the y-dimension (y-coordinates as dependent variable and z-coordinates as independent variable) and repeated for the left and right LC. Residuals from these regressions identified FT-segmented LC voxels that were distant from the fit line (outliers). For comparison purposes, the FT mask's linear fit was compared to that of a highly linear mask (the center of the LC search mask) and an inconsistently linear mask (created by permuting LC voxel positions within the LC search mask, 1000 permutations in bootstrapped participants)[143].

2.1.6. PET Acquisition and Analysis

All participants in Sample 1 had [^{18}F]AZD4694 and [^{18}F]MK6240 PET scans acquired to estimate brain levels of Aβ and tau respectively, using a brain-dedicated Siemens high resolution research tomograph. See previous studies for more detailed PET methods[154,155]. For the Aβ tracer, [^{18}F]AZD4694, SUVR values were extracted from a composite set of regions including

the precuneus, prefrontal, orbitofrontal, parietal, temporal, anterior, and posterior cingulate cortices[156]. Aβ positivity (Aβ status) was defined, similar to prior work[157], as SUVR value >1.55 at baseline or at a subsequent time point if [^{18}F]AZD4694 was not available at baseline. SUVR scores from the tau tracer [^{18}F]MK6240 were extracted from predefined ROIs to determine Braak stage, similar to prior work[158]. Tau positive cases were defined as those with SUVR >1.24 in the temporal ROI. Discordant cases (where regional tau burden did not follow the anatomical progression proposed by Braak) were excluded from analyses of Braak stage[143].

2.1.7. Statistical Analysis

Statistical tests were performed on MATLAB software. Intraclass Correlation Coefficient (ICC(3,K)) was used to test agreement between methods and between images. Dice Similarity Coefficient (DSC) was used to determine spatial overlap between LC masks. Linear regression and partial correlations were used to calculate effect-size measures relating LC-signal to clinical and biological measures of AD severity. Scan-rescan variability was calculated using the following equation[143]:

$$\frac{2 * |scan - rescan|}{scan + rescan}$$

2.2. Methods for Aims 2 and 3

2.2.1. Participants and clinical measures

Study participants (n=266) consisted of individuals over 50 years of age from the TRIAD cohort[141] (an expanded version of the sample used in Aim 1 that also included longitudinal data). Participants had a detailed clinical assessment, including the Clinical Dementia Rating Scale (CDR) and Mini Mental State examination (MMSE; for clinical and demographic description of the sample see Table 1b). Cognitively unimpaired participants had no objective cognitive impairment and a CDR score of 0. Mild cognitive impairment (MCI) individuals had subjective and objective cognitive impairment, preserved activities of daily living, and a CDR score of 0.5. Patients with mild-to-moderate sporadic AD dementia had a CDR score between 0.5 and 2 and met the National Institute on Aging and the Alzheimer's Association criteria for probable AD determined by a physician[142]. Participants were excluded if they had other inadequately treated conditions, active substance abuse, recent head trauma, major surgery, or MRI/PET safety contraindication. AD patients did not discontinue medications for this study. The Douglas Institute Research Ethics Board approved this study. All participants provided written informed consent.

Table 1b. Clinical, cognitive and demographic measures

	Aβ-negative (n=148)	Aβ-positive (n=118)	p-value
Age, mean ±SD	70.86 ±6.21	70.76 ±7.07	0.91
Male, No (%)	56 (37.8%)	44 (37.29%)	0.15
CDR, mean ±SD	0.12 ±0.23	0.55 ±0.56	<0.001
Years of Education, mean ±SD	15.76 ±3.56	15.08 ±3.52	0.12
APOE ε4 Carrier (%)	43 (29.1)	83 (70.34)	<0.001
Diagnosis (CN/AD/MCI)	117/3/28	34/40/44	<0.001
Global Cognition (MMSE), mean ±SD	29.08 ±1.53	25.85 ±5.18	<0.001
Object Recognition (BORB), mean ±SD	30.43 ±1.79	28.66 ±3.76	<0.001
Verbal Fluency, mean ±SD	39.64 ±10.32	32.48 ±13.40	<0.001
Executive Functioning (TMT-B), mean ±SD	56.32 ±28.55	37.74 ±29.44	<0.001
Speed of Processing (TMT-A), mean ±SD	52.63 ±29.87	40.76 ±29.32	0.013
Logical Memory (WAIS), mean ±SD	15.33 ±4.84	8.37 ±7.18	<0.001
Working Memory (digit span), mean ±SD	16.32 ±3.94	14.38 ±4.73	<0.001

p-value were from t-tests for continuous variables and chi-square tests for categorical variables.

2.2.2. Image acquisition

The same acquisition has been used as described in Aim 1 above.

2.2.3. PET Acquisition and Analysis

The same acquisition has been used as described in Aim 1 above.

2.2.4. NM-MRI processing

LC signal was measured using a semi-automated algorithm developed by our group (same as the one used for Aim 1); see previous papers for a more complete description of the algorithm and performance of the method in terms of reliability and performance in the context of AD[143,146]. This "funnel-tip" method performs an intensity-threshold-free cluster search within an overinclusive mask of the LC that has been transformed from standardized space to native space. It thereby estimates the signal from the LC at its hyperintense putative "core" on each cross-sectional (axial) slice through the structure. Similar to other algorithms, it calculates contrast-to-noise ratio (CNR) of the LC relative to a central pons reference region, applies an LC search mask on native space NM-MRI images[159] and divides the LC into rostrocaudal sections[147] (we calculated LC signal for 5 sections on the right and left side),

We used a multivariate approach, guided by work in other neuroimaging modalities[160], to generate a single metric of LC integrity that incorporates information from all LC sections and reflects the extent to which an individual's pattern of LC signal across sections is AD-like or healthy. To make this metric, we first carried out a mixed-effects logistic regression analysis with clinical diagnosis of AD as the dependent variable (MCI were excluded) and LC signal from all 10 LC sections as fixed factors and subject as a random factor. The regression

coefficient produced by this analysis for each LC section was saved (see Figure 4) and used to calculate the log of the odds ratio of CN status for each study participant based on their LC signal (this step was applied to all participants including those with MCI). We refer to this log of the odds ratio as the LC $pattern_{CN}$, participants with positive values have greater odds of being CN than AD. Figure 4 shows that the LC pattern linked to CN status is high signal in middle and mid-caudal LC sections relative to signal on the rostral and caudal ends of the LC. Note that LC $pattern_{CN}$ was highly correlated with a simpler LC integrity metric, LC signal averaged from bilateral middle LC sections ($r=0.77$, the middle section was selected because it was the one that was most affected in AD in our prior work in this cohort[143]).

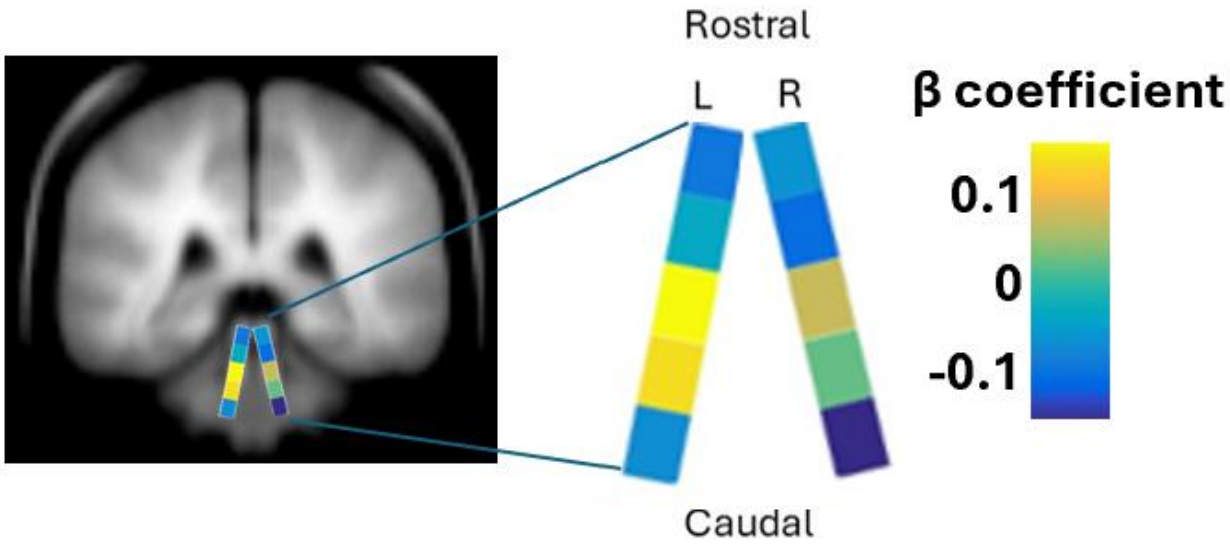

Figure 4. *Schematic map of the LC with colors reflecting coefficients for each LC section derived from a logistic regression with CN status as dependent variable. These coefficients were applied to calculate the log of the odds ratio of CN status for each participant (LC pattern$_{CN}$) the summary metric of LC integrity used for the current study.*

2.2.5. Cognitive Tests

For aim 3 of this doctoral thesis, we used cognitive tests to analyze the cognitive decline in healthy and AD patients such as MMSE, BORB, TMT, WAIS-III digit span test, Wechsler Memory Scale (WMS) logical memory test, and Verbal fluency test (letter and category fluency).

Mini-Mental State Examination (MMSE) is a widely used brief cognitive assessment tool to screen for cognitive impairments, especially in older adults. It evaluates various cognitive functions, including orientation, memory, attention, language, and visuospatial skills. The test consists of a series of questions or tasks that assess different cognitive domains[161]. The MMSE is scored out of 30 points, with each task contributing a certain number of points. higher scores indicate better cognitive function[161].

The Birmingham Object Recognition Battery (BORB) is a neuropsychological test used to assess object recognition abilities in individuals. It's often utilized to evaluate how well someone can identify and discriminate between various objects. The BORB consists matching and identifying objects based on their visual characteristics. performance in object recognition is based on accuracy and response time. The results are then compared to norms [162].

the Trail Making Test (TMT) is a neuropsychological assessment tool that evaluates cognitive functions such as executive function, attention, visual-motor tracking, and mental flexibility. It consists of two parts: Trail Making Test Part A (TMT-A) and Trail Making Test Part B (TMT-B). In TMT-A, participants are asked to connect a sequence of numbers (1, 2, 3, etc.) distributed randomly on a sheet of paper. The goal is to connect the numbers in ascending order as quickly as possible. While in TMT-B, participants are required to connect both numbers

(1, 2, 3, etc.) and letters (A, B, C, etc.) in alternating sequence (1-A-2-B-3-C, etc.). Lower scores on both TMT-A and TMT-B indicate better performance, as faster completion times are associated with more efficient cognitive processing and better attentional control[163].

The WAIS-III Digit Span Test is a component of the Wechsler Adult Intelligence Scale - Third Edition (WAIS-III), a widely used intelligence test to assess cognitive abilities in adults as working memory, attention, and auditory processing speed. The Digit Span Test measures a person's working memory and attention by evaluating their ability to repeat back a sequence of digits in the order they were presented (forward digit span) or in reverse order (backward digit span). The score is based on the longest sequence of digits the participant correctly repeats in either order[164].

Logical memory is a subtest in the Wechsler Memory Scale-IV (WMS-IV). based on two independent stories. In the first part of the test (logical memory I), the two narrative stories are verbally given, and the participants should try to immediately recall the stories as much as they can. In the second part of this test (logical memory II), a free recall for both stories is elicited after a 20-30 minute delay. For every correct detail the participant would score a point. The 30 yes/no recognition questions about these stories are provided subsequently to test the recognition ability[165].

The verbal fluency test is a short test of verbal functioning which has two tasks: category fluency and letter fluency. In this test every participant is given one minute to produce as many unique words as possible within a semantic category (animals, food, drink…) or starting with a given letter (S, R, L…). Then, the score in each task can be calculated by adding the number of unique correct words in each task[166].

2.2.6. Statistical Analysis

Statistical analyses employed linear mixed effects models and robust linear regression implemented in MATLAB software. Our initial analysis examined the impact of time on the LC signal. This linear mixed-effects model employed an LC $pattern_{CN}$ as dependent variable, a random subject factor, and the fixed factors were: time since baseline (time), Aβ status, time × Aβ status, age at baseline, sex, and scan date pre/post covid-19 pandemic onset. The pre/post covid-19 dummy covariate was included in analyses examining time effects on the LC because the pandemic occurred between the baseline and follow up scans of many participants and there is evidence that the LC may be vulnerable to covid-19 infection[167–171]. This analysis was repeated in different subgroups of participants examining the impact of time on LC signal with the same model except for exclusion of the Aβ status and time × Aβ status fixed factors.

Change-over-time metrics were calculated for the following measures: LC $pattern_{CN}$, tau burden in the Braak stage 1 ROI ([^{18}F]MK6240 SUVR), and performance on the object recognition task (BORB score). These change-over-time metrics are denoted by adding a Δ symbol before the variable name. They were calculated by extracting the slope from a linear regression performed for each subject with the measure of interest at all available time points as the dependent variable and the interval of time between assessments as the dependent variable.

The next analysis examined how Aβ and tau burden influence ΔLC $pattern_{CN}$ at the earliest stages of AD. We selected participants who were CN and at Braak stage 0 at study baseline and performed a robust regression to predict ΔLC $pattern_{CN}$ based on Aβ status, Δtau burden (SUVR) in the Braak stage 1 ROI, age, and sex. This analysis was performed with and without an interaction term for Aβ status × Δtau burden.

The next set of analyses examined the impact of LC signal on cognition. These linear mixed-effects models employed a cognitive measure as dependent variable, a random subject factor, and the following fixed factors: LC $pattern_{CN}$, age at study baseline, sex, and time. These were repeated for different cognitive measures and in different subgroups of participants. For the object recognition test (BORB), we also analyzed the correlation between LC change over time and performance change over time. We performed a robust regression analysis with ΔBORB performance as the dependent variable and Δ LC $pattern_{CN}$, age, and sex as dependent variables.

For purposes of visualization, we provide statistical maps displaying the time effect (Figure 8) and correlations to cognition (Figure 10) for all LC sections. These were generated by running the above-described linear-mixed effects regression models for all 10 LC sections.

Chapter 3. Aim 1: Characterization of an automated method to segment the human locus coeruleus (findings published in Human Brain Mapping)[143]

3.1. Evaluation of Different LC Segmentation Methods

This chapter's findings addressed the challenge of imaging the LC, a deep brainstem structure implicated in neurodegenerative diseases like AD, using NM-MRI. Due to its small size and the limitations of manual segmentation (e.g., time-consuming, subjective, and unsuitable for large or multisite studies), we developed a semi-automated method called the funnel-tip (FT) approach. This chapter evaluates the FT method's accuracy, reproducibility, and ability to detect LC signal loss associated with Alzheimer's disease (validated via tau-PET imaging), comparing it to manual and other automated segmentation techniques. By testing across multiple MRI sequences and assessing 3D structural outputs, this research aimed to establish FT segmentation as a reliable and scalable tool for studying LC integrity and its role in AD.

3.1.1. LC Signal Values

For the locus coeruleus (LC), three segmentation methods were used: segmentation in standardized space, manual, and a semi-automated (Funnel Tip, FT) method. Based on how many voxels were retained per axial slice, each method was further divided into two categories: a single voxel that represented the highest signal 'peak intensity' or a small cluster of 4-5 voxels (see Figures 2 and 3). These methods were used on 190 older adult participants' neuromelanin-sensitive MRI (NM-MRI) data (Sample 1)[143].

We utilized our chosen imaging metric, the contrast-to-noise ratio (CNR), to evaluate the LC signal. Peak-voxel CNR values from the manual and FT approaches were almost the same: 22.2% (±5.53) for the manual method and 22.0% (±5.22) for FT (Table 2a). Nevertheless, the standardized-space approach had significantly decreased CNR. In contrast to the standardized-space peak-voxel segmentation (15.0% ± 4.0), the peak-voxel FT technique yielded a much higher CNR (22.0% ± 5.2), with a very significant difference ($p < 10^{-89}$, paired t-test). These

findings imply that while the standardized space approach might be hampered by factors like voxel interpolation, resolution resampling, or inaccurate voxel targeting during spatial normalization, the FT method captures high-intensity LC voxels with similar efficacy to manual segmentation[143].

3.1.2. Agreement between LC metrics

When using masks of the same size, the FT and manual method demonstrated strong agreement, according to an evaluation of inter-method reliability. The range of the intraclass correlation coefficients (ICCs) was 0.89 to 0.91. On the other hand, with ICCs ranging from 0.52 to 0.66, masks produced using the standardized space method showed less agreement with the other peak-voxel-based techniques (refer to Table 2a). Additionally, there was a significant degree of agreement between the left and right LC for the manual peak-voxel and FT peak-voxel methods (ICC(2,k) = 0.85 and 0.89, respectively)[143].

There was a bias when comparing masks of different sizes (e.g., single-voxel vs. 4 voxel), where the peak-voxel masks had higher CNR values, and slightly lower ICCs (Table 2a). However, ICC(3,k) values above 0.83 indicated that consistency was excellent across all approaches (Table 2b). According to Bland-Altman plot, there was little proportional bias between our manual and FT methods (Figure 5). Dice similarity coefficients (DSCs) on the same axial slice were used to evaluate the spatial overlap between FT and manual segmentations. The findings showed a substantial overlap: peak-voxel masks had a DSC of 0.64 ± 0.47 and 4-voxel masks had a DSC of 0.54 ± 0.40 (Figure 6). The manual method's tendency to choose different axial slices because of cruder anatomical targeting along the rostrocaudal axis was one of its limiting factors, which restricted the upper limit of DSC to 0.67, thus it about two thirds of the cases in which both methods searched for the LC on the same axial slice (121 and 132 cases

for the left and right LC respectively, Figure 2). Spatial agreement between peak-voxel FT and manual methods significantly increased when studying only these cases that were searching on the same 2D image, reaching 0.98 ± 0.13 (right LC) and 0.95 ± 0.23 (left LC)[143].

Lastly, we investigated whether automatic segmentation was hampered by decreased LC signal contrast in tau-positive individuals due to LC degeneration. Nevertheless, tau pathology had no effect on the high level of agreement. The resilience of the FT approach even in pathological instances is demonstrated by the fact that the ICC for tau-positive persons (0.94) was marginally higher than that for tau-negative participants (0.90), and the DSC values were equal (0.64 in both groups)[143].

Table 2a. LC signal (CNR) as measured by different LC segmentation approaches and level of agreement (ICC (2,k)) between these metrics

	CNR mean±std	Agreement between methods (ICC(2,k)); constant bias reported in parentheses							
		Manual 5-voxel	Manual 4-voxel	Manual peak-voxel	FT 4-voxel	FT peak-voxel	FT 4-voxel unfixed	FT peak-voxel unfixed	SS mask 1 peak-voxel
Manual 5-voxel	13.8±3.7	-	-	-	-	-	-	-	-
Manual 4-voxel	15.9±4.0	0.92 (2.1)	-	-	-	-	-	-	-
Manual peak-voxel	22.2±5.5	0.49 (8.4)	0.65 (6.3)	-	-	-	-	-	-
FT 4-voxel	16.7±3.9	0.78 (2.9)	0.90 (0.8)	0.62 (-5.5)	-	-	-	-	-
FT peak-voxel	22.0±5.2	0.44 (8.2)	0.60 (6.1)	0.91 (-0.2)	0.70 (5.3)	-	-	-	-
FT 4-voxel unfixed	16.7±3.8	0.77 (2.9)	0.89 (0.8)	0.61 (-5.5)	1.0 (0.0)	0.70 (-5.3)	-	-	-
FT peak-voxel unfixed	22.1±5.2	0.42 (8.3)	0.57 (6.2)	0.90 (-0.1)	0.69 (5.4)	0.99 (0.1)	0.70 (5.4)	-	-
SS mask 1 peak voxel	15.0±4.0	0.85 (1.2)	0.87 (-0.9)	0.52 (-7.2)	0.90 (-1.7)	0.57 (-7.0)	0.89 (-1.7)	0.55 (-7.1)	-
SS mask 2 peak voxel	16.1±4.0	0.81 (2.3)	0.90 (0.2)	0.60 (-6.1)	0.96 (-0.6)	0.66 (-5.9)	0.95 (-0.6)	0.64 (-6.0)	0.94 (1.1)

FT=funnel-tip segmentation method, SS mask 1=standardized space from Dahl et al1, SS mask 2=standardized space created from this dataset, unfixed=fully automated funnel-tip method with no manual corrections applied[143].

Table 2b. LC signal (CNR) as measured by different LC segmentation approaches and level of agreement (ICC (3,k)) between these metrics

	Agreement between methods (ICC(3,k))								
	Manual 5-voxel	Manual 4-voxel	Manual peak-voxel	FT 4-voxel	FT peak-voxel	FT 4-voxel unfixed	FT peak-voxel unfixed	SS mask 1 peak voxel	SS mask 2 peak voxel
Manual 5-voxel	-	-	-	-	-	-	-	-	-
Manual 4-voxel	0.99	-	-	-	-	-	-	-	-
Manual peak-voxel	0.91	0.94	-	-	-	-	-	-	-
FT 4-voxel	0.90	0.91	0.86	-	-	-	-	-	-
FT peak-voxel	0.85	0.88	0.91	0.95	-	-	-	-	-
FT 4-voxel unfixed	0.89	0.90	0.85	1.0	0.95	-	-	-	-
FT peak-voxel unfixed	0.84	0.87	0.90	0.94	0.99	0.95	-	-	-
SS mask 1 peak voxel	0.87	0.86	0.85	0.94	0.92	0.93	0.91	-	-
SS mask 2 peak voxel	0.89	0.90	0.87	0.97	0.94	0.96	0.93	0.96	-

FT=funnel-tip segmentation method, SS mask 1=standardized space from Dahl et al1, SS mask 2=standardized space created from this dataset, unfixed=fully automated funnel-tip method with no manual corrections applied[143].

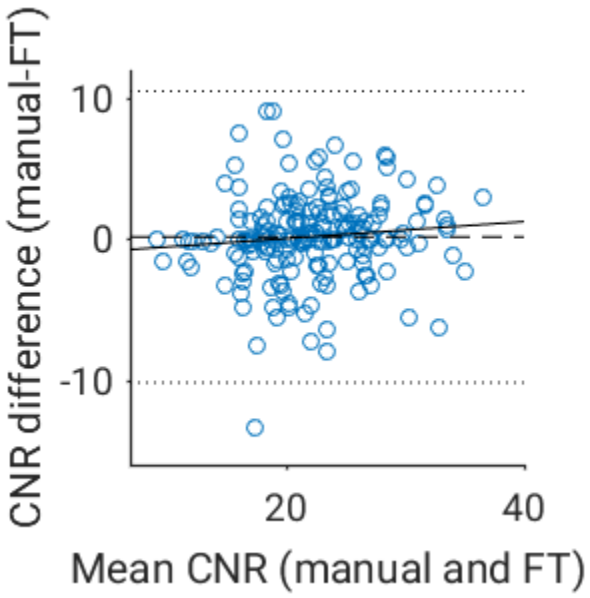

Figure 5: Bland-Altman plot examining proportional bias between LC signal measured using the manual and FT methods (peak-voxel version). Nearly flat regression slopes (solid line) suggest little evidence of proportional bias: constant bias or mean difference was also very small (dashed line). Dotted lines are two standard deviations above and below the mean difference[143].

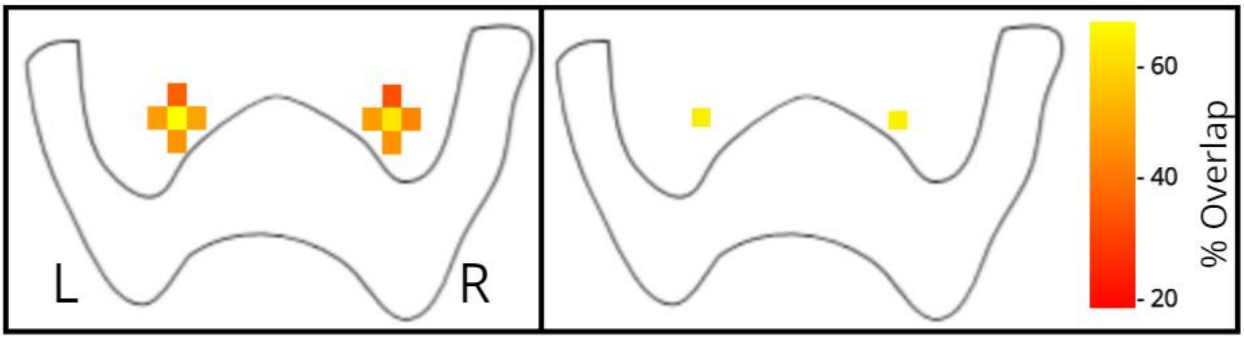

Figure 6: Heatmap showing proportion of subjects where the manual and FT LC masks overlapped. Overlap between the 5-voxel manual mask and the 4-voxel FT mask is shown at left and overlap between the peak-intensity voxels derived form these masks at right. Failure of peak-intensity voxels to overlap was almost always due to discordance regarding the axial slice wherein to search for the LC[143].

3.1.3. *Sensitivity to Signal Loss Associated with AD*

Correlations between LC signal values and clinical/pathological AD markers were calculated in order to assess each segmentation method's capacity to capture AD related LC signal loss (Table 3). Similar correlation strengths were demonstrated by the manual and FT techniques, usually falling within the medium effect size range. The greatest numerical effects were demonstrated by the FT approach employing peak-intensity voxels, which included a correlation of $r = –0.35$ with Braak stage and Cohen's $d = 0.64$ for differentiating tau-positive cases. the corrected FT variant numerically outperformed a fully automated version of the FT approach (i.e., without manual corrections). The standardized space approach, showed worse relationships with measures related to AD[143] and therefore was excluded from further analyses.

Table 3. Effect size estimates of the relationship between LC signal metrics and AD severity measures

	Control vs AD (excluding MCI) (n=139)	Tau positivity (n=190)	Tau burden (n = 189)	Braak stage (n = 160)	Cognitive impairment (MMSE) (n = 187)	Dementia severity (CDR) (n = 187)
	Cohen's d	Cohen's d	Pearson R	Pearson R	Pearson R	Pearson R
Manual 5-voxel	0.39	0.45	-0.24	-0.25	0.19	-0.14
Manual 4-voxel	0.45	0.47	-0.27	-0.28	0.21	-0.18
Manual peak-voxel	0.57	0.48	-0.31	-0.31	0.25	-0.23
FT 4-voxel	0.42	0.58	-0.29	-0.29	0.21	-0.21
FT peak-voxel	0.56	0.64	-0.33	-0.35	0.25	-0.26
FT 4-voxel unfixed	0.37	0.59	-0.26	-0.28	0.16	-0.25
FT peak-voxel unfixed	0.48	0.63	-0.29	-0.32	0.18	-0.25
SS mask 1 peak voxel	0.43	0.53	-0.27	-0.26	0.21	-0.17
SS mask 2 peak voxel	0.46	0.48	-0.28	-0.25	0.22	-0.19

FT=funnel-tip segmentation method, SS mask 1=standardized space from Dahl et al1, SS mask 2=standardized space created from this dataset, unfixed=fully automated funnel-tip method with no manual corrections applied. Tau positivity and tau burden were measured in the temporal cortex. All analyses controlled for age and sex[143].

3.2. Reproducibility Across and within NM-MRI sequences

3.2.1. Reliability of Scan-Rescan and LC location

A separate cohort (Sample 2, n = 12) underwent two scans on the same day utilizing a 2D-GRE NM-MRI sequence with magnetization transfer (MT) in order to evaluate test–retest stability. With ICCs above 0.7 for bilateral CNR values, both the FT and manual segmentation methods demonstrated excellent reliability (Table 4). Scan-to-rescan variability was modest across all methods, ranging between 8.4% and 12.0%[143].

Additionally, we evaluated whether the LC spatial localization held steady across scan-rescan sessions by testing the overlap between the images following rigid-body registration of the rescan images and LC masks to the original scan. a 4-voxel mask was used in this analysis as interpolation during registration may impair the accuracy of single-voxel masks. All cases showed at least partial overlap between scan and rescan masks, indicating reliable localization across sessions using the FT method (mean DSC = 0.48 ± 0.15). Crucially, the CNR of overlapping voxels was greater (19.2% ± 3.2) than that of non-overlapping ones (15.3% ± 2.5), indicating that the FT approach may more accurately capture the core (higher intensity) LC region. The manual mask (4-voxel), on the other hand, produced a lower average DSC (0.24 ± 0.26), most likely as a result of inconsistent axial slice selection[143].

Table 4. Reproducibility of LC signal[143]

	CNR, Bilateral LC (n = 12)	Reliability of CNR values				Scan-rescan variability (Bilateral LC, %)
	mean±std	ICC (3,k) Bilateral LC	ICC (2,k) Bilateral LC	ICC (2,k) Left LC	ICC (2,k) Right LC	mean±std
Manual 5-voxel	16.9±3.3	0.85	0.85	0.88	0.59	12.0±7.4
Manual 4-voxel	19.0±3.3	0.87	0.88	0.88	0.71	8.4±7.2
Manual peak-voxel	24.8±3.6	0.78	0.79	0.51	0.71	10.2±6.2
FT 4-voxel	19.5±2.6	0.75	0.73	0.81	0.57	10.7±8.6
FT peak-voxel	24.5±3.0	0.82	0.82	0.86	0.62	8.4±5.7
FT 4-voxel unfixed	19.4±2.7	0.73	0.73	0.80	0.58	11.3±8.5
FT peak-voxel unfixed	24.6±2.9	0.79	0.79	0.67	0.61	9.3±5.3

3.2.2. Consistency across NM-MRI sequences

We studied data from Sample 3 (n = 30), where subjects were scanned using both a 2D-GRE MT sequence and a turbo spin echo (TSE) sequence on the same day, in order to investigate the performance of the FT approach across various NM-MRI acquisition protocols. Compared to the TSE (CNR = 17.3 ± 5.0), the MT sequence had a greater LC signal intensity (CNR = 28.8 ± 4.3). Despite these variations, the two modalities' signal consistency was still high, as evidenced by the FT peak-voxel approach's ICC(3,k) of 0.71, which shows good cross-sequence agreement[143].

3.3. Structural Validity of automated LC segmentation

Because manual segmentation is usually restricted to 2D axial views, many previous studies were restricted to a single rostrocaudal slice of the LC. Thus, complete three-dimensional reconstruction of the LC is an advantage of the FT method. We examined whether the segmented LC matched the anticipated rod-like, linear structure of the nucleus in order to assess the anatomical realism of this reconstruction (Figure 2)[143].

For all Sample 3 cases, the spatial coordinates of FT-derived peak-intensity voxels along the rostrocaudal length of the LC were subjected to linear regression. Also to closely observe the variability in performance across implementations, and further establish the utility of our method, we assessed the data from both MT and TSE sequences. The residuals from these regressions demonstrated LC voxels that were distant from the straight line estimating the LC 3D anatomy (Figure 7 shows fit lines, and Table 5 shows angles relative to the y axis)[143].

The idealized LC trajectory was depicted by the fit lines that were produced (Figure 7). For the left LC, 96.1% (TSE) and 91.7% (MT) of LC voxels fell within one voxel diameter on

the x-axis, indicating that the majority of voxels closely followed these lines. Moreover, table 6 shows lower variance along the y-axis. Lastly, the middle section (section 3; Table 7) had smaller residual errors, compared to the rostral and caudal sections (sections 1 and 5) which showed larger residual errors[143].

Our comparison of FT-based voxel fits to two reference models—(1) a "positive control" based on the LC search mask center (the LC core) and (2) randomly permuted coordinates within the LC search mask (permuted 1000 times in bootstrapped subjects, which should lead to highly variable linear fits)—helped put the regression accuracy into context. Particularly in the y-axis dimension, FT-derived fits had significantly less error than the permuted model across both MT and TSE sequences, while many subjects showed error consistent with the ‘LC core’ positive control (Figure 7, Table 8)[143].

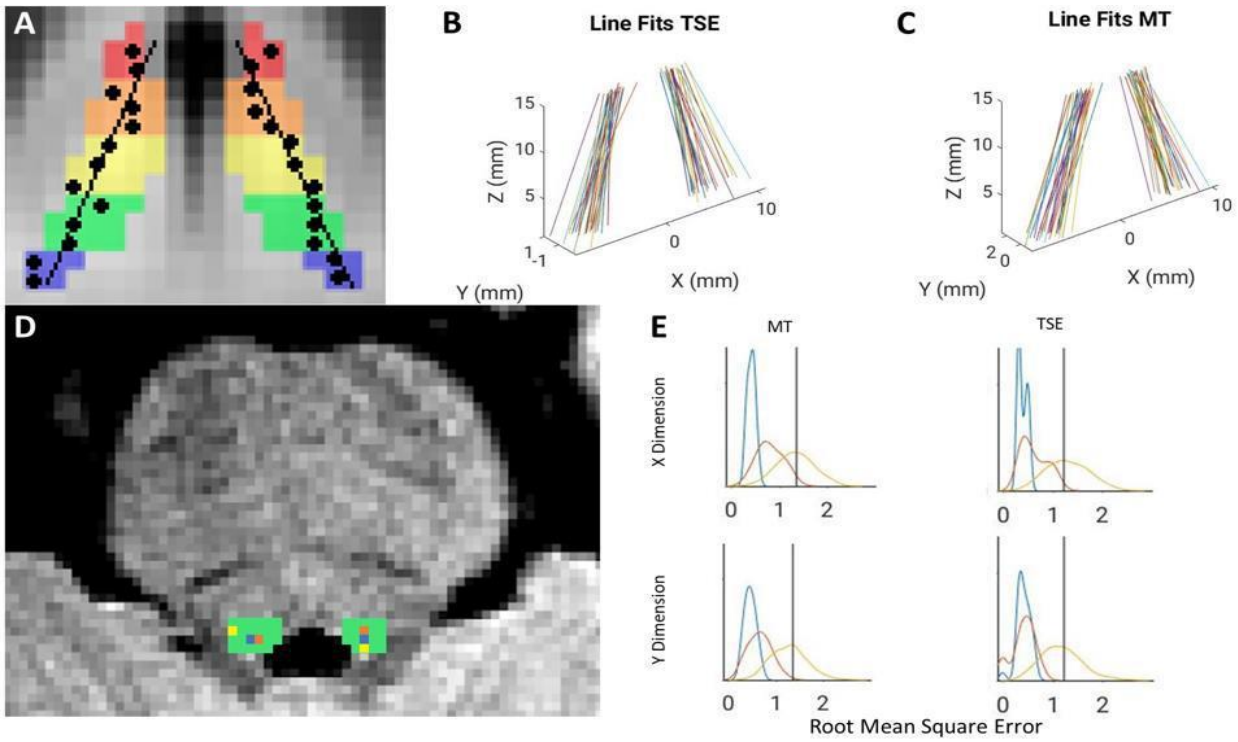

Figure 7. *Linear structure of the FT LC mask. A: schematic of hypothetical data showing linear fit of peak-intensity voxels (black circles) segmented using the FT method within the LC search mask (rainbow colors). B, C: Idealized LC structure revealed by linear regression on LC peak voxel coordinates from the FT method. Lines for all participants are overlaid in native space after setting the origin as the midpoint between the left and right middle LC sections. D: Axial view of the pons of a representative subject overlaid with the LC search mask (green). FT peak voxel coordinates are shown in orange, the center coordinate of the LC search mask is shown in blue ('LC core' positive control), and a permuted coordinate is shown in yellow. E: The distribution of linear fit error for all these types of coordinates for the right LC is shown with curves in matching colors. The LC core (blue) showed minimal error and the permuted coordinates (yellow) showed highly variable error. The FT peak-intensity voxels (orange) often showed error of a similar magnitude to the LC core and never showed greater error than the mean of permuted voxels (black vertical line)*[143].

Table 5. Angle of LC fit lines relative to y-axis[143]

	X-dimension (Left)	X-dimension (Right)	Y-dimension (Left)	Y-dimension (Right)
TSE	15.2°±5.4	-14.0°±5.0	1.4°±4.1	2.0°±3.7
MT	15.6°±3.4	-17.0°±4.2	-0.0°±3.79	-0.0°±3.7

Table 6. Fraction of FT peak-intensity voxels deviating from linear structure[143]

	>1 voxel diameter away				>2 voxels diameter away			
	X - dimension (Left)	X - dimension (Right)	Y - dimension (Left)	Y - dimension (Right)	X - dimension (Left)	X - dimension (Right)	Y - dimension (Left)	Y - dimension (Right)
TSE	8 (3.9%)	7 (3.4%)	2 (1.0%)	3 (1.5%)	0 (0%)	0 (0%)	0 (0%)	0 (0%)
TSE fully automated	6 (3.0%)	9 (4.5%)	0 (0%)	4 (2.0%)	0 (0%)	0 (0%)	0 (0%)	0 (0%)
MT	21 (8.3%)	23 (9.1%)	10 (4.0%)	12 (4.8%)	0 (0%)	1 (0.4%)	1 (0.4%)	0 (0%)
MT fully automated	22 (8.8%)	26 (10.3%)	11 (4.4%)	11 (4.4%)	3 (1.2%)	3 (1.2%)	0 (0%)	1 (0.4%)

Table 7. Error in linear fit of LC coordinates per LC section[143]

	X-dimension (Left) (mean±std)		X-dimension (Right) (mean±std)		Y-dimension (Left) (mean±std)		Y-dimension (Right) (mean±std)	
	MT	TSE	MT	TSE	MT	TSE	MT	TSE
1 (rostral)	0.69±0.45	0.50±0.29	0.57±0.37	0.41±0.30	0.53±0.35	0.38±0.29	0.58±0.47	0.23±0.20
2	0.73±0.46	0.51±0.26	0.57±0.33	0.44±0.35	0.54±0.41	0.38±0.32	0.57±0.31	0.30±0.31
3 (middle)	0.53±0.41	0.42±0.25	0.53±0.28	0.42±0.31	0.42±0.25	0.33±0.21	0.45±0.29	0.27±0.24
4	0.54±0.29	0.50±0.37	0.65±0.38	0.49±0.39	0.50±0.32	0.38±0.19	0.41±0.27	0.27±0.26
5 (caudal)	0.62±0.40	0.43±0.38	0.86±0.48	0.52±0.29	0.53±0.42	0.34±0.19	0.55±0.38	0.38±0.27

Table 8. Error in linear fit of LC coordinates from FT method and control conditions[143]

Sequence		X-dimension (Left) (mean±std)	X-dimension (Right) (mean±std)	Y-dimension (Left) (mean±std)	Y-dimension (Right) (mean±std)
TSE	FT Peak Voxel	0.64±0.21	0.63±0.26	0.47±0.18	0.41±0.23
	LC Core	0.41±0.10	0.40±0.10	0.47±0.17	0.42±0.13
	Permuted Voxel	1.23±0.40	1.30±0.43	1.12±0.39	1.17±0.41
TSE Fully Automated	FT Peak Voxel	0.64±0.22	0.66±0.33	0.44±0.22	0.42±0.25
	LC Core	0.41±0.10	0.40±0.10	0.47±0.17	0.42±0.13
	Permuted Voxel	1.23±0.40	1.30±0.43	1.12±0.39	1.17±0.41
MT	FT Peak Voxel	0.81±0.24	0.82±0.26	0.66±0.24	0.67±0.23
	LC Core	0.44±0.08	0.43±0.08	0.50±0.14	0.47±0.11
	Permuted Voxel	1.37±0.39	1.35±0.39	1.25±0.37	1.28±0.38
MT Fully Automated	FT Peak Voxel	0.87±0.35	0.83±0.30	0.66±0.21	0.66±0.27
	LC Core	0.44±0.09	0.43±0.08	0.50±0.14	0.47±0.11
	Permuted Voxel	1.37±0.39	1.35±0.39	1.25±0.37	1.28±0.37

Chapter 4. longitudinal investigation of locus coeruleus norepinephrine system integrity and cognitive performance across the Alzheimer's spectrum (Paper under review, NPP).

4.1. Longitudinal Change in LC signal

The locus coeruleus (LC), the brain's primary source of norepinephrine, is increasingly recognized for its central role in cognitive function and its early vulnerability in AD. NM-MRI enables non-invasive in vivo assessment of LC integrity, and growing evidence suggests that LC signal loss may precede clinical symptoms and relate to tau pathology and cognitive decline. However, longitudinal investigations of these relationships remain limited. This chapter's findings addressed this gap by examining LC signal loss over time in a large cohort of older adults. Using a validated automated LC segmentation method (FT-method), we quantified the NM-MRI signal and studied its association with a broad set of cognitive domains, including global cognition, verbal memory (via two distinct measures), working memory, executive function, speed processing, object recognition, and verbal fluency. Participants were stratified by amyloid-β and tau PET imaging biomarkers, allowing us to investigate group-level and within-group associations between LC integrity and cognition.

To assess LC change over time, n=266 study participants were included in a linear mixed effects model. We did not see evidence that the LC $pattern_{CN}$ was differentially changing over time between Aβ-positive and Aβ-negative individuals (time × Aβ status interaction t_{474}=-0.47). Therefore, we reasoned that further division into early and later phase AD groups may be needed to reveal AD-associated LC degeneration over time. We did not measure significant change over time in a healthy aging group (CN, Aβ-negative, and at Braak stage 0, n=86; ΔLC $pattern_{CN}$/year=-0.023, CI=-0.24—0.19, t_{139}=-0.21, p=0.83, linear mixed effects model controlling for age at baseline, sex, and scan date prior to covid-19 pandemic), nor in patients with later stage AD (Aβ-positive and braak stage 4-6, n=56) who actually showed a non-significant *increase* over time (ΔLC $pattern_{CN}$/year=0.13, CI=-0.096—0.35, t_{80}=1.14, p=0.26). It

was the early-stage AD group (Aβ-positive and Braak stage<4, n=59) who showed a marked decrease in LC signal over time (ΔLC $pattern_{CN}$/year=-0.43, CI=-0.66—-0.20, t_{95}=-3.72, p=0.0003). For detailed visualization of how the LC signal changed over time in all rostro-caudal sections, see Figure 8 and Supplementary Figure 1 for raw data scores for every subject across all Braak stages.

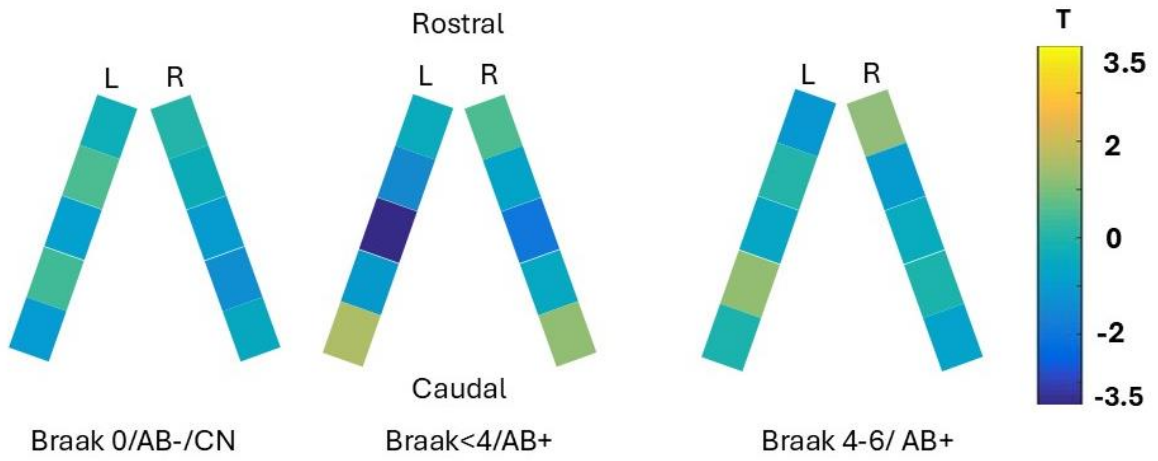

Figure 8. *Effect of time on LC integrity. Schematic LC maps showing LC signal loss over time for all rostrocaudal sections in sub-groups of participants (left: healthy aging, middle: early AD, right: later AD).*

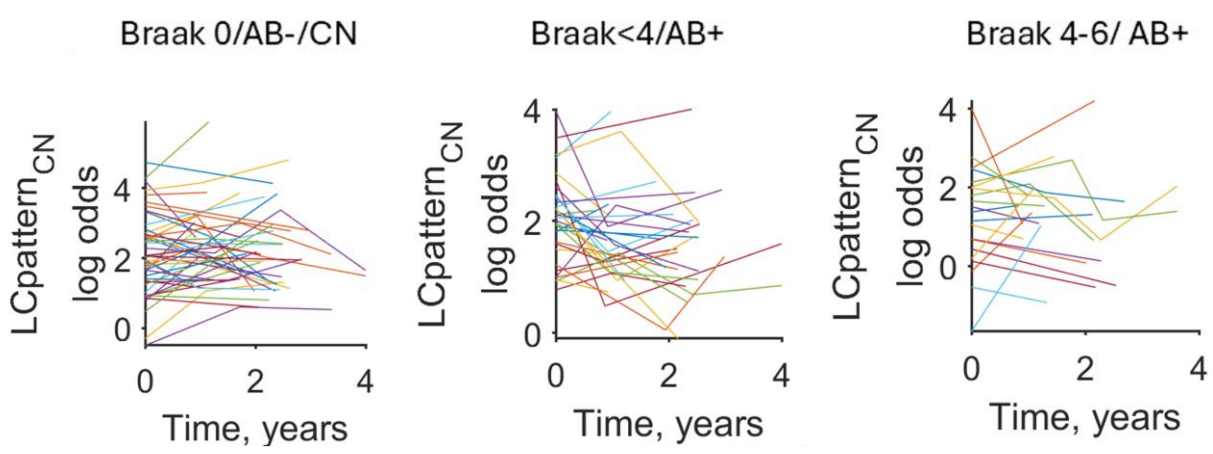

Supplementary Figure 1. *Raw data of LC patternCN metric change over time in every single participant across all Braak stages.*

4.2. LC change proximal to AD onset

Next, given our observation of pronounced LC loss in the early stages of AD and prior evidence that the LC may be one of the first brain regions affected in AD[172,173], we examined a group who had little or no indication of AD at baseline (all were CN and at Braak stage 0 though some were Aβ-positive) and examined the relationship between Δtau (in the Braak stage 1 ROI) and ΔLC $pattern_{CN}$ over time in a robust linear regression (Figure 9). We found that Aβ positivity was associated with reduction over time in LC $pattern_{CN}$ (t_{52}=-2.83, p=0.0065). In contrast to Aβ, a positive Δtau over time was correlated with an *increase* in ΔLC $pattern_{CN}$ over time (t_{52}=3.82, p=0.0004). Rerunning this analysis with an Aβ-positivity × Δtau interaction term, revealed a near-significant interaction (t_{51}=-1.95, p=0.057) that we broke down to find a strong positive correlation between ΔLC $pattern_{CN}$ and Δtau in the Aβ-negative group (t_{44}=4.28, p=0.0001) but not in the Aβ-positive group (t_5=-0.52, p=0.62).

The Aβ finding is intuitive (suggesting that the LC is becoming more AD-like over time in Aβ-positive individuals). On the other hand, the finding that tau accumulation is linked to a positive ΔLC $pattern_{CN}$ reflecting a shift toward an apparent *improvement* in LC health, is surprising. This appeared to be driven by three participants who, of all participants in this subgroup, had both the most positive Δtau in the Braak 1 ROI and the most positive ΔLC $pattern_{CN}$ over the follow-up interval (Figure 9). There were other AD-risk signs in these three cases, one had a substantial increase in tau burden in the Braak stage 2 ROI, another had a substantial drop in MMSE score, and two were APOE4 carriers.

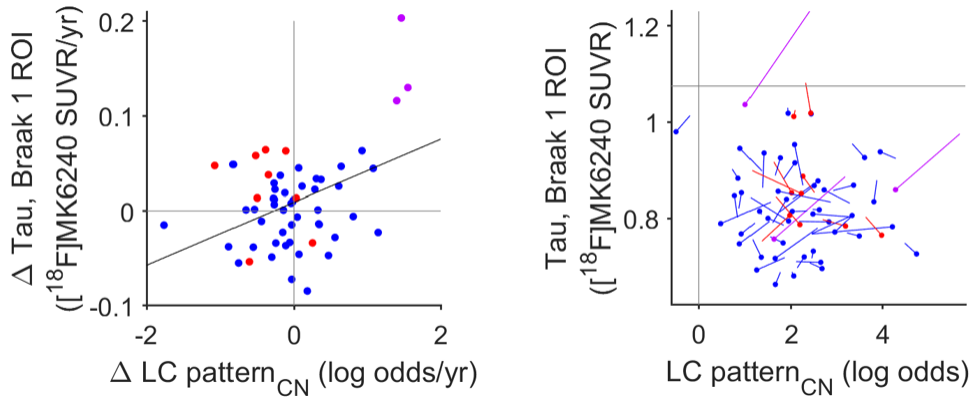

Figure 9. *Relationship between change in LC integrity and tau accumulation over time in older adults with little to no evidence of AD at study baseline (CN and at Braak stage 0). Left: scatterplot showing change in tau burden over time in the Braak stage 1 ROI versus change in LC pattern$_{CN}$ over time. Aβ-positive cases (red) were more likely to decrease in LC pattern$_{CN}$ over time (become more AD-like) compared to Aβ-negative cases (blue). A positive ΔLC pattern$_{CN}$, reflecting a more CN-like pattern, was paradoxically correlated to positive Δtau accumulation over time. This was driven by three participants (shown in violet) who had the greatest increase in both tau and LC pattern$_{CN}$. Right: vector plot of the same data. Each line represents a different participant. The dots plot the value of LC pattern$_{CN}$ and tau burden at baseline and the other end of the line plots the value after 1 year of follow-up (based on the slope fitted to all available time points). The three influential cases (violet) show long vectors pointing towards the top right corner. The vertical line at LC pattern$_{CN}$=0 represents the point where the odds of CN:AD =1. The horizontal line represents the threshold to convert to Braak stage 1.*

4.3. Association of LC integrity to cognition

Next, we considered the association between LC integrity and multiple domains of cognition in healthy aging and AD individuals taking into account data from all available time points using linear mixed effects model with additional fixed factors: time, age at baseline, and sex. When merging Aβ-positive individuals from Braak stage 1-6, all cognitive measures correlated positively to LC $pattern_{CN}$, the strongest association was with the novel object recognition test (BORB: T_{125}=4.10, p=0.00007, Table 9, correlations of BORB combined score versus LC patternCN across the Braak stages is presented in Supplementary Figure 2.). In the healthy aging group, only working memory (WAIS digit span) showed a significant correlation to LC $pattern_{CN}$ (T_{129}=2.50, p=0.014, Table 9, correlations of working memory versus LC patternCN across the Braak stages is presented in Supplementary Figure 3).

To minimize the risk of correlation strength being inflated by examining measures across such a broad range of AD severity, and in line with evidence from the prior section that LC signal may be impacted differently across the AD spectrum, we performed subsequent analysis dividing the AD group into early (Aβ-positive, Braak stage<4) and later (Aβ-positive, Braak stage 4-6) groups. In the early AD group, LC $pattern_{CN}$ correlated positively to general cognitive impairment (MMSE score, t_{93}=2.31, p=0.023) and executive function (TMT-B test, t_{48}=2.87, p=0.006, Table 9). In the later AD group, LC $pattern_{CN}$ correlated positively to several measures including object recognition (BORB test, t_{64}=3.41, p=0.0011), logical memory (t_{64}=2.57, p=0.013, correlations of logical memory versus LC patternCN across the Braak stages is presented in Supplementary Figure 4), and verbal fluency (t_{66}=2.41, p=0.019, Table 9, correlations of verbal fluency versus LC patternCN across the Braak stages is presented in Supplementary Figure 5). The findings from the AD subgroups that survived FDR correction

were the relationship of LC pattern$_{CN}$ to TMT-B in early AD and its relationship to object recognition, logical memory, and verbal fluency in later AD (for these measures that survived FDR correction, maps visualizing the relationships across all LC sections in later AD are provided in Figure 10).

Given the strong relationship we observed in AD between object recognition and LC integrity, we reasoned that this cognitive test may be sensitive enough to reveal a relationship between change over time in task performance and change over time in LC pattern$_{CN}$. We tested this in the later AD group and found a significant correlation suggesting loss of LC integrity over time is associated with increasing impairment in object recognition (t_{11}=2.69, p=0.021, Figure 11). We further examined subscale scores of this object recognition test and found that the relationships to LC integrity both in the full AD sample and the later AD group were apparent when attempting to recognize novel stimuli (imaginary animals comprising the 'unreal subscale', t=4.02 and 3.66 respectively) but were not significant when recognizing familiar stimuli (common animals on the 'real subscale', t=1.97 and 1.04 respectively).

Table 9. Relation of LC pattern$_{CN}$ to cognitive measures in study subgroups

	CN & Braak 0 & AB-	AB+ Braak 1-6	Braak <4 & AB+	Braak 4-6 & AB+
Global Cognition	T_{137}=-0.36	T_{141}=2.24*	T_{93}=2.31*	T_{78}=1.93
Logical memory	T_{130}=1.18	T_{125}=2.82**	T_{85}=-0.01	T_{64}=2.57*
Working Memory	T_{129}=2.50*	T_{125}=2.87**	T_{84}=0.40	T_{65}=2.19*
Speed of Processing	T_{71}=1.33	T_{56}=2.50*	T_{48}=1.81	T_{22}=1.08
Executive Functioning	T_{71}=1.25	T_{53}=3.51***	T_{48}=2.87**	T_{19}=0.00
Verbal Fluency	T_{130}=1.24	T_{127}=2.98**	T_{85}=1.19	T_{66}=2.41*
Object Recognition	T_{129}=-0.43	T_{125}=4.10***	T_{85}=1.71	T_{64}=3.41**

***p<0.001, **p<0.01, *p<0.05

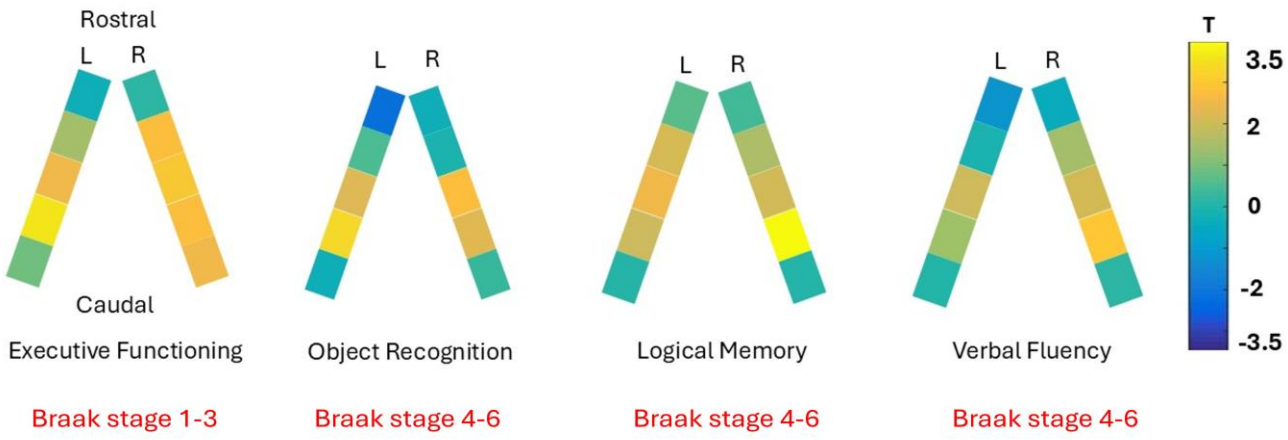

Figure 10. *LC schematic maps association of NM-MRI signal across all LC sections to cognitive measures. Relationships to executive function (TMT-B performance) are shown for the subgroup of early AD participants (Braak<4 & AB+) and the other measures are shown for the subgroup of later AD participants (Braak>3 & AB+).*

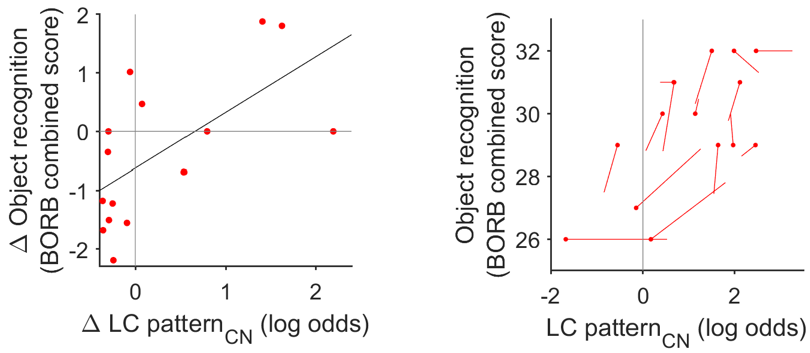

Figure 11. *Longitudinal loss in LC integrity is associated with reduction in object recognition over time in AD participants (Aβ-positive, Braak stage<4). Scatterplot at left shows change in object recognition performance versus change in LC integrity over time. The same data is plotted at right as a vector plot with the dots plotting baseline values of object recognition and LC pattern$_{CN}$ and the other end of the line plotting the value after 1 year of follow-up (based on the slope fitted to all available time points). Most lines are running between the top right and bottom left corner, consistent with the positive line fitted on the scatterplot at left.*

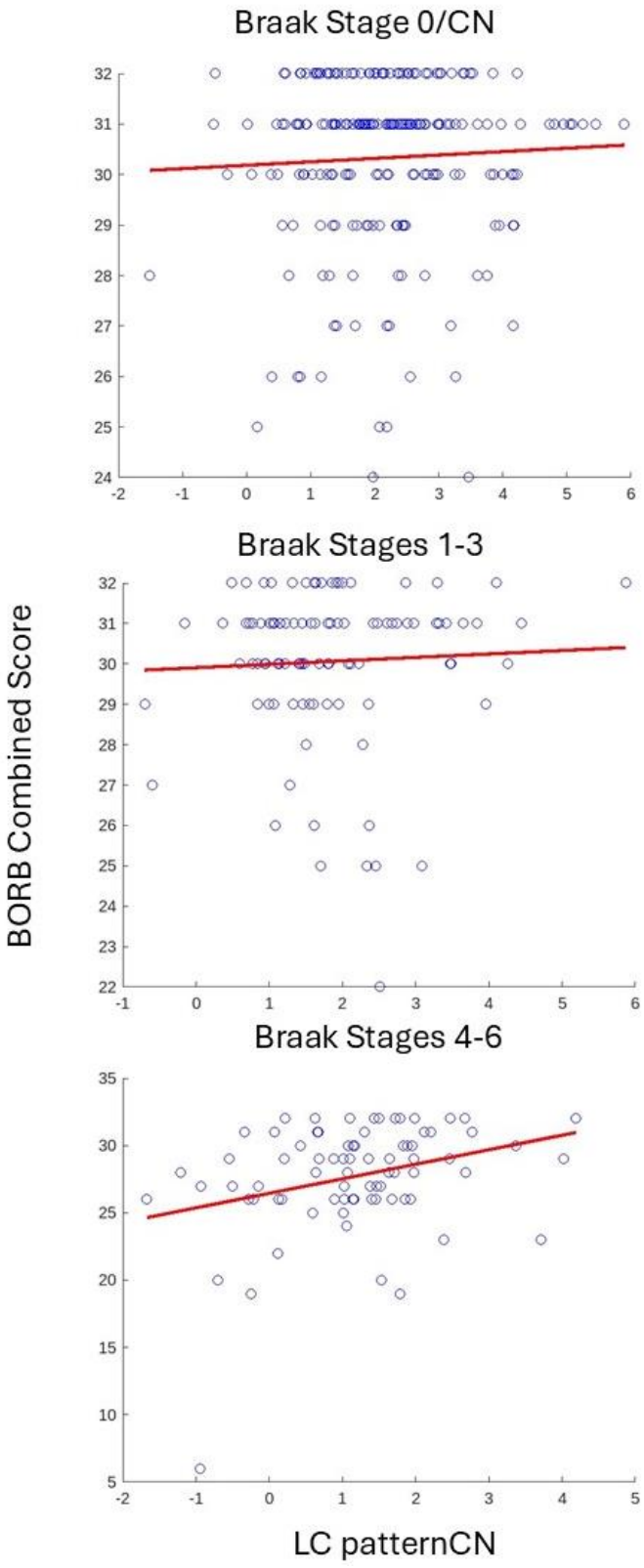

Supplementary Figure 2. *BORB combined scores versus LC patternCN across Braak staging.*

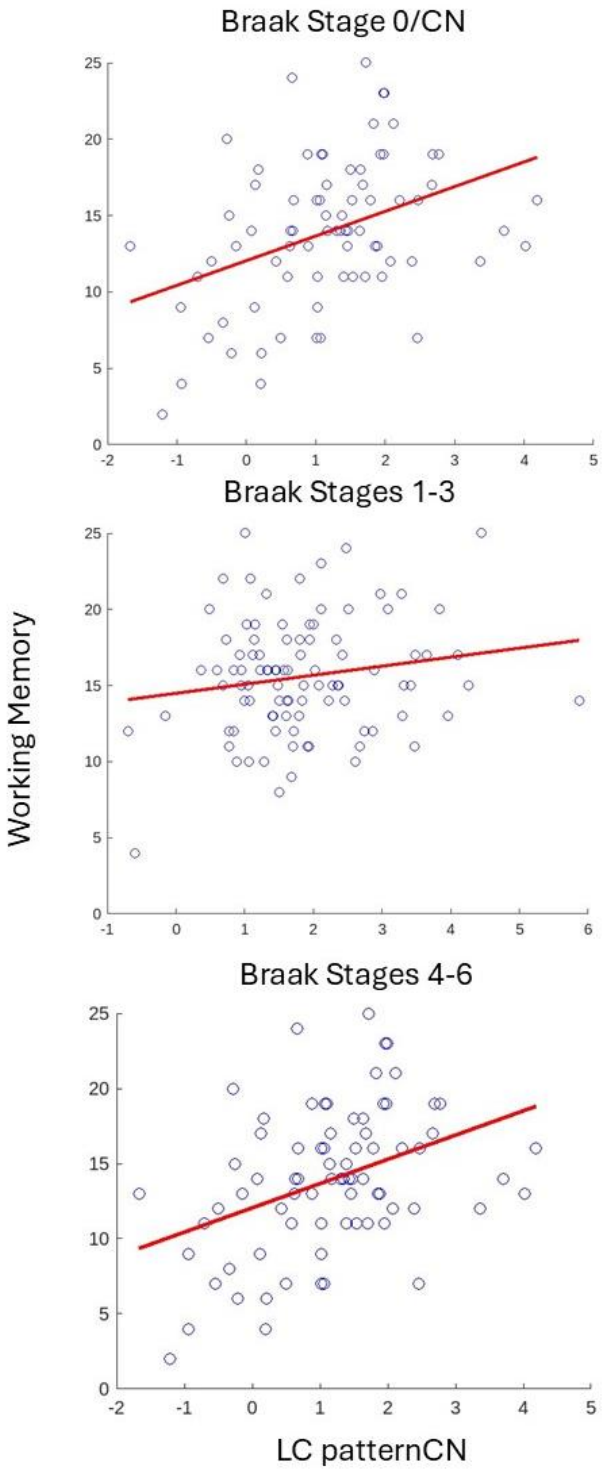

Supplementary Figure 3. *Working Memory scores versus LC patternCN across Braak staging.*

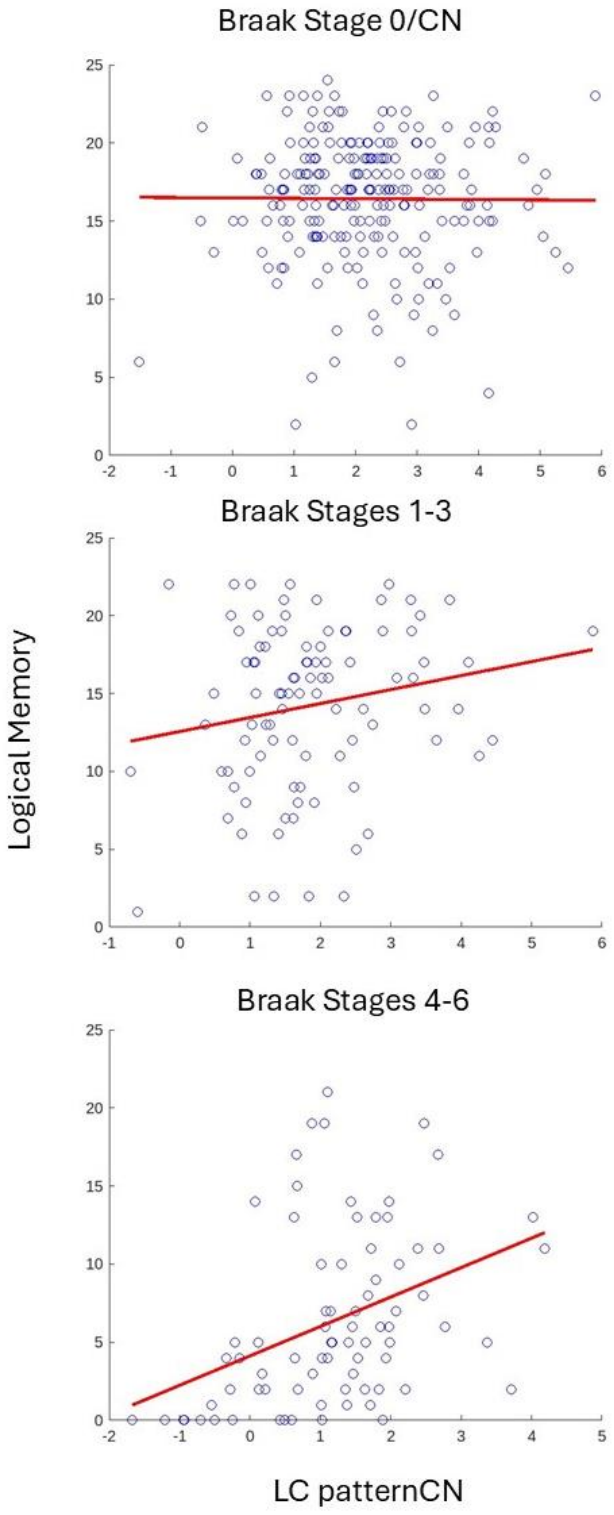

Supplementary Figure 4. *Logical Memory scores versus LC patternCN across Braak staging.*

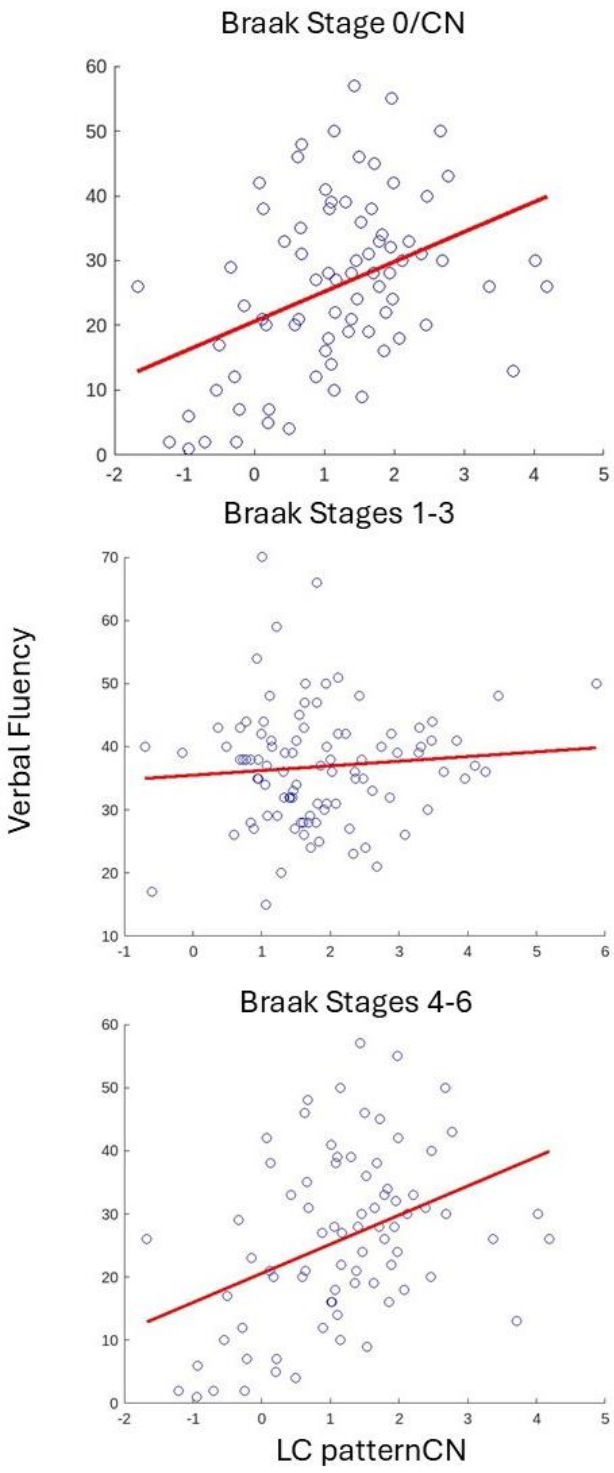

Supplementary Figure 5. *Verbal Fluency scores versus LC patternCN across Braak staging.*

Chapter 5. Discussion

5.1. Discussion for Aim 1

Our results endorse a semi-automated approach for segmenting the LC (FT method). The FT method demonstrated a high level of agreement with the manual segmentation regarding LC localization and signal (ICC=0.91), which is comparable to previous automated techniques (ICCs ranging from 0.90 to 0.93)[130,145]. In comparison to manual segmentation, the FT method demonstrated a comparable level of correlation with clinical and pathophysiological indicators of Alzheimer's disease severity, thereby establishing convergent validity due to the recognized influence of Alzheimer's disease on the LC[144], and indicating its efficacy in assessing the LC signal in both healthy and degenerated conditions. The FT method demonstrated exceptional scan-rescan reliability (ICC=0.82 for the peak-voxel method), approaching the upper range of prior findings of LC signal ICC, which varied from 0.36 to 0.875, and exhibited consistent spatial targeting of high-contrast voxels across repeated scans . The structure of the locus coeruleus produced by this FT method was congruent with the established morphology of the LC, characterized as a continuous, rod-like structure[174]. This method also revealed good performance when processing data from the two most commonly used NM-MRI sequence types (TSE and MT), and displayed high consistency in extracting LC signal across these sequences.

Our analysis revealed that a more straightforward automated LC segmentation utilizing a fixed mask in standardized space exhibited a decrease in the contrast-to-noise ratio (CNR) and a reduced capacity to detect Alzheimer's disease-associated degeneration relative to alternative methodologies, including a fully automated FT approach. Other groups have documented promising outcomes utilizing analogous methodologies[97,175,176], and it is probable that this technique could be refined compared to our implementation (e.g., improving reference region signal extraction methods, selecting LC voxels, optimizing the mask, or warping the mask,

excluding artifacts, and extracting signals in native space). A challenge with averaging all voxels[130,144] in a fixed LC mask is that the mask must be tiny to avoid overlapping with the surrounding tissue or cerebrospinal fluid; nevertheless, at this size, it might still inadequately target the LC. Techniques related to FT address this issue by beginning with a larger overinclusive mask (LC search mask) that covers adjacent tissue and cerebrospinal fluid, thereby minimizing the likelihood of missing the LC due to their large size.

Conversely, the risk associated with these methodologies is that, in segmenting the LC within this search mask, they depend not only on external anatomical location data but also on the image intensity itself, so generating circularity and a positive bias. They may occasionally choose voxels that are not the LC but exhibit hyperintensity due to noise, artifacts, or other tissue characteristics. This risk may be intensified in the context of LC degeneration when the disparity in signal intensity between the LC and adjacent tissue diminishes. The approach minimizes the possibility of selecting an isolated hyperintense voxel, which is less likely to indicate LC, by first identifying a hyperintense cluster of nearby voxels ('narrowing the funnel') before locating the brightest single voxel inside this cluster. The risk of inaccurate segmentation is decreased by visual examination and manual adjustments; however, this process hinders full automation and involves subjectivity. Considering the theoretical advantages and disadvantages of the FT approach, it seems that the strengths may surpass the limitations, as the method effectively captured LC signal loss in AD more proficiently than a standardized space ROI approach and comparably to manual segmentation. Additionally, the agreement with manual segmentation remained unaffected despite the reduction of LC signal intensity in AD.

We evaluated different methodologies by altering the size of the LC cross-section and implementing manual adjustments to the FT approach. Smaller LC cross-sections (a single peak-

intensity voxel) had a higher correlation numerically with AD severity compared to larger cross-sections, while masks of varying sizes showed comparable performance regarding agreement with manual segmentation and scan-rescan reliability. Nevertheless, our data may not have been ideally suited to ascertain the appropriate dimensions of the LC mask. Our images exhibited worse in-plane resolution relative to other studies (including those that established the manual segmentation protocol[128]), and within a 4-voxel cross-section, certain voxels are likely affected by partial voluming. Utilizing a greater resolution may yield advantages by incorporating many voxels in the cross-section to comprehensively analyze the structure and diminish noise. Conversely, analyzing the peak-intensity voxel may increase the range of LC signal values, thereby enhancing the identification of correlations. The FT method, whether applied to a cluster of voxels or an individual voxel, is not intended to define the axial boundaries of the LC. Even at high resolution, it cannot extract signals from all LC voxels, but only from a central portion of the LC in each axial slice.

Concerning manual corrections, our data indicates that they are advantageous when possible but may not be critical, as there was virtually excellent agreement between the corrected and uncorrected versions of the FT segmentation (ICC=0.99), with both reflecting AD-related signal loss. The requirement for manual correction may vary based on the specific dataset, as we have observed discrepancies across NM-MRI acquisition protocols regarding error rates (ranging from less than 1% to 6.5%), influenced by factors such as signal-to-noise ratio or the occurrence of hyperintense artifacts in the fourth ventricle, which are more prevalent in certain acquisitions. The influence of segmentation errors in our dataset (Sample 1) appears to be moderate compared to others we have seen, as the error rate was low (1.2%); yet, some errors were attributable to artifacts, resulting in significant CNR values. The FT technique provides a filtering option to

automatically reject extreme CNR values; nevertheless, it must be employed judiciously, possibly necessitating study-specific criteria. These findings instill confidence that it is plausible to establish an acquisition strategy that would mitigate the likelihood of errors and provide substantial assurance for employing the FT approach in a completely automated manner, particularly in clinical settings where manual correction would be difficult.

The FT technique offers a notable advantage by enabling the evaluation of LC signals in up to five subsections along the complete rostrocaudal extent of the LC. Nevertheless, several research studies in this area focused solely on the middle LC region to better conform to the prevailing manual technique. Therefore, we developed a test to assess the capacity of the FT technique to reconstruct an LC with a conformation that aligns with its recognized form as an almost linear, rod-like structure. The LC is a continuous nucleus, and it is expected that its position on adjacent slices will be close and often overlapping. The majority of LC voxels classified by the FT method were situated adjacent to a linear regression line. The variations from the line may have arisen from segmentation issues or the inherent structure of the LC diverging from linearity. This is anticipated to occur intermittently in both the rostral and especially the caudal regions of the LC, where cell counting studies have demonstrated more fluctuation in LC cell location[153]. Consistent with this, the discrepancy in the linear fit was typically more pronounced at the extremes of the LC.

In this doctoral thesis, we developed and validated the funnel-tip (FT) segmentation method for extracting locus coeruleus (LC) signal from neuromelanin-sensitive MRI, demonstrating high reliability, anatomical accuracy, and strong associations with Alzheimer's disease (AD) pathology and cognition. This work formed the foundation for a successful Mitacs internship with Terran Biosciences, a biotechnology company that integrated the FT method into

NM-101, the first FDA-approved software for neuromelanin MRI analysis in a clinical context[177]. During this internship, I contributed directly to refining and validating the software's LC processing pipeline, applying it to large-scale longitudinal datasets and helping establish its clinical utility. This hands-on experience deepened my understanding of medical imaging software development and regulatory pathways, while allowing me to translate my PhD research into a clinically applicable tool for early AD detection.

5.2. Discussion for Aims 2 and 3

This thesis leveraged the use of NM-MRI, measured for the full extent of the LC, by collecting neuroimaging data to perform longitudinal assessments for a large sample of tau-positive and tau-negative subjects, in addition to gathering longitudinal PET scans and seven cognitive measures. This would be the first longitudinal study to connect all these measures and factors for a better understanding of LC signal over time and its relation to cognition in AD and healthy subjects.

This study examined longitudinal changes in locus coeruleus integrity and its correlation with cognition in a substantial and well-defined cohort of an older population across the Alzheimer's disease spectrum. Several significant findings emerged, starting with the decline in LC integrity which was most pronounced during the early stages of Alzheimer's disease (Braak stages 1-3), while no substantial change was observed in the later stages of Alzheimer's or in healthy aging. Upon closer examination of people without baseline symptoms of Alzheimer's disease, we observed a counterintuitive correlation between tau accumulation and changes in our LC metric over time. This may be pertinent to the onset of Alzheimer's disease. Then we investigated the correlation between LC integrity and cognition across many domains. Our analysis revealed that, over the whole spectrum of Alzheimer's disease severity, the integrity of the locus coeruleus was associated with performance on all cognitive assessments. A more rigorous examination aimed at minimizing spurious correlations arising from illness progression and restricting analyses to either early Alzheimer's disease (Braak stage < 4) or late Alzheimer's disease (Braak stage > 3) revealed that numerous cognitive metrics continued to exhibit substantial correlations with LC integrity.

Although many cognitive assessments have previously been associated with the locus coeruleus's role in Alzheimer's disease (e.g., logical memory[40,134,140]), the measure demonstrating the most significant correlation, object recognition, has not been examined in this context. This assessment indicated a deficiency in the recognition of imaginary animals, which may highlight the significant contibution of the LC-NE system in compromised novelty detection in Alzheimer's disease, while the reason that there was no relation of LC to BORB in early AD/ healthy aging may be that variability in this cognitive metric is low in these groups, it is an easy test and probably not sensitive enough in these groups. Ultimately, our work successfully examined healthy aging using a more stringent criteria than most previous findings that omitted Aβ and tau imaging. We discovered that, excluding working memory, in the context of healthy aging, LC integrity had no significant correlation with cognition, aligning with findings that indicate minimal LC degradation in healthy aging[136].

The work in this thesis also produced a singular metric of locus coeruleus (LC) integrity across all rostrocaudal LC sections, LC pattern$_{CN}$, representing the log of the odds that an individual is cognitively normal or has Alzheimer's disease based on their LC signal. This multivariate approach offers advantages over analyzing an average of the entire LC or particular LC sections without accounting for information from other parts. For instance, based on the pattern, an individual exhibiting a high LC signal in the middle of the LC is more protected against AD if they simultaneously possess a low signal at the rostral-caudal ends of the LC, in contrast to another individual with a high LC signal at both the middle and the ends of the LC. We had reasoned that a multivariate LC measure would aid in quantifying LC signal loss over time, as various biological or imaging factors may affect LC signal in a manner distinct from AD-related degeneration across LC sections. This strategy demonstrated that the most

significant degeneration of the locus coeruleus (LC) occurred during the early stages of Alzheimer's disease, specifically between Braak stages 1-3. Notably, an analysis of LC signal variation over time across all LC sections during this phase (Figure 8, middle) revealed a pattern that is different from the cross-sectional pattern associated with cognitive normality (LC $pattern_{CN}$, see Figure 4): a reduction in the middle section of the LC while showing an increase trend at the extremities of the LC.

The decline in LC signal observed in early Alzheimer's disease aligns with previous research investigating the early or at-risk phase of the condition. We acknowledge two previous imaging studies addressing this issue, both of which identified a substantial reduction in LC signal, either in individuals genetically predisposed to AD[40] or in a heterogeneous cohort of AD and MCI[138]. Postmortem analysis has similarly revealed the most significant decline in LC volume between Braak stages 0 and 1 in middle LC[136]. Conversely, a substantial sample of older adults exhibited no significant change in LC signal over time, even demonstrating a numerical increase, which was unexpected yet aligned with our findings in the healthy aging cohort[134].

Autopsy investigations have played a crucial role in confirming the early and progressive degeneration of the locus coeruleus in Alzheimer’s disease. The LC, known for its dense population of neuromelanin-pigmented noradrenergic neurons, exhibits substantial neuronal loss in AD, with estimates suggesting that more than half of these neurons may be lost by the time of late-stage disease[135]. Neuropathological assessments have shown that this degeneration often begins early, even in preclinical stages, preceding substantial cortical involvement[136]. Importantly, this loss of neuromelanin-containing neurons tends to follow the trajectory of tau pathology, which is known to first accumulate in the LC before spreading to connected brain

regions[94]. This temporal relationship suggests that LC degeneration may play a seeding or accelerating role in broader neurodegenerative cascades associated with AD[78].

Detailed postmortem histological analyses have further revealed that reductions in neuromelanin pigmentation within the LC are strongly correlated with disease severity and cognitive decline[135]. The extent of neuromelanin depletion has been found to increase across Braak stages, aligning with the progression of tau pathology and neurofibrillary tangle burden[136]. Some studies have also highlighted that neuromelanin-rich neurons are especially vulnerable to tau aggregation and neurodegeneration, suggesting a possible role of neuromelanin in modulating neuronal susceptibility[94]. Moreover, the pigment's known ability to chelate redox-active metals such as iron implicates it in oxidative stress pathways, providing a potential mechanistic link between neuromelanin loss and neuroinflammation[178]. Together, these findings position LC neuromelanin as both a marker of noradrenergic neuron integrity and a window into the molecular mechanisms underpinning AD-related degeneration.

The inability of our study to detect longitudinal change in LC signal during healthy aging or in the later AD group may be attributed to various factors. Minor variations in LC signal may not rise above the threshold of test-retest noise, perhaps necessitating an extended follow-up period beyond the 2-4 year interval to detect substantial change. Moreover, we do not directly assess LC degeneration but instead evaluate LC signal, which is influenced by various factors that might potentially enhance the signal (e.g., alterations in neuromelanin, iron, cell size, or macromolecule content) and mitigate a degeneration-associated decline. We noted significant increases in signal over time for certain people, particularly in the later AD group (with larger magnitudes compared to decreases over time, as illustrated in Figure 11). This may hide LC

degradation and could have contributed to our inability to identify a decline in signal over time in the later AD group if some of these impacts vary more significantly at this stage of the illness.

The dataset revealed a noteworthy significant correlation between ΔLC $pattern_{CN}$ and Δtau binding in Braak stage 1 among people who had no evidence of AD at baseline (Figure 9). We chose to meticulously analyze this sample to identify individuals that exhibit initial indications of Alzheimer's Disease (AD) only after the baseline evaluation, thereby showing how LC signal changes with the onset of AD, as indicated by Δtau in the Braak 1 region of interest (ROI). Three patients were identified with significant Δtau and additional Alzheimer's disease risk variables determined post-hoc. Remarkably, these were the three cases among the group exhibiting the most positive ΔLC $pattern_{CN}$, resulting in a strong positive correlation with Δtau. An increase in LC $pattern_{CN}$ may indicate improvement in LC health; however, we propose that this could result from an elevation in LC signal not secondary to improved LC integrity, but rather due to an alternative cause that could elevate LC signal as a preliminary step prior to LC damage. Biological factors that enhance the LC signal comprise iron accumulation, neuromelanin accumulation, and neuronal swelling. All of these factors could be plausibly enhanced by Alzheimer's disease pathogenesis. Accelerated neuromelanin buildup may arise from APOE ε4-mediated inhibition of VMAT, and there is substantial evidence of elevated iron levels in the brain in Alzheimer's disease, which could be a critical factor leading to neuronal damage[176–179].

Future research must integrate LC imaging with iron imaging to examine this hypothesis. The topography of this change across the LC reveals that the positive shift in LC $pattern_{CN}$ suggests the signal increase predominantly affects the same LC region that shows reduced signal in AD, aligning with the hypothesis that this increase signifies an insult directed at the same LC

subregion that will eventually experience integrity loss. It is significant that the rise in LC signal was seen solely in Aβ-negative patients, whereas nearly all Aβ-positive cases at Braak stage 0 exhibited a decline in LC signal. The limited sample of emerging AD cases does not provide sufficient data for confident conclusions, prompting the inquiry of whether Aβ might inhibit the increase in LC signal.

Numerous studies have demonstrated a substantial association between LC integrity and cognitive performance in healthy individuals, those with mild cognitive impairment, and Alzheimer's disease patients. This work confirms the longitudinal correlation between LC and many cognitive domains, as illustrated in Table 9, which includes global cognition[138,141], episodic memory[140,180], and processing speed[40,137], as documented in the literature. This study established and confirmed the correlation between LC and verbal fluency, logical memory, and object recognition, although it does not specify if any of these associations are stronger than others. To directly investigate the relationship between LC signal and cognition while minimizing spurious correlation from sampling across a wide range of AD severity, we analyzed early and later AD subgroups and identified numerous significant associations. In the early AD subgroup, the sole measure that survived multiple-comparisons correction was the TMT-B test. This finding aligns with extensive evidence regarding the LC-NE system's involvement in executive function and warrants replication in a larger sample (this test was administered to fewer participants than most tests in our sample) and utilizing a paradigm capable of examining specific aspects of executive function (e.g., cognitive flexibility, inhibitory control).

In the later AD cohort, we identified multiple cognitive assessments that correlated with LC integrity, including logical memory, a frequently examined metric in previous LC imaging studies, the majority of which have demonstrated a positive correlation between this type of

memory and LC signal in AD or AD-risk populations[135,138,180]. Our observation of a correlation between LC signal and verbal fluency aligns with a previous publication involving older persons with and without MCI[131].

It is noteworthy that the cognitive metric most closely associated with LC integrity, object recognition, has not been examined in previous LC imaging research to our knowledge. This measure was correlated just at the later stages of Alzheimer's Disease, potentially due to ceiling effects in individuals with milder impairment. We contend that this measure functions as a novelty detection test by requiring participants to identify images of animals that do not exist in nature. A substantial body of literature exists regarding the function of the LC-NE system in novelty detection and the associated deficiencies in novelty detection shown in Alzheimer's disease[181–184]. This test may be particularly sensitive in illustrating the effect of LC damage on behavior in AD, aligning with our capacity to identify a correlation between alterations in LC integrity and variations in task performance.

Our findings indicate that, in healthy aging, our LC metric did not substantially correlate with cognition, except for working memory, aligning with our observation of no LC signal loss in this cohort and previous evidence suggesting minor LC degeneration in healthy aging[136,137]. Consequently, any factors influencing LC signal variability without LC degeneration (such as neuromelanin and iron levels, cell size, or cell density) may have little impact on cognitive performance in healthy aging. Multiple previous studies[40,135,185] also reported no significant correlation between LC signal and cognitive performance in healthy aging, while other investigations identified a correlation between LC signal and memory[129,130,134,186], global cognition[139], and executive function[186]. These correlations may, in certain instances, result from the unintentional inclusion of individuals with

prodromal Alzheimer's disease, as numerous studies lack the capability to screen for brain Alzheimer's disease markers. This ambiguity prompted us to adopt a stringent criterion of healthy aging (absence of Aβ or tau, even in the Braak 0 region of interest). The finding that working memory performance is correlated with LC signal in healthy aging is noteworthy; nonetheless, it contradicts previous research[134] and requires replication.

Despite the growing body of evidence linking LC neuromelanin loss to Alzheimer's disease (AD) progression, several methodological limitations and confounding variables remain insufficiently resolved in both imaging and postmortem literature. One significant concern involves the potential influence of pharmacological treatments on the structural and functional integrity of the LC. Participants in both autopsy and neuromelanin-sensitive MRI (NM-MRI) studies are often on various medications for cognitive, psychiatric, or cardiovascular conditions, which could potentially alter noradrenergic tone or neuromelanin metabolism[128]. However, detailed medication histories are frequently unavailable, similar to our dataset, or inconsistently recorded, making it difficult to disentangle disease-related changes in LC signal from medication-induced alterations. This limitation may particularly impact studies relying on cross-sectional designs or mixed clinical cohorts.

Furthermore, demographic variables such as sex, age, and race may also influence LC neuromelanin signal but are often underexplored or inconsistently accounted for. Age is a well-known factor, as neuromelanin accumulates with age until midlife and may decline later due to neuronal loss, potentially confounding interpretations of LC signal in older adults[129]. Biological sex may also influence noradrenergic regulation due to hormonal modulation of LC activity, yet few studies are sufficiently powered to detect sex differences or stratify findings accordingly[190]. Racial and ethnic variation remains critically understudied; neuromelanin

content may vary with genetic background, and racial disparities in AD risk factors and access to care may further influence LC-related outcomes[191]. In our own dataset, we did not observe significant differences in LC signal based on sex or race; however, the very small proportion of non-White participants limits the strength and generalizability of this conclusion. The predominance of White individuals in both clinical and research samples introduces a bias that may obscure population-specific vulnerabilities or resilience patterns[190]. Future research must address these gaps by incorporating more demographically diverse and well-characterized samples, and by employing statistical models that can account for intersectional factors.

In summary, this doctoral thesis provides the first longitudinal evidence linking locus coeruleus (LC) signal dynamics, tau accumulation, and cognitive performance across the Alzheimer's disease (AD) spectrum using multimodal imaging and automated LC segmentation. The findings reveal that LC degeneration is most pronounced during early AD and that changes in LC signal may precede neuronal loss, offering a potential early biomarker of AD risk. Importantly, our novel multivariate LC metric, LC pattern$_{CN}$, enhances detection of disease-related changes and highlights the LC-NE system’s critical role in memory, novelty detection, and executive function, thereby informing both diagnosis and intervention strategies.

Chapter 6. Limitations, Strengths, Future Directions, and Conclusions

6.1. Strengths and Limitations of LC Segmentation Methods Development Experiments (Chapter 3)

Our work had many strengths, including a substantial sample size comprising both healthy individuals and those with neurodegenerative illness (Sample 1), which was accessible for the majority of the tests performed. A notable strength of our study was the confirmation of Alzheimer's disease diagnosis and severity (Braak stage[187]) for all people in this sample using tau PET imaging. However, our study also possessed certain limitations. Although the FT method demonstrated high scan-rescan reliability, in accordance with other LC segmentation techniques, our sample size for this assessment (n=12) was comparatively limited, constraining the accuracy of ICC estimates. Moreover, although we showed good agreement of our method when utilized with both prevalent NM-MRI sequence types (TSE and MT) and indicated good agreement between these sequences, both types were not accessible for all assessments.

Although we created a test to assess the FT segmentation along the rostrocaudal axis, it would have been preferable to compare its performance against manual segmentation for all LC sections. While previous research has developed manual techniques to segment the entire LC[131], applying these approaches to a sample of this magnitude would be exceedingly laborious. Moreover, the critical validation step about Alzheimer's disease severity would be less effective in certain segments of the LC that exhibit do not show clear signal loss in AD[126].

Consequently, the ICC, DSC, and effect size metrics discussed herein solely represent the performance of the FT method for the middle section of the LC and cannot be extrapolated to the rostral and caudal regions of the LC, despite our 3D structural analyses offering some assurance

that the FT method attains adequate localization of the rostral and caudal LC. As previously mentioned, it would have aligned more closely with other research employing the manual technique if we had acquired NM-MRI images at a higher resolution, given that the fixed-shape LC mask (a 5-voxel cross) included a broader area at this resolution. This may have impeded the performance of the manual technique to some extent, but we endeavored to alleviate this risk by incorporating 4-voxel and 1-voxel manual LC masks. Additionally, concerning resolution, there was diversity among samples in slice thickness, ranging from 1.5 to 2.0 mm. We generally recommend a slice thickness of approximately 1.5 mm for best performance of the FT technique to maximize the number of measurements per LC section. Nonetheless, a slice thickness of 2.0 mm may be enough, as all LC sections were identifiable in every individual at this thickness.

Lastly, although we examined a substantial cohort of healthy older adults and patients within the Alzheimer's disease spectrum, it would be advantageous to evaluate the performance of our technique in Parkinson's disease, another disorder characterized by significant degeneration of the locus coeruleus[173,188,189].

6.2. Strengths and Limitations of longitudinal investigation of LC integrity and cognition (Chapter 4)

This work had numerous strengths as the largest longitudinal LC imaging investigation known in Alzheimer's disease, including the entire spectrum of AD and incorporating PET imaging of tau and Aβ. However, not all participants possessed longitudinal data, and after subgroup split, the sample sizes remained small. It is exciting to contemplate that we may have identified a few instances in the initial phases of conversion to Alzheimer's disease. Nonetheless, their scarcity renders generalization challenging. Moreover, we cannot assert with certainty that these patients will develop Alzheimer's disease, as this hypothesis was predominantly reliant on continuous SUVR scores in the Braak stage 1 ROI. This challenges the boundaries of inference, as the SUVR of the tau tracer is not a quantitative metric and may be more effective in identifying tracer presence exceeding a normal threshold than in quantifying quantities of this Alzheimer's disease marker. Nevertheless, given the rarity of longitudinal studies on the initial onset of Alzheimer's disease in the brain and the significant variations in SUVR among a few individuals, we cautiously interpret these fortuitous observations as indicative of the early stage of Alzheimer's pathophysiology in these subjects.

Another restriction is the potential for circularity, given that our LC metric (LC $pattern_{CN}$) was both calculated and utilized within the same sample. We believe this risk is negligible in our situation, as this metric was established through a group comparison (CN vs AD), and very few analyses in the study were conducted across groups; the most significant findings were noted in analyses limited to participants predominantly from one of these groups. Future research may utilize the LC $pattern_{CN}$ measure established in this study for an out-of-sample analysis to ascertain if this metric facilitates superior diagnostic differentiation compared

to a more rudimentary metric (e.g., entire LC or middle LC signal). While this metric was established to separate CN from AD, it may not facilitate optimal differentiation within AD, specifically regarding the patterns of LC signal that differentiate early from later phases of AD.

6.3. Future Directions

The results of this work provide new understanding of the intricate details of locus coeruleus (LC) signal changes along the Alzheimer's disease (AD) spectrum and open many significant directions for further investigation. Since early AD showed the greatest LC signal drop, future research should incorporate extended follow-up times outside the present 2–4 year range. This would improve the temporal window of preclinical LC degeneration and enable identification of more slow or delayed signal alterations that might develop in later phases of AD. Furthermore, another important measure would be extended tracking to ascertain whether the transient rise in LC signal observed close to the start of tau pathology is predictive of later degeneration and whether this characteristic can be exploited as a consistent early biomarker.

Though our work concentrated on normal AD development, it is important to evaluate LC signal trajectories in variant forms of AD and other neurodegenerative dementias (e.g., Parkinson's disease dementia, Lewy body dementia, frontotemporal dementia). By means of comparison of LC signal patterns under various settings, one can construct disease-specific neurodegenerative signatures and clarify the function of the LC-NE system over several neuropathological processes which could be useful for potential as biomarker supporting differential diagnosis.

Moreover, analyzing LC signal responsiveness to treatment interventions in AD patients as well as cognitively healthy people becomes a crucial next step. Future work could target studying neuroprotective treatments, as well as pre- and post-treatment NM-MRI scans to evaluate whether particular interventions, such as cholinesterase inhibitors, noradrenergic medications, or lifestyle changes (e.g., exercise, mindfulness), can protect or decrease LC damage and consequent cognitive deterioration. Emerging data imply that, depending on disease

status, pharmaceutical regulation of the noradrenergic system can produce varied cognitive effects. For instance, although having no impact in healthy controls, clonidine, an alpha-2 adrenergic agonist, was demonstrated to cause cognitive abnormalities in subjects with pre-existing cognitive impairment. Especially with early-stage or prodromal AD, there are results that emphasize the significance of looking at how different pharmacological drugs change LC signal and affect cognition[190]. Also, another study done by our lab showed how the LC imaging ability in help to decide who would benefit from noradrenergic drugs used to treat neuropsychiatric symptoms like agitation and aggressivity[126]. By establishing these relationships, focused treatments will be discovered and created to support LC function and stop neurodegeneration.

Since our FDA cleared funnel-tip (FT) LC segmentation technique (NM 101 software), has shown great accuracy and repeatability, future endeavors should use it to evaluate generalizability over several separate cohorts around the world. Also, integrate multimodal imaging (e.g., iron-sensitive MRI sequences, diffusion tensor imaging) to better define structural and biological sources to LC signal variability.

Lastly, we see LC imaging as a potential technique to identify people at high risk for AD even before overt cognitive signs emerge. To fully understand the function of the LC-NE system in Alzheimer's disease, future studies should aim to combine longitudinal imaging, cross-disease comparisons, and therapeutic intervention trials employing consistent LC segmentation techniques. These guidelines will not only deepen our knowledge of AD pathophysiology but also help to create new clinical instruments for early diagnosis, disease monitoring, and focused therapy.

6.4. Conclusions

This doctoral thesis advances our understanding of locus coeruleus (LC) signal change and its significance across the Alzheimer's disease spectrum by integrating longitudinal neuromelanin-sensitive MRI (NM-MRI), tau and amyloid PET imaging, and cognitive assessments. Through this multifaceted approach, we offer critical insight into both the timing and behavioral relevance of LC degeneration, as well as a novel, validated automated segmentation method (FT method) that supports robust and scalable LC imaging in both research and potential clinical settings. Developing this method was essential to support the findings reported here but also has the potential to accelerate research on this topic by providing a convenient tool to extract useful information about the LC-NE system integrity in AD that could be used in future by researchers examining its clinical and pathophysiological correlates. As a potential biomarker, this tool could have potential for multiple applications in AD or other neurodegenerative conditions including supporting differential diagnosis, early diagnosis, predicting treatment response, and monitoring progression of neurodegeneration. While it is not yet proven as a clinically useful biomarker, this tool has already proceeded a long way on the path of steps needed for a biomarker. Started with development of the LC segmentation algorithm, demonstration and validation of its performance as a marker of LC degeneration (Aim 1), harmonization of LC signal across scanners using ComBat[196] to allow results to be compared across scanners, translation of the algorithm into a commercial software package suitable for clinical use, and regulatory clearance by the FDA. Finally, the next step would be conducting a large and well-controlled study in AD showing clinical utility for the biomarker applications listed above.

NM-MRI is considered a new inexpensive and reliable tool to measure the LC signal in

vivo. Our results showed that our FT method of LC segmentation has high agreement with a manual method it is highly reproducible, eliminates interrater concerns, consistently targets the LC in 3D space, and has a better ability to detect AD-related LC degeneration (Cohen's d = 0.64). Unlike other methods that either fail to capture subregional alterations or show reduced performance in advanced stages of degeneration, the FT method supports accurate, full-length segmentation of the LC along its rostrocaudal axis. Standardizing LC integrity assessments between individuals and scanners not only lessens the burden and subjectivity of manual tracing but also makes large-scale investigations more practical.

Our longitudinal data suggest that LC signal loss is most noticeable in early-stage AD, in line with postmortem and imaging data displaying middle LC susceptibility during the earliest phases of disease progression. Especially in those lacking AD pathology at baseline, we found a counterintuitive rise in LC signal over time linked with early tau accumulation in Braak stage I. Rather than an increase in LC function, this surprising signal spike may reflect pathophysiological precursors to LC degeneration—such as iron buildup, neuroinflammation, or alterations in neuromelanin metabolism. These results imply that LC signal dynamics are temporally sensitive and non-linear, which emphasizes the need of longitudinal imaging in catching transitory phases maybe indicating neurodegeneration and the potential benefit of multimodal imaging, for instance to monitor iron content (e.g. using quantitative susceptibility mapping) at the same time as NM-MRI.

Our results confirm earlier research tying LC signal to episodic memory ability, especially logical memory, and extend this knowledge by pointing to a robust correlation between LC integrity and object recognition—a cognitive domain that is not being studied in the literature in terms of LC function and AD. We interpret this result in the larger context of the

function of the LC-norepinephrine (LC-NE) system in novelty detection and suggest that poor object identification in later-stage AD may represent a breakdown in novelty-related brain processing. Other domains, including executive function (e.g., TMT-B), also exhibited substantial correlations with LC integrity, especially in early AD. While working memory emerged as the only LC-correlated domain in healthy aging, consistent with maintained LC structure in this group,

These findings taken together indicate the LC imaging is an invaluable tool for research into the role of the LC-NE system in the pathophysiology of AD. Furthermore, it is a possible early biomarker for AD risk. When combined with PET imaging and cognitive tests, the FT segmentation approach helps to more precisely define the LC's involvement during and even before the onset of AD. Moreover, the discovery of signal changes in people prior to appearance cognitive symptoms emphasizes the biomarker possibility of LC imaging as a marker of AD risk.

References

1. Jack CR, Bennett DA, Blennow K, Carrillo MC, Dunn B, Haeberlein SB, et al. NIA-AA Research Framework: Toward a biological definition of Alzheimer's disease. Alzheimer's and Dementia. 2018;14:535–562.

2. Thies W, Bleiler L. 2011 Alzheimer's disease facts and figures. Alzheimer's and Dementia. 2011;7:208–244.

3. Livingston G, Huntley J, Sommerlad A, Ames D, Ballard C, Banerjee S, et al. Dementia prevention, intervention, and care: 2020 report of the Lancet Commission. The Lancet. 2020;396:413–446.

4. Wimo A, Guerchet M, Ali GC, Wu YT, Prina AM, Winblad B, et al. The worldwide costs of dementia 2015 and comparisons with 2010. Alzheimer's and Dementia. 2017;13:1–7.

5. Martin Prince A, Wimo A, Guerchet M, Gemma-Claire Ali M, Wu Y-T, Prina M, et al. World Alzheimer Report 2015 The Global Impact of Dementia An AnAlysIs of prevAlence, IncIDence, cosT AnD TrenDs.

6. Health Organization W. Global status report on the public health response to dementia. 2021.

7. Safiri S, Ghaffari Jolfayi A, Fazlollahi A, Morsali S, Sarkesh A, Daei Sorkhabi A, et al. Alzheimer's disease: a comprehensive review of epidemiology, risk factors, symptoms diagnosis, management, caregiving, advanced treatments and associated challenges. Front Med (Lausanne). 2024;11.

8. 2023 Alzheimer's disease facts and figures. Alzheimer's and Dementia. 2023;19:1598–1695.

9. Corder EH, Saunders AM, Gaskell PC, Pericak-Vance MA, Strittmatter WJ, Roses AD, et al. some 14. The frequency of APOE-E4 was not elevated in these and 12 other early onset families (6). Members of 42 late onset. vol. 261. 1993.

10. Farrer LA, Cupples ; L Adrienne, Haines JL, Hyman B, Kukull WA, Mayeux R, et al. Effects of Age, Sex, and Ethnicity on the Association Between Apolipoprotein E Genotype and Alzheimer Disease A Meta-analysis.

11. Selkoe DJ, Hardy J. The amyloid hypothesis of Alzheimer's disease at 25 years. EMBO Mol Med. 2016;8:595–608.

12. Long JM, Holtzman DM. Alzheimer Disease: An Update on Pathobiology and Treatment Strategies. Cell. 2019;179:312–339.

13. De Strooper B, Karran E. The Cellular Phase of Alzheimer's Disease. Cell. 2016;164:603–615.

14. Guerreiro RJ, Baquero M, Blesa R, Boada M, Brás JM, Bullido MJ, et al. Genetic screening of Alzheimer's disease genes in Iberian and African samples yields novel mutations in presenilins and APP. Neurobiol Aging. 2010;31:725–731.

15. Livingston G, Huntley J, Sommerlad A, Ames D, Ballard C, Banerjee S, et al. Dementia prevention, intervention, and care: 2020 report of the Lancet Commission. The Lancet. 2020;396:413–446.

16. Norton S, Matthews FE, Barnes DE, Yaffe K, Brayne C. Potential for primary prevention of Alzheimer's disease: An analysis of population-based data. Lancet Neurol. 2014;13:788–794.

17. Scarmeas N, Stern Y, Tang MX, Mayeux R, Luchsinger JA. Mediterranean diet and risk for Alzheimer's disease. Ann Neurol. 2006;59:912–921.

18. Stern Y. Cognitive reserve in ageing and Alzheimer's disease. Lancet Neurol. 2012;11:1006–1012.

19. Gorelick PB, Scuteri A, Black SE, Decarli C, Greenberg SM, Iadecola C, et al. Vascular contributions to cognitive impairment and dementia: A statement for healthcare professionals from the American Heart Association/American Stroke Association. Stroke. 2011;42:2672–2713.

20. De La Monte SM. Contributions of Brain Insulin Resistance and Deficiency in Amyloid-Related Neurodegeneration in Alzheimer's Disease.

21. Ngandu T, Lehtisalo J, Solomon A, Levälahti E, Ahtiluoto S, Antikainen R, et al. A 2 year multidomain intervention of diet, exercise, cognitive training, and vascular risk monitoring versus control to prevent cognitive decline in at-risk elderly people (FINGER): A randomised controlled trial. The Lancet. 2015;385:2255–2263.

22. Peters R, Ee N, Peters J, Booth A, Mudway I, Anstey KJ. Air Pollution and Dementia: A Systematic Review. Journal of Alzheimer's Disease. 2019;70:S145–S163.

23. Pettigrew C, Soldan A. Defining Cognitive Reserve and Implications for Cognitive Aging. Curr Neurol Neurosci Rep. 2019;19.

24. Sweeney MD, Sagare AP, Zlokovic B V. Blood-brain barrier breakdown in Alzheimer disease and other neurodegenerative disorders. Nat Rev Neurol. 2018;14:133–150.

25. Chen X, Drew J, Berney W, Lei W. Neuroprotective natural products for alzheimer's disease. Cells. 2021;10.

26. Sun P, Yin JB, Liu LH, Guo J, Wang SH, Qu CH, et al. Protective role of dihydromyricetin in Alzheimer's disease rat model associated with activating AMPK/SIRT1 signaling pathway. Biosci Rep. 2019;39.

27. Cali F, Cantone M, Cosentino FII, Lanza G, Ruggeri G, Chiavetta V, et al. Interpreting genetic variants: Hints from a family cluster of Parkinson's disease. J Parkinsons Dis. 2019;9:203–206.

28. Maseeha Banu, H.N Prakash. Forecasting alzheimer's disease in its early stages with the use of machine learning algorithms. Global Journal of Engineering and Technology Advances. 2024;20:231–241.

29. Erkkinen MG, Kim MO, Geschwind MD. Clinical neurology and epidemiology of the major neurodegenerative diseases. Cold Spring Harb Perspect Biol. 2018;10.

30. Mohamed MAG, Mahmud WMHW, Izaham RMAR. Hippocampus Segmentation of Brain MRI Images for Possible Progression Detection of Alzheimer's Disease. Journal of Advanced Research in Applied Sciences and Engineering Technology. 2023;32:234–241.

31. Bourin M. How to Diagnose an Alzheimer Disease? Theranostics of Brain, Spine & Neural Disorders. 2017;01.

32. Odusami M, Maskeliūnas R, Damaševičius R. An Intelligent System for Early Recognition of Alzheimer's Disease Using Neuroimaging. Sensors. 2022;22.

33. Dickerson BC, McGinnis SM, Xia C, Price BH, Atri A, Murray ME, et al. Approach to atypical Alzheimer's disease and case studies of the major subtypes. CNS Spectr, vol. 22, Cambridge University Press; 2017. p. 439–449.

34. Paroni G, BP, & SD. Understanding the amyloid hypothesis in alzheimer's disease. Journal of Alzheimer S Disease,. 2019;2:493–510.

35. Braak H, Braak E. Frequency of stages of Alzheimer-related lesions in different age categories. Neurobiol Aging. 1997;18.

36. Therriault J, Pascoal TA, Lussier FZ, Tissot C, Chamoun M, Bezgin G, et al. Biomarker modeling of Alzheimer's disease using PET-based Braak staging. Nat Aging. 2022;2:526–535.

37. Rullmann M, Brendel M, Schroeter ML, Saur D, Levin J, Perneczky RG, et al. Multicenter18F-PI-2620 PET for In Vivo Braak Staging of Tau Pathology in Alzheimer's Disease. Biomolecules. 2022;12.

38. Attems J, Lintner F, Jellinger KA. Olfactory involvement in aging and Alzheimer's disease: An autopsy study. vol. 7. IOS Press; 2005.

39. Alorfi NM. Public Awareness of Alzheimer's Disease: A Cross-Sectional Study from Saudi Arabia. Int J Gen Med. 2022;15:7535–7546.

40. Jacobs HIL, Becker JA, Kwong K, Munera D, Ramirez-Gomez L, Engels-Domínguez N, et al. Waning locus coeruleus integrity precedes cortical tau accrual in preclinical autosomal dominant Alzheimer's disease. Alzheimer's and Dementia. 2023;19:169–180.

41. Baldock D, Miller JB, Leger GC, Banks SJ. Memory Test Performance on Analogous Verbal and Nonverbal Memory Tests in Patients with Frontotemporal Dementia and Alzheimer's Disease. Dement Geriatr Cogn Dis Extra. 2016;6:20–27.

42. Zachary A Miller, et al. TDP-43 frontotemporal lobar degeneration and autoimmune disease. J Neurol Neurosurg Psychiatry. 2013;84:946.

43. Valera E, Spencer B, Masliah E. Immunotherapeutic Approaches Targeting Amyloid-β, α-Synuclein, and Tau for the Treatment of Neurodegenerative Disorders. Neurotherapeutics. 2016;13:179–189.

44. Corriveau-Lecavalier N, Barnard LR, Botha H, Graff-Radford J, Ramanan VK, Lee J, et al. Uncovering the distinct macro-scale anatomy of dysexecutive and behavioural degenerative diseases. Brain. 2024;147:1483–1496.

45. Loi SM, Eratne D, Goh AMY, Wibawa P, Farrand S, Kelso W, et al. A 10 year retrospective cohort study of inpatients with younger-onset dementia. Int J Geriatr Psychiatry. 2021;36:294–301.

46. Bruun M, Rhodius-Meester HFM, Koikkalainen J, Baroni M, Gjerum L, Lemstra AW, et al. Evaluating combinations of diagnostic tests to discriminate different dementia types. Alzheimer's and Dementia: Diagnosis, Assessment and Disease Monitoring. 2018;10:509–518.

47. Steketee RME, Bron EE, Meijboom R, Houston GC, Klein S, Mutsaerts HJMM, et al. Early-stage differentiation between presenile Alzheimer's disease and frontotemporal dementia using arterial spin labeling MRI. Eur Radiol. 2016;26:244–253.

48. Burke JF, Albin RL, Koeppe RA, Giordani B, Kilbourn MR, Gilman S, et al. Assessment of mild dementia with amyloid and dopamine terminal positron emission tomography. Brain. 2011;134:1647–1657.

49. Rizzo G, Arcuti S, Copetti M, Alessandria M, Savica R, Fontana A, et al. Accuracy of clinical diagnosis of dementia with Lewy bodies: A systematic review and meta-analysis. J Neurol Neurosurg Psychiatry. 2018;89:358–366.

50. Van Vliet D, De Vugt ME, Bakker C, Pijnenburg YAL, Vernooij-Dassen MJFJ, Koopmans RTCM, et al. Time to diagnosis in young-onset dementia as compared with late-onset dementia. Psychol Med. 2013;43:423–432.

51. Yeo JM, Lim X, Khan Z, Pal S. SYSTEMATIC REVIEW OF THE DIAGNOSTIC UTILITY OF SPECT IMAGING IN DEMENTIA. J Neurol Neurosurg Psychiatry. 2013;84:e2.209-e2.

52. Turnbull MT, Boskovic Z, Coulson EJ. Acute down-regulation of BDNF signaling does not replicate exacerbated amyloid-β levels and cognitive impairment induced by cholinergic basal forebrain lesion. Front Mol Neurosci. 2018;11.

53. Das S. Alzheimer's Type Neuropathological Changes in a Patient with Depression and Anxiety: A Case Report and Literature Review of Neuropathological Correlates of Neuropsychiatric Symptoms in Alzheimer's Disease. Case Rep Neurol Med. 2023;2023:1–3.

54. Hampel H, Mesulam MM, Cuello AC, Farlow MR, Giacobini E, Grossberg GT, et al. The cholinergic system in the pathophysiology and treatment of Alzheimer's disease. Brain. 2018;141:1917–1933.

55. Cavedo E, Grothe MJ, Colliot O, Lista S, Chupin M, Dormont Di, et al. Reduced basal forebrain atrophy progression in a randomized Donepezil trial in prodromal Alzheimer's disease. Sci Rep. 2017;7.

56. Eu WZ, Chen YJ, Chen WT, Wu KY, Tsai CY, Cheng SJ, et al. The effect of nerve growth factor on supporting spatial memory depends upon hippocampal cholinergic innervation. Transl Psychiatry. 2021;11.

57. Ademiluyi AO, Oyesomi AA, Ogunsuyi OB, Oyeleye SI, Oboh G. Influence of cooking on the neuroprotective properties of pepper (bird pepper and cayenne pepper) varieties in scopolamine-induced neurotoxicity in rats. J Food Process Preserv. 2020;44.

58. Sultzer DL, Leskin LP, Melrose RJ, Harwood DG, Narvaez TA, Ando TK, et al. Neurobiology of delusions, memory, and insight in alzheimer disease. American Journal of Geriatric Psychiatry. 2014;22:1346–1355.

59. Rosenberg PB, Nowrangi MA, Lyketsos CG. Neuropsychiatric symptoms in Alzheimer's disease: What might be associated brain circuits? Mol Aspects Med. 2015;43–44:25–37.

60. Rothenberg KG. Assessment and Management of Psychiatric Symptoms in Alzheimer's Disease. Biomed J Sci Tech Res. 2020;28.

61. Betts MJ, Cardenas-Blanco A, Kanowski M, Jessen F, Düzel E. In vivo MRI assessment of the human locus coeruleus along its rostrocaudal extent in young and older adults. Neuroimage. 2017;163:150–159.

62. Watanabe T, Tan Z, Wang X, Martinez-Hernandez A, Frahm J. Magnetic resonance imaging of noradrenergic neurons. Brain Struct Funct. 2019;224:1609–1625.

63. Kelly SC, He B, Perez SE, Ginsberg SD, Mufson EJ, Counts SE. Locus coeruleus cellular and molecular pathology during the progression of Alzheimer's disease. Acta Neuropathol Commun. 2017;5:8.

64. Sommerauer M, Fedorova TD, Hansen AK, Knudsen K, Otto M, Jeppesen J, et al. Evaluation of the noradrenergic system in Parkinson's disease: An 11 C-MeNER PET and neuromelanin MRI study. Brain. 2018;141:496–504.

65. Betts MJ, Kirilina E, Otaduy MCG, Ivanov D, Acosta-Cabronero J, Callaghan MF, et al. Locus coeruleus imaging as a biomarker for noradrenergic dysfunction in neurodegenerative diseases. Brain. 2019;142:2558–2571.

66. Sullivan RM, Stackenwalt G, Nasr F, Lemon C, Wilson DA. Association of an odor with activation of olfactory bulb noradrenergic β-receptors or locus coeruleus stimulation is sufficient to produce learned approach responses to that odor in neonatal rats. Behavioral Neuroscience. 2000;114:957–962.

67. Ye R, Hezemans FH, O'Callaghan C, Tsvetanov KA, Rua C, Jones PS, et al. Reduced locus coeruleus integrity linked to response inhibition deficits in parkinsonian disorders. 2021.

68. Theofilas P, Ehrenberg AJ, Dunlop S, Di Lorenzo Alho AT, Nguy A, Leite REP, et al. Locus coeruleus volume and cell population changes during Alzheimer's disease progression: A stereological study in human postmortem brains with potential implication for early-stage biomarker discovery. Alzheimer's and Dementia. 2017;13:236–246.

69. O'callaghan C, Hezemans FH, Ye R, Rua C, Jones PS, Murley AG, et al. Locus coeruleus integrity and the effect of atomoxetine on response inhibition in Parkinson's disease. https://doi.org/10.1093/brain/awab142/6203808.

70. Li J, Wei Y, Zhou J, Zou H, Ma L, Liu C, et al. Activation of locus coeruleus-spinal cord noradrenergic neurons alleviates neuropathic pain in mice via reducing neuroinflammation from astrocytes and microglia in spinal dorsal horn. J Neuroinflammation. 2022;19.

71. Eduardo E. Benarroch. The locus ceruleus norepinephrine system. Neurology. 2009;73 (20):1699–1704.

72. Robertson SD, Plummer NW, De Marchena J, Jensen P. Developmental origins of central norepinephrine neuron diversity. Nat Neurosci. 2013;16:1016–1023.

73. Hansen N, Manahan-Vaughan D. Locus Coeruleus Stimulation Facilitates Long-Term Depression in the Dentate Gyrus That Requires Activation of β-Adrenergic Receptors. Cerebral Cortex. 2015;25:1889–1896.

74. Hayat H, Regev N, Matosevich N, Sales A, Paredes-Rodriguez E, Krom AJ, et al. Locus coeruleus norepinephrine activity mediates sensory-evoked awakenings from sleep. 2020.

75. Carter ME, Brill J, Bonnavion P, Huguenard JR, Huerta R, De Lecea L. Mechanism for Hypocretin-mediated sleep-to-wake transitions. Proc Natl Acad Sci U S A. 2012;109.

76. Vazey EM, Aston-Jones G. Designer receptor manipulations reveal a role of the locus coeruleus noradrenergic system in isoflurane general anesthesia. Proc Natl Acad Sci U S A. 2014;111:3859–3864.

77. Hofmeister J, Sterpenich V. A role for the locus ceruleus in reward processing: Encoding behavioral energy required for goal-directed actions. Journal of Neuroscience. 2015;35:10387–10389.

78. Heneka MT, Nadrigny F, Regen T, Martinez-Hernandez A, Dumitrescu-Ozimek L, Terwel D, et al. Locus ceruleus controls Alzheimer's disease pathology by modulating microglial functions through norepinephrine. Proc Natl Acad Sci U S A. 2010;107:6058–6063.

79. Zucca FA, Segura-Aguilar J, Ferrari E, Muñoz P, Paris I, Sulzer D, et al. Interactions of iron, dopamine and neuromelanin pathways in brain aging and Parkinson's disease. Prog Neurobiol. 2017;155:96–119.

80. Morris LS, McCall JG, Charney DS, Murrough JW. The role of the locus coeruleus in the generation of pathological anxiety. Brain Neurosci Adv. 2020;4:239821282093032.

81. Grandjean A, Mathieu A, Chen S, Widmann A, Wetzel N, Bidet-Caulet A. Enhancing tonic arousal improves voluntary but not involuntary attention in humans. 2024.

82. Bast N, Poustka L, Freitag CM. The locus coeruleus–norepinephrine system as pacemaker of attention – a developmental mechanism of derailed attentional function in autism spectrum disorder. European Journal of Neuroscience. 2018;47:115–125.

83. Matchett BJ, Grinberg LT, Theofilas P, Murray ME. The mechanistic link between selective vulnerability of the locus coeruleus and neurodegeneration in Alzheimer's disease. Acta Neuropathol. 2021;141:631–650.

84. Hussain S, Menchaca I, Shalchy MA, Yaghoubi K, Langley J, Seitz AR, et al. Locus coeruleus integrity predicts ease of attaining and maintaining neural states of high attentiveness. 2022.

85. Iannitelli AF, Kelberman MA, Lustberg DJ, Korukonda A, McCann KE, Mulvey B, et al. The Neurotoxin DSP-4 Dysregulates the Locus Coeruleus-Norepinephrine System and Recapitulates Molecular and Behavioral Aspects of Prodromal Neurodegenerative Disease. ENeuro. 2023;10.

86. Bekar LK, Wei HS, Nedergaard M. The locus coeruleus-norepinephrine network optimizes coupling of cerebral blood volume with oxygen demand. Journal of Cerebral Blood Flow and Metabolism. 2012;32:2135–2145.

87. Takeuchi T, Duszkiewicz AJ, Sonneborn A, Spooner PA, Yamasaki M, Watanabe M, et al. Locus coeruleus and dopaminergic consolidation of everyday memory. Nature. 2016;537:357–362.

88. Beas BS, Wright BJ, Skirzewski M, Leng Y, Hyun JH, Koita O, et al. The locus coeruleus drives disinhibition in the midline thalamus via a dopaminergic mechanism. Nat Neurosci. 2018;21:963–973.

89. Martins ARO, Froemke RC. Coordinated forms of noradrenergic plasticity in the locus coeruleus and primary auditory cortex. Nat Neurosci. 2015;18:1483–1492.

90. Liu Y, Chen J, Li Q, Guo YX, Chen YJ, Zhao YJ. Locus coeruleus activation contributes to masseter muscle overactivity induced by chronic restraint stress in mice. Neuroreport. 2024;35:763–770.

91. Rorabaugh JM, Chalermpalanupap T, Botz-Zapp CA, Fu VM, Lembeck NA, Cohen RM, et al. Chemogenetic locus coeruleus activation restores reversal learning in a rat model of Alzheimer's disease. Brain. 2017;140:3023–3038.

92. Carter ME, Yizhar O, Chikahisa S, Nguyen H, Adamantidis A, Nishino S, et al. Tuning arousal with optogenetic modulation of locus coeruleus neurons. Nat Neurosci. 2010;13:1526–1535.

93. Hansen N, Manahan-Vaughan D. Locus Coeruleus Stimulation Facilitates Long-Term Depression in the Dentate Gyrus That Requires Activation of β-Adrenergic Receptors. Cerebral Cortex. 2015;25:1889–1896.

94. Kelly SC, He B, Perez SE, Ginsberg SD, Mufson EJ, Counts SE. Locus coeruleus cellular and molecular pathology during the progression of Alzheimer's disease. Acta Neuropathol Commun. 2017;5:8.

95. Jacki M. Rorabaugh, et al. Chemogenetic locus coeruleus activation restores reversal learning in a rat model of Alzheimer's disease. Brain. 2017;140:2770–2773.

96. Wang Q. Amyloid β redirects norepinephrine signaling to activate the pathogenic GSK3β/tau cascade. Alzheimer's & Dementia. 2020;16.

97. Betts MJ, Cardenas-Blanco A, Kanowski M, Jessen F, Düzel E. In vivo MRI assessment of the human locus coeruleus along its rostrocaudal extent in young and older adults. Neuroimage. 2017;163.

98. Bennett IJ, Langley J, Sun A, Solis K, Seitz AR, Hu XP. Locus Coeruleus Contrast and Diffusivity: Effects of Age and Relations to Memory. 2024.

99. Betts MJ, Kirilina E, Otaduy MCG, Ivanov D, Acosta-Cabronero J, Callaghan MF, et al. Locus coeruleus imaging as a biomarker for noradrenergic dysfunction in neurodegenerative diseases. Brain. 2019;142:2558–2571.

100. Bueichekú E, Diez I, Kim CM, Becker JA, Koops EA, Kwong K, et al. Spatiotemporal patterns of locus coeruleus integrity predict cortical tau and cognition. Nat Aging. 2024;4:625–637.

101. Mather M, Harley CW. The Locus Coeruleus: Essential for Maintaining Cognitive Function and the Aging Brain. Trends Cogn Sci. 2016;20.

102. Zarow C, Lyness SA, Mortimer JA, Chui HC. Neuronal Loss Is Greater in the Locus Coeruleus Than Nucleus Basalis and Substantia Nigra in Alzheimer and Parkinson Diseases. Arch Neurol. 2003;60:337.

103. Theofilas P, Ehrenberg AJ, Dunlop S, Di Lorenzo Alho AT, Nguy A, Leite REP, et al. Locus coeruleus volume and cell population changes during Alzheimer's disease progression: A stereological study in human postmortem brains with potential implication for early-stage biomarker discovery. Alzheimer's and Dementia. 2017;13.

104. Kalinin S, Polak PE, Lin SX, Sakharkar AJ, Pandey SC, Feinstein DL. The noradrenaline precursor L-DOPS reduces pathology in a mouse model of Alzheimer's disease. Neurobiol Aging. 2012;33:1651–1663.

105. Sperling RA, Donohue MC, Raman R, Sun CK, Yaari R, Holdridge K, et al. Association of Factors with Elevated Amyloid Burden in Clinically Normal Older Individuals. JAMA Neurol. 2020;77:735–745.

106. Young CB, Winer JR, Younes K, Cody KA, Betthauser TJ, Johnson SC, et al. Divergent Cortical Tau Positron Emission Tomography Patterns among Patients with Preclinical Alzheimer Disease. JAMA Neurol. 2022;79:592–603.

107. Liu J, van Beusekom H, Bu X, Chen G, Henrique Rosado de Castro P, Chen X, et al. Preserving cognitive function in patients with Alzheimer's disease: The Alzheimer's disease neuroprotection research initiative (ADNRI). Neuroprotection. 2023;1:84–98.

108. Salvatore C, Cerasa A, Castiglioni I. MRI characterizes the progressive course of AD and predicts conversion to Alzheimer's dementia 24 months before probable diagnosis. Front Aging Neurosci. 2018;10.

109. Wachinger C, Reuter M, Klein T. DeepNAT: Deep convolutional neural network for segmenting neuroanatomy. Neuroimage. 2018;170:434–445.

110. Matchett BJ, Grinberg LT, Theofilas P, Murray ME. The mechanistic link between selective vulnerability of the locus coeruleus and neurodegeneration in Alzheimer's disease. Acta Neuropathol. 2021;141:631–650.

111. Giorgi FS, Galgani A, Puglisi-Allegra S, Limanaqi F, Busceti CL, Fornai F. Locus Coeruleus and neurovascular unit: From its role in physiology to its potential role in Alzheimer's disease pathogenesis. J Neurosci Res. 2020;98:2406–2434.

112. Martí-Juan G, Sanroma-Guell G, Piella G. A survey on machine and statistical learning for longitudinal analysis of neuroimaging data in Alzheimer's disease. Comput Methods Programs Biomed. 2020;189.

113. Ali I, Manda VK. Artificial intelligence for predicting progression and personalizing healthcare to Alzheimer's disease patients. AI-Driven Personalized Healthcare Solutions, IGI Global; 2025. p. 155–189.

114. Rizzi L, Aventurato ÍK, Balthazar MLF. Neuroimaging Research on Dementia in Brazil in the Last Decade: Scientometric Analysis, Challenges, and Peculiarities. Front Neurol. 2021;12.

115. Lizarraga G, Li C, Cabrerizo M, Barker W, Loewenstein DA, Duara R, et al. A neuroimaging web services interface as a cyber physical system for medical imaging and data management in brain research: Design study. JMIR Med Inform. 2018;20.

116. Priovoulos N, Jacobs HIL, Ivanov D, Uludağ K, Verhey FRJ, Poser BA. High-resolution in vivo imaging of human locus coeruleus by magnetization transfer MRI at 3T and 7T. Neuroimage. 2018;168:427–436.

117. Riley E, Cicero N, Swallow K, De Rosa E, Anderson A. Locus coeruleus neuromelanin accumulation and dissipation across the lifespan. 2023.

118. Watanabe T, Tan Z, Wang X, Martinez-Hernandez A, Frahm J. Magnetic resonance imaging of noradrenergic neurons. Brain Struct Funct. 2019;224:1609–1625.

119. Xing Y, Sapuan A, Dineen RA, Auer DP. Life span pigmentation changes of the substantia nigra detected by neuromelanin-sensitive MRI. Movement Disorders. 2018;33:1792–1799.

120. Priovoulos N, Jacobs HIL, Ivanov D, Uludağ K, Verhey FRJ, Poser BA. High-resolution in vivo imaging of human locus coeruleus by magnetization transfer MRI at 3T and 7T. Neuroimage. 2018;168:427–436.

121. Simões RM, Castro Caldas A, Grilo J, Correia D, Guerreiro C, Pita Lobo P, et al. A distinct neuromelanin magnetic resonance imaging pattern in parkinsonian multiple system atrophy. BMC Neurol. 2020;20.

122. Tang F, Liu H, Zhang XJ, Zheng HH, Dai YM, Zheng LY, et al. Evidence for Dopamine Abnormalities Following Acute Methamphetamine Exposure Assessed by Neuromelanin-Sensitive Magnetic Resonance Imaging. Front Aging Neurosci. 2022;14.

123. Madelung CF, Meder D, Fuglsang SA, Marques MM, Boer VO, Madsen KH, et al. Locus Coeruleus Shows a Spatial Pattern of Structural Disintegration in Parkinson's Disease. Movement Disorders. 2022;37:479–489.

124. Bachman SL, Dahl MJ, Werkle-Bergner M, Düzel S, Forlim CG, Lindenberger U, et al. Locus coeruleus MRI contrast is associated with cortical thickness in older adults. Neurobiol Aging. 2021;100:72–82.

125. Madelung CF, Meder D, Fuglsang SA, Marques MM, Boer VO, Madsen KH, et al. The locus coeruleus shows a spatial pattern of structural disintegration in Parkinson's disease. 2021.

126. Ye R, Rua C, O'Callaghan C, Jones PS, Hezemans FH, Kaalund SS, et al. An in vivo probabilistic atlas of the human locus coeruleus at ultra-high field. Neuroimage. 2021;225:117487.

127. Beardmore R, Durkin M, Zayee-Mellick F, Lau LC, Nicoll JAR, Holmes C, et al. Changes in the locus coeruleus during the course of Alzheimer's disease and their relationship to cortical pathology. Neuropathol Appl Neurobiol. 2024;50.

128. Cassidy CM, Therriault J, Pascoal TA, Cheung V, Savard M, Tuominen L, et al. Association of locus coeruleus integrity with Braak stage and neuropsychiatric symptom severity in Alzheimer's disease. Neuropsychopharmacology. 2022;47:1128–1136.

129. Zhou C, Guo T, Wu J, Wang L, Bai X, Gao T, et al. Locus Coeruleus Degeneration Correlated with Levodopa Resistance in Parkinson's Disease: A Retrospective Analysis. J Parkinsons Dis. 2021;11:1631–1640.

130. Clewett D V., Lee TH, Greening S, Ponzio A, Margalit E, Mather M. Neuromelanin marks the spot: identifying a locus coeruleus biomarker of cognitive reserve in healthy aging. Neurobiol Aging. 2016;37.

131. Liu KY, Acosta-Cabronero J, Cardenas-Blanco A, Loane C, Berry AJ, Betts MJ, et al. In vivo visualization of age-related differences in the locus coeruleus. Neurobiol Aging. 2019;74:101–111.

132. Dahl MJ, Mather M, Düzel S, Bodammer NC, Lindenberger U, Kühn S, et al. Rostral locus coeruleus integrity is associated with better memory performance in older adults. Nat Hum Behav. 2019;3.

133. Jeremy A Elman, Olivia K Puckett, Asad Beck, Christine Fennema-Notestine, Latonya K Cross, Anders M Dale, et al. MRI-assessed locus coeruleus integrity is heritable and associated with cognition, Alzheimer's risk, and sleep-wake disturbance. Alzheimer's Dement. 2021;17:1017–1025.

134. Van Egroo M, Riphagen JM, Ashton NJ, Janelidze S, Sperling RA, Johnson KA, et al. Ultra-high field imaging, plasma markers and autopsy data uncover a specific rostral locus coeruleus vulnerability to hyperphosphorylated tau. Mol Psychiatry. 2023;28:2412–2422.

135. Galgani A, Giorgi FS. Exploring the Role of Locus Coeruleus in Alzheimer's Disease: a Comprehensive Update on MRI Studies and Implications. Curr Neurol Neurosci Rep. 2023;23:925–936.

136. Dahl MJ, Bachman SL, Dutt S, Düzel S, Bodammer NC, Lindenberger U, et al. The integrity of dopaminergic and noradrenergic brain regions is associated with different aspects of late-life memory performance. Nat Aging. 2023;3:1128–1143.

137. Jacobs HIL, Becker JA, Kwong K, Engels-Domínguez N, Prokopiou PC, Papp K V., et al. In vivo and neuropathology data support locus coeruleus integrity as indicator of Alzheimer's disease pathology and cognitive decline. Sci Transl Med. 2021;13.

138. Galgani A, Lombardo F, Frijia F, Martini N, Tognoni G, Pavese N, et al. The degeneration of locus coeruleus occurring during Alzheimer's disease clinical progression: a neuroimaging follow-up investigation. Brain Struct Funct. 2024;229:1317–1325.

139. Liu KY, Kievit RA, Tsvetanov KA, Betts MJ, Düzel E, Rowe JB, et al. Noradrenergic-dependent functions are associated with age-related locus coeruleus signal intensity differences. Nat Commun. 2020;11.

140. Olivieri P, Lagarde J, Lehericy S, Valabrègue R, Michel A, Macé P, et al. Early alteration of the locus coeruleus in phenotypic variants of Alzheimer's disease. Ann Clin Transl Neurol. 2019;6:1345–1351.

141. Therriault J, Benedet AL, Pascoal TA, Mathotaarachchi S, Chamoun M, Savard M, et al. Association of Apolipoprotein E ε4 With Medial Temporal Tau Independent of Amyloid-β Supplemental content. JAMA Neurol. 2020;77:470–479.

142. McKhann GM, Knopman DS, Chertkow H, Hyman BT, Jack CR, Kawas CH, et al. The diagnosis of dementia due to Alzheimer's disease: Recommendations from the National Institute on Aging-Alzheimer's Association workgroups on diagnostic guidelines for Alzheimer's disease. Alzheimer's and Dementia. 2011;7.

143. Sibahi A, Gandhi R, Al-Haddad R, Therriault J, Pascoal T, Chamoun M, et al. Characterization of an automated method to segment the human locus coeruleus. Hum Brain Mapp. 2023;44:3913–3925.

144. Dahl MJ, Mather M, Werkle-Bergner M, Kennedy BL, Guzman S, Hurth K, et al. Locus coeruleus integrity is related to tau burden and memory loss in autosomal-dominant Alzheimer's disease. Neurobiol Aging. 2022;112:39–54.

145. Gallant SN, Kennedy BL, Bachman SL, Huang R, Lee T-H, Mather M. Behavioral and fMRI evidence that arousal enhances bottom-up attention and memory selectivity in young but not older adults. https://doi.org/10.1101/2021.07.02.450802.

146. Cassidy CM, Therriault J, Pascoal TA, Cheung V, Savard M, Tuominen L, et al. Association of locus coeruleus integrity with Braak stage and neuropsychiatric symptom severity in Alzheimer's disease. https://doi.org/10.1038/s41386-022-01293-6.

147. Jacobs HIL, Priovoulos N, Poser BA, Pagen LHG, Ivanov D, Verhey FRJ, et al. Dynamic behavior of the locus coeruleus during arousal-related memory processing in a multi-modal 7T fMRI paradigm. Elife. 2020;9.

148. García-Lorenzo D, Longo-Dos Santos C, Ewenczyk C, Leu-Semenescu S, Gallea C, Quattrocchi G, et al. The coeruleus/subcoeruleus complex in rapid eye movement sleep behaviour disorders in Parkinson's disease. Brain. 2013;136.

149. Naidich TP, Duvernoy HM, Delman BN, Sorensen AG, Kollias SS, Haacke EM. Duvernoy's Atlas of the Human Brain Stem and Cerebellum: High-Field MRI, Surface Anatomy, Internal Structure, Vascularization and 3 D Sectional Anatomy. 2009.

150. German DC, Walker BS, Manaye K, Smith WK, Woodward DJ, North AJ. The human locus coeruleus: Computer reconstruction of cellular distribution. Journal of Neuroscience. 1988;8.

151. Chen X, Huddleston DE, Langley J, Ahn S, Barnum CJ, Factor SA, et al. Simultaneous imaging of locus coeruleus and substantia nigra with a quantitative neuromelanin MRI approach. Magn Reson Imaging. 2014;32.

152. Clewett D V., Huang R, Velasco R, Lee T-H, Mather M. Locus Coeruleus Activity Strengthens Prioritized Memories Under Arousal. The Journal of Neuroscience. 2018;38:1558–1574.

153. German DC, Manaye KF, White CL, Woodward DJ, McIntire DD, Smith WK, et al. Disease-specific patterns of locus coeruleus cell loss. Ann Neurol. 1992;32.

154. Lussier FZ, Pascoal TA, Chamoun M, Therriault J, Tissot C, Savard M, et al. Mild behavioral impairment is associated with β-amyloid but not tau or neurodegeneration in cognitively intact elderly individuals. Alzheimer's and Dementia. 2020;16.

155. Therriault J, Benedet AL, Pascoal TA, Savard M, Ashton NJ, Chamoun M, et al. Determining Amyloid-b Positivity Using 18 F-AZD4694 PET Imaging. 2021. 2021. https://doi.org/10.2967/jnumed.120.245209.

156. Jack CR, Wiste HJ, Weigand SD, Therneau TM, Lowe VJ, Knopman DS, et al. Defining imaging biomarker cut points for brain aging and Alzheimer's disease. Alzheimer's and Dementia. 2017;13.

157. Therriault J, Benedet AL, Pascoal TA, Savard M, Ashton NJ, Chamoun M, et al. Determining amyloid-b positivity using 18F-AZD4694 PET imaging. Journal of Nuclear Medicine. 2021;62:247–252.

158. Pascoal TA, Therriault J, Benedet AL, Savard M, Lussier FZ, Chamoun M, et al. 18F-MK-6240 PET for early and late detection of neurofibrillary tangles. Brain. 2020;143.

159. García-Lorenzo D, Longo-Dos Santos C, Ewenczyk C, Leu-Semenescu S, Gallea C, Quattrocchi G, et al. The coeruleus/subcoeruleus complex in rapid eye movement sleep behaviour disorders in Parkinson's disease. Brain. 2013;136:2120–2129.

160. Horga G, Cassidy CM, Xu X, Moore H, Slifstein M, Van Snellenberg JX, et al. Dopamine-related disruption of functional topography of striatal connections in unmedicated patients with schizophrenia. JAMA Psychiatry. 2016;73:862–870.

161. Shigemori K, Ohgi S, Okuyama E, Shimura T, Schneider E. The factorial structure of the mini mental state examination (MMSE) in Japanese dementia patients. vol. 10. 2010.

162. St-Hilaire A, Blackburn MC, Wilson MA, Laforce R, Hudon C, Macoir J. Object decision test (BORB): normative data for the adult Quebec population and performance in Alzheimer's disease and the semantic variant of primary progressive aphasia. Aging, Neuropsychology, and Cognition. 2018;25:427–442.

163. 'Haines Ciolek C, 'Lee SY. Cognitive Issues in the Older Adult. Guccione's Geriatric Physical Therapy. 2020:425–452.

164. ’Lichtenberger EO, ’Kaufman AS. Essentials of WAIS-IV Assessment. John Wiley & Sons. 2009. 2009.

165. Ahn YD, Yi D, Joung H, Seo EH, Lee YH, Byun MS, et al. Normative data for the logical memory subtest of the wechsler memory scale-iv in middle-aged and elderly korean people. Psychiatry Investig. 2019;16:793–799.

166. Shao Z, Janse E, Visser K, Meyer AS. What do verbal fluency tasks measure? Predictors of verbal fluency performance in older adults. Front Psychol. 2014;5.

167. Hugon J, Queneau M, Sanchez Ortiz M, Msika EF, Farid K, Paquet C. Cognitive decline and brainstem hypometabolism in long COVID: A case series. Brain Behav. 2022;12.

168. Rogers JP, Chesney E, Oliver D, Pollak TA, McGuire P, Fusar-Poli P, et al. Psychiatric and neuropsychiatric presentations associated with severe coronavirus infections: a systematic review and meta-analysis with comparison to the COVID-19 pandemic. Lancet Psychiatry. 2020;7:611–627.

169. Emmi A, Rizzo S, Barzon L, Sandre M, Carturan E, Sinigaglia A, et al. Detection of SARS-CoV-2 viral proteins and genomic sequences in human brainstem nuclei. NPJ Parkinsons Dis. 2023;9.

170. Martin EM, Rupprecht S, Schrenk S, Kattlun F, Utech I, Radscheidt M, et al. A hypoarousal model of neurological post-COVID syndrome: the relation between mental fatigue, the level of central nervous activation and cognitive processing speed. J Neurol. 2023;270:4647–4660.

171. Jacobs HIL, Ibrahim T, Vahidy FS, Girard TD, Hosseini AA, Alkateeb S, et al. Lower locus coeruleus integrity in older COVID-19 survivors: initial findings from an international 7T MRI consortium. Alzheimer’s & Dementia. 2023;19.

172. Grudzien A, Shaw P, Weintraub S, Bigio E, Mash DC, Mesulam MM. Locus coeruleus neurofibrillary degeneration in aging, mild cognitive impairment and early Alzheimer’s disease. Neurobiol Aging. 2007;28:327–335.

173. Arendt T, Brückner MK, Morawski M, Jäger C, Gertz HJ. Early neurone loss in Alzheimer’s disease: cortical or subcortical? Acta Neuropathol Commun. 2015;3:10.

174. Fernandes P, Regala J, Correia F, Gonçalves-Ferreira AJ. The human locus coeruleus 3-D stereotactic anatomy. Surgical and Radiologic Anatomy. 2012;34.

175. Castellanos G, Lorenzo-Betancor Q, Ortega-Cubero de, Uranga J, Pastor P. Automated neuromelanin imaging as a diagnostic biomarker for Parkinson’s disease. Mov Disord. 2015;30:945–952.

176. Dünnwald M, Betts MJ, Sciarra A, Düzel E, Oeltze-Jafra S. Automated segmentation of the locus coeruleus from neuromelanin-sensitive 3t MRI using deep convolutional neural networks. Informatik aktuell, 2020.

177. Imaging Technology News. NM-101 Software. Https://WwwItnonlineCom/Content/Terran-Biosciences-Receives-Fda-Clearance-Nm-101-Industry%E2%80%99s-First-Software-Analysis. 2023.

178. Akagawa M, Ishii Y, Ishii T, Shibata T, Yotsu-Yamashita M, Suyama K, et al. Metal-Catalyzed Oxidation of Protein-Bound Dopamine. Biochemistry. 2006;45:15120–15128.

179. Spotorno N, Acosta-Cabronero J, Stomrud E, Lampinen B, Strandberg OT, van Westen D, et al. Relationship between cortical iron and tau aggregation in Alzheimer's disease. Brain. 2020;143:1341–1349.

180. Belaidi AA, Masaldan S, Southon A, Kalinowski P, Acevedo K, Appukuttan AT, et al. Apolipoprotein E potently inhibits ferroptosis by blocking ferritinophagy. Mol Psychiatry. 2024;29:211–220.

181. Ayton S, Faux NG, Bush AI, Weiner MW, Aisen P, Petersen R, et al. Ferritin levels in the cerebrospinal fluid predict Alzheimer's disease outcomes and are regulated by APOE. Nat Commun. 2015;6.

182. Levi S, Ripamonti M, Moro AS, Cozzi A. Iron imbalance in neurodegeneration. Mol Psychiatry. 2024;29:1139–1152.

183. Wolters AF, Heijmans M, Priovoulos N, Jacobs HIL, Postma AA, Temel Y, et al. Neuromelanin related ultra-high field signal intensity of the locus coeruleus differs between Parkinson's disease and controls. Neuroimage Clin. 2023;39.

184. Schneider C, Prokopiou PC, Papp K V., Engels-Domínguez N, Hsieh S, Juneau TA, et al. Atrophy links lower novelty-related locus coeruleus connectivity to cognitive decline in preclinical AD. Alzheimer's and Dementia. 2024;20:3958–3971.

185. Bastin C, Delhaye E, Moulin C, Barbeau EJ. Novelty processing and memory impairment in Alzheimer's disease: A review. Neurosci Biobehav Rev. 2019;100:237–249.

186. Omoluabi T, Torraville SE, Maziar A, Ghosh A, Power KD, Reinhardt C, et al. Novelty-like activation of locus coeruleus protects against deleterious human pretangle tau effects while stress-inducing activation worsens its effects. Alzheimer's and Dementia: Translational Research and Clinical Interventions. 2021;7.

187. Lustberg D, Tillage RP, Bai Y, Pruitt M, Liles LC, Weinshenker D. Noradrenergic circuits in the forebrain control affective responses to novelty. Psychopharmacology (Berl). 2020;237:3337–3355.

188. Giorgi FS, Lombardo F, Galgani A, Hlavata H, Della Latta D, Martini N, et al. Locus Coeruleus magnetic resonance imaging in cognitively intact elderly subjects. Brain Imaging Behav. 2022;16:1077–1087.

189. Bell TR, Elman JA, Beck A, Fennema-Notestine C, Gustavson DE, Hagler DJ, et al. Rostral-middle locus coeruleus integrity and subjective cognitive decline in early old age. Journal of the International Neuropsychological Society. 2023;29:763–774.

190. Vila-Castelar C, Fox-Fuller JT, Guzmán-Vélez E, Schoemaker D, Quiroz YT. A cultural approach to dementia — insights from US Latino and other minoritized groups. Nat Rev Neurol. 2022;18:307–314.

191. Bell TR, Elman JA, Beck A, Fennema-Notestine C, Gustavson DE, Hagler DJ, et al. Rostral-middle locus coeruleus integrity and subjective cognitive decline in early old age. Journal of the International Neuropsychological Society. 2023;29:763–774.

192. Pascoal TA, et al. 18F-MK-6240 PET for early and late detection of neurofibrillary tangles. Brain. 2020;143:2634–2636.

193. Ohtsuka C, Sasaki M, Konno K, Koide M, Kato K, Takahashi J, et al. Changes in substantia nigra and locus coeruleus in patients with early-stage Parkinson's disease using neuromelanin-sensitive MR imaging. Neurosci Lett. 2013;541:93–98.

194. Reimão S, Pita Lobo P, Neutel D, Correia Guedes L, Coelho M, Rosa MM, et al. Substantia nigra neuromelanin magnetic resonance imaging in de novo Parkinson's disease patients. Eur J Neurol. 2015;22.

195. Schneider JS, Tinker JP, Decamp E. Clonidine improves attentional and memory components of delayed response performance in a model of early Parkinsonism. Behavioural Brain Research. 2010;211:236–239.

196. Wengler K, Cassidy C, van der Pluijm M, Weinstein JJ, Abi-Dargham A, van de Giessen E, et al. Cross-Scanner Harmonization of Neuromelanin-Sensitive MRI for Multisite Studies. Journal of Magnetic Resonance Imaging. 2021;54:1189–1199.